TOWARDS NOVEL PARADIGM OF SEISMIC SIGNAL PROCESSING

BY

Arbab Latif

A Thesis Presented to the
DEANSHIP OF GRADUATE STUDIES

KING FAHD UNIVERSITY OF PETROLEUM & MINERALS

DHAHRAN, SAUDI ARABIA

In Partial Fulfillment of the
Requirements for the Degree of

MASTER OF SCIENCE

In

ELECTRICAL ENGINEERING

May 2014

KING FAHD UNIVERSITY OF PETROLEUM & MINERALS
DHAHRAN 31261, SAUDI ARABIA

DEANSHIP OF GRADUATE STUDIES

This thesis, written by **ARBAB LATIF** under the direction of his thesis adviser and approved by his thesis committee, has been presented to and accepted by the Dean of Graduate Studies, in partial fulfillment of the requirements for the degree of **MASTER OF SCIENCE IN ELECTRICAL ENGINEERING**.

Thesis Committee

Dr. Wail A. Mousa (Adviser)

Dr. Tareq Y. Al-Naffouri (Member)

Dr. Abdullatif A. Al-Shuhail (Member)

Dr. Ali Ahmad Al-Shaikhi
Department Chairman

Dr. Salam A. Zummo
Dean of Graduate Studies

27/5/14
Date

عمادة الدراسات العليا
DEANSHIP OF GRADUATE STUDIES

Dedicated to my beloved Baba, Mama and sweet Bajjay!

ACKNOWLEDGMENTS

I would like to thank KFUPM for providing me the opportunity to complete my Master degree. Foremost, I want to thank my advisor, Dr. Wail A. Mousa, for introducing me to the seismic signal processing. His enthusiasm, advice, immense knowledge and guidance made this research possible. I could not have imagined having a better advisor for my MS thesis.

I would like to thank the committee members: Dr. Tareq Y. Al-Naffouri and Dr.Abdullatif A. Al-Shuhail for their valuable comments and insightful suggestions throughout the research work.I would like to thank Deanship of graduate studies for providing me the scholarship for this MS degree. I would also like to thank my friends for their support throughout the research work.

I can never give enough thanks to my parents, sister for their great encouragement and trust in me during difficult times. In particular, the patience and understanding shown by my mother, father and sister during the honors year is greatly appreciated.

TABLE OF CONTENTS

LIST OF TABLES

LIST OF FIGURES

THESIS ABSTRACT

NAME: Arbab Latif

TITLE OF STUDY: Towards Novel Paradigm of Seismic Signal Processing

MAJOR FIELD: Electrical Engineering

DATE OF DEGREE: May 2014

Acquisition of seismic data is one of the most crucial step in the seismic exploration. Once acquired, the data is abundant, mostly stored in terabytes. Processing of such large amounts of data is expensive; hence, it requires time and lots of resources. Therefore, techniques that can acquire high resolution data of the Earth's subsurfaces, but with few samples, are needed. In this thesis, one such technique, known as compressive sensing, is investigated for different seismic applications. Radon transform is used as sparsifying transform for the compressive sensing. By utilizing the compressive sensing and different variants of Radon transform, new techniques for first arrival picking, multiple reflection removal, seismic deconvolution, reconstruction of missing traces and classification of seismic events are presented. The proposed method are computationally more efficient than the existing methods and are robust under noisy conditions. The methods were tested on

synthetic and real seismic data set, with different compression levels and various levels of additive white Gaussian noise. Therefore, since the new methods require fewer samples and computation time than existing techniques, it is believed that the proposed methods are an appropriate new addition to the existing compressive sensing methods for seismic data processing.

ملخص الرسالة

الاسم الكامل: أرباب لطيف

عنوان الرسالة: نحو رواية باراديم من معالجة الإشارات الزلزالية

التخصص: الهندسة الكهربائية

تاريخ الدرجة العلمية: مايو 2014

الحصول على البيانات الزلزالية هي واحدة من أهم الخطوات في التنقيب الزلزالي. وبمجرد الحصول عليها ، البيانات وفيرة، تخزن معظمها في تيرابايت . معالجة مثل هذه الكميات الضخمة من البيانات مكلفة ؛ وبالتالي، فإنه يتطلب وقتا والكثير من الموارد. وبالتالي، التقنيات التي يمكن من خلالها الحصول على بيانات عالية الدقة من سطوح الأرض ، ولكن مع بعض القياسات ، ضرورية . في هذه الأطروحة ، واحدة من هذه التقنيات، المعروفة باسم الاستشعار عن الضغط، لتطبيقات الزلزالية المختلفة . تحويل الرادون يستخدم كأساس لل تحويل الاستشعار عن الضغط . من خلال الاستفادة من الاستشعار عن بعد و مختلف المتغيرات الضغط من غاز الرادون تحويل ، يتم عرض تقنيات جديدة ل أول قطف صوله، و إزالة انعكاس متعددة ، وإعادة بناء آثار المفقودين وتصنيف الأحداث الزلزالية. الطريقة المقترحة هي حسابيا أكثر كفاءة من الطرق القائمة وقوي في ظل ظروف صاخبة. تم اختبار الأساليب الاصطناعية و الحقيقية على مجموعة البيانات الزلزالية ، مع مستويات ضغط مختلفة ومستويات مختلفة من الضوضاء المضافة جاوس الأبيض. لذلك، بما ان الأساليب جديدة تتطلب قدرا أقل من العينات و حساب الوقت من التقنيات الموجودة ،يعتقد أن الأساليب المقترحة هي إضافة جديدة ملائمة ل أساليب الضغط الاستشعار الموجودة لمعالجة البيانات الزلزالية

CHAPTER 1

INTRODUCTION

The consumption of oil and gas is increasing at rapid rate due to, which discovered reservoirs are diminishing with the passage of time. So not only the exploration but the accurate exploration of new reservoirs of oil and gas is becoming more important with the passage of time [1]. The ultimate aim of the seismic exploration is to obtain accurate information (images) of the earth subsurface so one can identify the hydrocarbons structure present below the earth surface, without any expensive /or time consuming drilling.

Seismic data processing plays an important role in achieving this goal [2]. Earth is composed of different layers with different physical properties. The acquired seismic data contain reflections from these different layers [3,4]. By analyzing these layers, geologists, after obtaining the final image of the subsurface, can predict the likelihood of hydrocarbons existence. Due to the complex geological conditions, different kinds of reflections are generated. The acquired data has low resolution due to the presence of noise and unwanted energies (e.g,; multiple re-

flection and ground roll) from the same layer, which in turn make the processing of seismic data more difficult.In general, as the complexity of the earth structure of the concerned area is increased, increasing the resolution and the removal of noise become more challenging and require more sophisticated processing techniques. Besides difficulty in identification of primary reflections, one also face difficulties in the data analysis and interpretation [5].

The most crucial step in seismic exploration is the acquisition of data. Once acquired, the data is abundant, mostly stored in terabytes [6]. Processing of such large amounts of data is expensive; hence, it requires time and lots of resources. Therefore, techniques that can acquire high resolution data of the Earth's subsurfaces, but with few samples, are needed. The 'curse of dimensionality' is the main barricade [7] and is governed by the Nyquist-Shannon theorem. If one is interested to increase the resolution, he/she has to increase the sampling rate (number of samples). To bypass the Nyquist–Shannon theorem, there exists a new nonlinear sampling theory known as Compressive Sensing [8]. This enables the capture of high resolution signals only using small numbers of measurement-far less compared to the Nyquist-Shannon theorem [9]. Currently, in almost all devices, first the data is captured and then it is compressed by throwing away the non-significant(mainly redundant data) part of the signal. Compressive sensing takes sampling to another level by combining both of these steps into a step where the signal can be compressed on the fly. It uses two key concepts: sparseness and incoherence [11] of the signal in a certain domain. Compressive sensing is effec-

tive for a particular type of signals that are sparse in nature. The signal can be sparse in some transform domain. Compressive sensing exploits the fact that all most all the signals are sparse in some particular domain. The existing acquisition techniques do not utilize the structure of the seismic data.

The feature, that seismic data is sparse in some specific domain, enables us to use this new sampling scheme (compressive sensing) for which the sampling rate depends upon the sparsity of the data. One of the challenges is to identify an appropriate transform where the signal (seismic data) is sparse. Seismic data is sparse in curvelets [12] and wave atoms [13]. The curvelet transform, composes wavefields as a superposition of multi scale, and highly localized waveforms, due to which we get needle-like curvelets at small scales. It has been shown in [14] that curvelet transform is suitable for compressing the seismic data, due to their near invariance under wave propagation. For oscillatory wave fronts, wave atoms are more suitable.

The generalized Radon transform is the tool that is heavily used in many application for the image processing [15], medical imaging [16, 17], solution of mathematical problems [18, 19] and, most importantly in the field of reflection seismic data processing [20–24]. Radon transform is robust in nature and has attracted the attention of seismic data processing scientists an engineers during the last two decades. It is being used for quite some time in different applications which includes seismic deconvolution [20], multiple removal as discussed in [23, 24, 24–26], first arrival picking or enhancement [21]. There exists three types of

Radon transform that are used for seismic data processing [27]. These transforms are the linear Radon transformation (slant-stack), the parabolic Radon transform, and the hyperbolic Radon transform. The parabolic Radon transform is mostly used due to its effectiveness as compared the linear Radon transform and low computational cost [22]. The Radon transform transforms the data from the time-space domain (t, x) to the linear Radon domain $(\tau - p)$ or parabolic or hyperbolic Radon domain$(\tau - q)$. One of the distinct feature of the Radon transform is that the $\tau - p$ and $\tau - q$ domains provide the sparse representation of the linear and parabolic(or hyperbolic) seismic events, respectively [27].

In this thesis, Radon transform [28] is used as an alternate sparsifying transform for reflection seismic data, instead of curvelets and wave-atoms. Radon transform is robust, easier to compute, a well-established mathematical theory, and is part of many seismic data processing work-flows. There are faster methods to evaluate Radon transform, so computationally, it is efficient [22, 29]. These features make Radon transform, as a sparsifying transform for compressive sensing, a better choice than curvelet transform. Additionally, different application of compressive sensing to the seismic data are studied. The applications includes interpolation of missing seismic traces, first arrival picking of the seismic refraction data, classification of different seismic events from the acquired data, deconvolution of seismic data, and attenuation of multiple reflection attenuation from the seismic data. Various results will be shown on synthetic and real seismic data and are compared with compressive sensing methods using state of the art seismic

sparse domain, namely, the curvelet domain.

The thesis is structured as follows. Chapter 2 provides a brief information about the origin, history of compressive sensing and Radon transform. Chapter 3 includes linear Radon transform and how can it be used as a sparsifying transform for compressive sensing of the seismic data. Various applications of the linear Radon transform on the seismic data will be shown for the interpolation, first arrival(break) picking, deconvolution and classification of linear events.

In chapter 4, the use of the parabolic Radon transform as sparsifying transform for the compressive sensing is described. It includes different application of the proposed formulation on the seismic data. Applications discussed in chapter 4 includes interpolation of non-linear events, deconvolution of seismic data, classification of non-linear reflections and attenuation of multiple reflection attenuation from the seismic data. Concluding remarks of this thesis and future work are presented in Chapter 5.

CHAPTER 2

REVIEW OF COMPRESSIVE SENSING AND GENERALIZED RADON TRANSFORM

2.1 Introduction

Compressive sensing has attracted many researchers in the field of signal and image processing as well as the field of exploration seismic [7, 30–36]. For the sake of completion and clarity for the thesis readers, chapter presents a brief review of compressive sensing and Radon transform. First a brief introduction of the compressive sensing will be provided. Then the basic properties and mathematical formulation of the compressive sensing is presented. Some applications of compressive sensing and how it is currently being used in seismic data processing, are also discussed.

Afterwards the generalized Radon transform is introduced. This is followed by the applications, properties and Inversion of Radon transform. Finally, the application of Radon transforms in seismic signal processing is discussed. For the linear and parabolic compressed Radon transform refer to chapter 3 and chapter 4, receptively.

2.2 Compressive Sensing

2.2.1 Introduction

The traditional approach for sampling signals or images follow Shannon's sampling theorem, according to which the sampling rate should be at least twice the maximum frequency content of the sampled signal, this rate is referred as the Nyquist rate [37]. This is the basic principle that has been adopted in almost all the acquisition techniques used in different visual and audio devices, medical imaging, radio transceivers, etc. [38]. Currently in almost all the devices, first the data is captured and then it compressed by throwing away the non-significant part of the signal.

In 2004, Candes accidentally discovered the fact that L_1-minimization helps to fill the blanks of an under-sampled signal(picture) effectively [39]. The recovered picture was not just slightly better than the original, rather, the picture looks sharp and perfect in every detail. D.Donoho, E. Candes, J. Romberg, and T. Tao [8,40–42] are considered as the pioneers of the compressive sensing, also known

as compressed sensing. Compressive sensing can be used to reduce the amount of data required at acquisition step. Compressive sensing is highly efficient and simple protocol for acquisition according to which you can sample the signal at a low rate(far less than the Nyquist rate) [8].

According to the theory of compressive sensing, the sampling rate does not depend on the frequency content of the signal but it depends upon the information content of the signal or the image. A signal or an image with low information content can be recovered back, without any error, only using small number of measurements [40]. The logic behind compressive sensing is that if one already have captured enough samples then increasing the sample rate will not increase the resolution of the signal. Almost all the real world signals have low information content [43], where low information content means that the signal of interest is sparse in nature. Compressed sensing uses the fact that most of the real life signals have low information content to bypass the Shannon theorem [44].

Compressive sensing currently a hot topic and a plenty of research is undergoing on how one can use this sampling technique in various applications.

Compressive sensing can be used for image compression. In [45], authors have presented a new camera architecture. It is based on micro-mirror devices. The comparison between the conventional imaging and compressive imaging is presented in [46]. More details about the image compression can be found in [47–50].

Compressive sensing can be used for compression of other data as discussed in

[51]. Compressive sensing can play a big part in communication as well. It is used for channel coding in [52], equalization [53, 54], and channel estimation [55–57]. It can also be used to solve inversion problems.

A very important use of compressive sensing can be in the medical field. By using compressive sensing, some valuable time can be saved in medical imaging problems. Magnetic resonance angiography is one example of inversion problem, where wavelet transform can be used for basis as proposed in [58]. Rapid magnetic resonance imaging concept is discussed in [59, 60]. It can be used for fast tomography as presented in [61, 62].

The most important use of compressive sensing is for the data acquisition. As in some situations it is not possible to obtain a lot of samples, like the case of seismic data, and computationally it could have an enormous impact. In such cases compressive sensing can help a lot in acquiring the data in a compressed way.

2.2.2 The Basic Concept of Compressive Sensing

As discussed earlier, compressive sampling is a new technique that enables us to capture high resolution signals only using small number of measurement, far less than govern by the Shannon theorem. It is the technique that goes against the common wisdom in data acquisition and enables one to recover signal with less samples than the Nyquist. To make this possible, compressive sensing relies on two principles: sparsity and incoherence of the signal in a particular domains [63, 64].

Sparsity uses the fact that the informational content of the signal might be much less than suggested by the bandwidth of the signal. Simply,sparsity deals with the number of non-zero elements in a signal. A signal of size N is said to be K sparse if it has maximum K non-zero elements. Incoherence covers the duality between transformed domain and the captured domain (e.g., time and frequency). If a signal is sparse in time, then it will be spread out in frequency domain or vice versa. In other words, incoherence is needed to measure the signal in such a way that the maximum amount of information can be extracted from the signal by using small amounts of measurement [9]. Mathematical techniques necessary to implement compressive sensing include the selection of appropriate transforms. Particularly, l_1 optimization is used for the representation of the signal in the sparse domain. The l_1 minimization concentrates the energy of the signal onto a few non-zero coefficients.

Mathematically, Let $g(n)$ be the seismic data, acquired using traditional sampling techniques. Once acquired, the data contains N uniformly spaced samples and can be represented as follows:

$$g(n) = \sum_{i=1}^{N} x_i \psi_i, \tag{2.1}$$

where x_i are the coefficients sequence of $g(n)$, with ψ_i as orthonormal basis. To make the formulation easier the signal $g(n)$ in terms of matrix is as follows:

$$\boldsymbol{g} = \boldsymbol{\psi x}. \tag{2.2}$$

For the multiplication to hold the dimension of $\boldsymbol{\psi}$ should be $N \times N$. If $\boldsymbol{\psi}$ is a sparsifying transform then $g(n)$ is a sparse vector with size N. Let the number of non zero entries in $\boldsymbol{g}$ be K. In other words, $\boldsymbol{g}$ is a K sparse vector with length N, when represented in basis $\boldsymbol{\psi}$.

As $\boldsymbol{g}$ is K sparse vector, so instead of sampling all the elements of $\boldsymbol{g}$, the signal can be recovered by less number of samples, as suggested by the compressive sensing. Let $\boldsymbol{\phi}$ be another basis matrix, known as sensing matrix, with size $M \times N$, where $M \ll N$. The sampled signal $\boldsymbol{g}$ can be represented in terms of new basis $\boldsymbol{\phi}$, as follows:

$$\boldsymbol{y} = \boldsymbol{\phi g} \tag{2.3}$$

$$\boldsymbol{y} = \boldsymbol{A x} \tag{2.4}$$

Here $\boldsymbol{A} = \boldsymbol{\phi\psi}$, sometimes referred as measurement matrix, is a matrix with dimension $M \times N$. So instead of using $\boldsymbol{\psi}$ for sampling, one can use $\boldsymbol{A}$ for sampling the signal. To recover the original signal, one have to find the coefficient vector $\hat{\boldsymbol{x}}$ by solving the following relation

$$\boldsymbol{A}\hat{\boldsymbol{x}} = \boldsymbol{b} \tag{2.5}$$

where

$$\boldsymbol{b} = \boldsymbol{\phi g} \tag{2.6}$$

Here $\boldsymbol{A}$, is a rectangular matrix, with less rows than the columns. So $\boldsymbol{A}$ is an

under-determined system of linear equations, number of unknowns are greater than the number of equations. Restricted isometric property(RIP) can be utilized for the perfect reconstruction of the under-sampled data [63] . The sensing matrix ϕ, satisfies the RIP, of order, K, if there exists a $\delta_K \in (0,1)$, such that;

$$(1-\delta_K)\|x\|_2^2 \leq \|\phi x\|_2^2 \leq (1+\delta_K)\|x\|_2^2 \tag{2.7}$$

The RIP is a sufficient condition for many sparsifying recovery theorem. Besides RIP the sensing matrix and representation matrix should have incoherence.

$$\mu(\phi,\psi) = \sqrt{n} \times \max_{1\leq K, j\leq n} |\langle \phi_K . \psi_j \rangle| \tag{2.8}$$

The incoherence lies between

$$\mu(\phi,\psi) \in [1,\sqrt{n}] \tag{2.9}$$

If the RIP and incoherence is satisfied then the l_1-norm can be used to solve this ill-conditioned relation (2.5). By using the l_1-norm for the reconstruction, the following model is obtained:

$$\min \|\boldsymbol{x}\|_1 \text{subject to } \boldsymbol{Ax} = \boldsymbol{b} \tag{2.10}$$

Once the coefficients are estimated by l_1-norm then the original signal can be

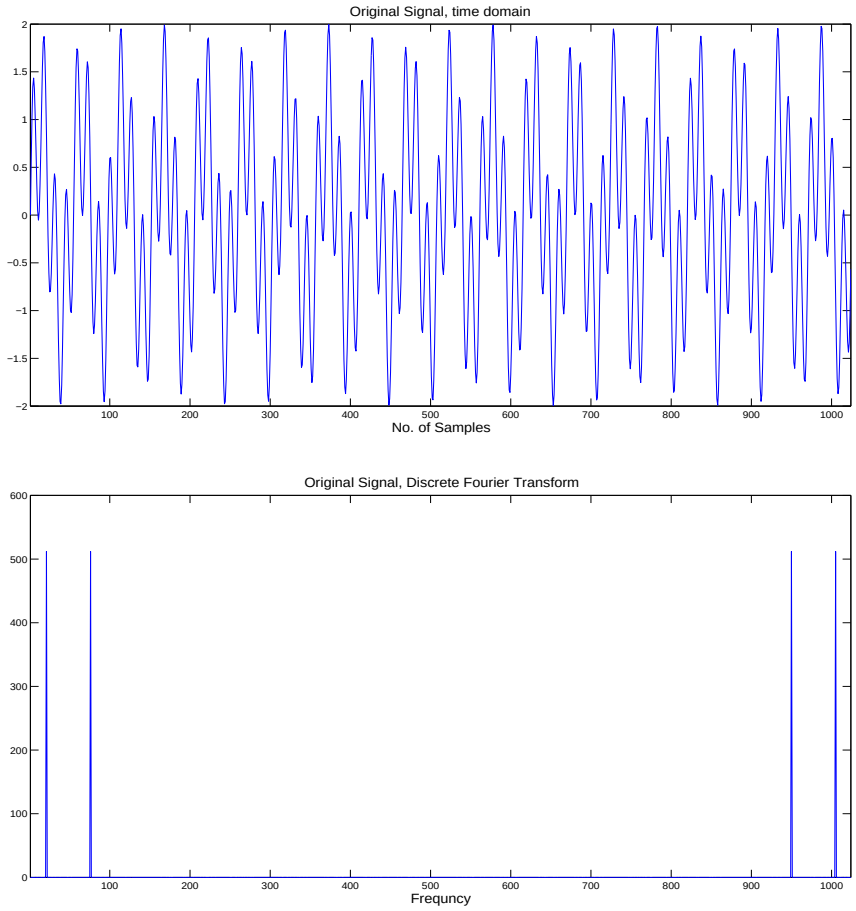

Figure 2.1: Compressive Sensing Example:(a)the original signal with N=1024 and (b) its sparse frequency representation

recovered by using the following relation

$$g = \psi \hat{x} \tag{2.11}$$

An example of a one-dimensional (1D) signal is presented here. The signal $g(t) = cos(2\pi 20t) + cos(2\pi 75t)$, is sampled in time with 1024 samples (N=1024). The signal and its frequency content is shown in Figure 2.1. From the frequency response it is evident that the signal is sparse in frequency domain and only has two frequencies. As the signal is sparse, one can use compressive sensing to acquire

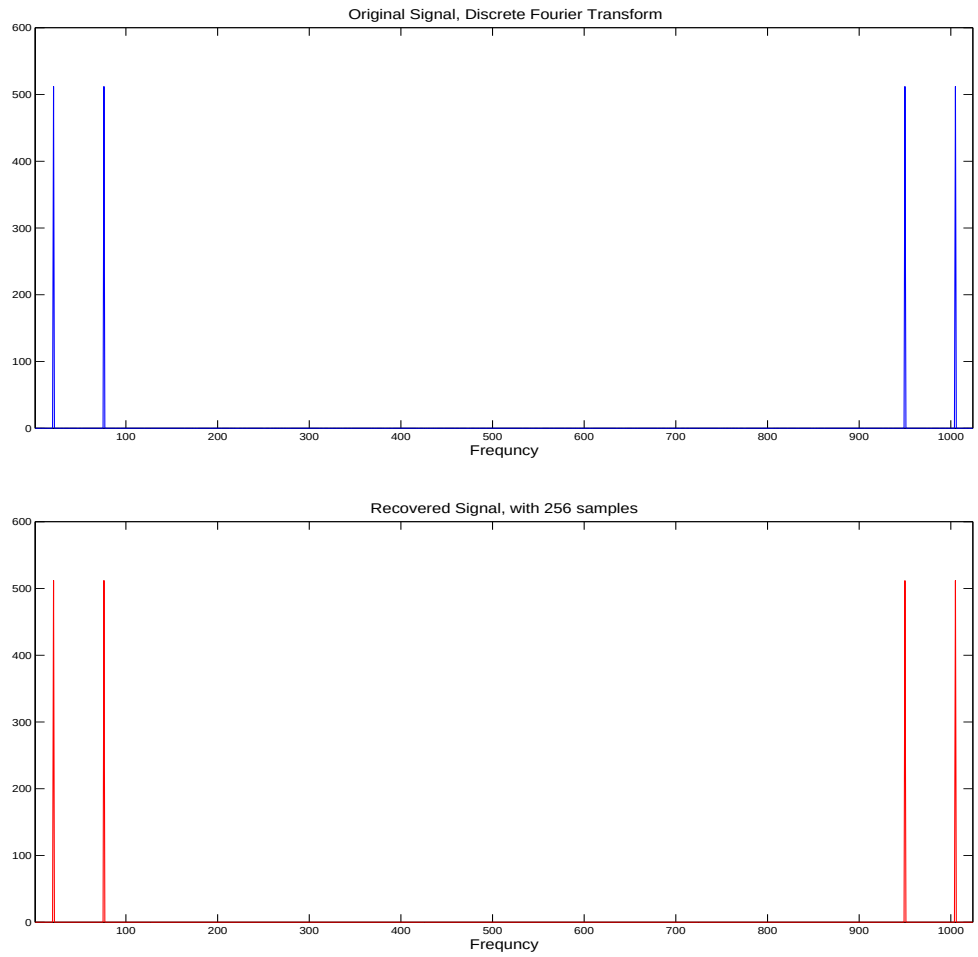

Figure 2.2: Compressive Sensing Example: (a)the sparse frequency representation of the signal after traditional sampling N=1024, and (b) the recovered signal in frequency domain after applying compressive sensing with M=256

the same signal with far less sample. For this example M=256 is used along with the discrete cosine transform (DCT) as its sparsifying transform. The recovered signal and the signal without the compression in frequency response is shown in Figure 2.2. The signal and recovered signal in time domain is shown in Figure 2.3. The error between the original signal and the compressed signal is also plotted in Figure 2.3

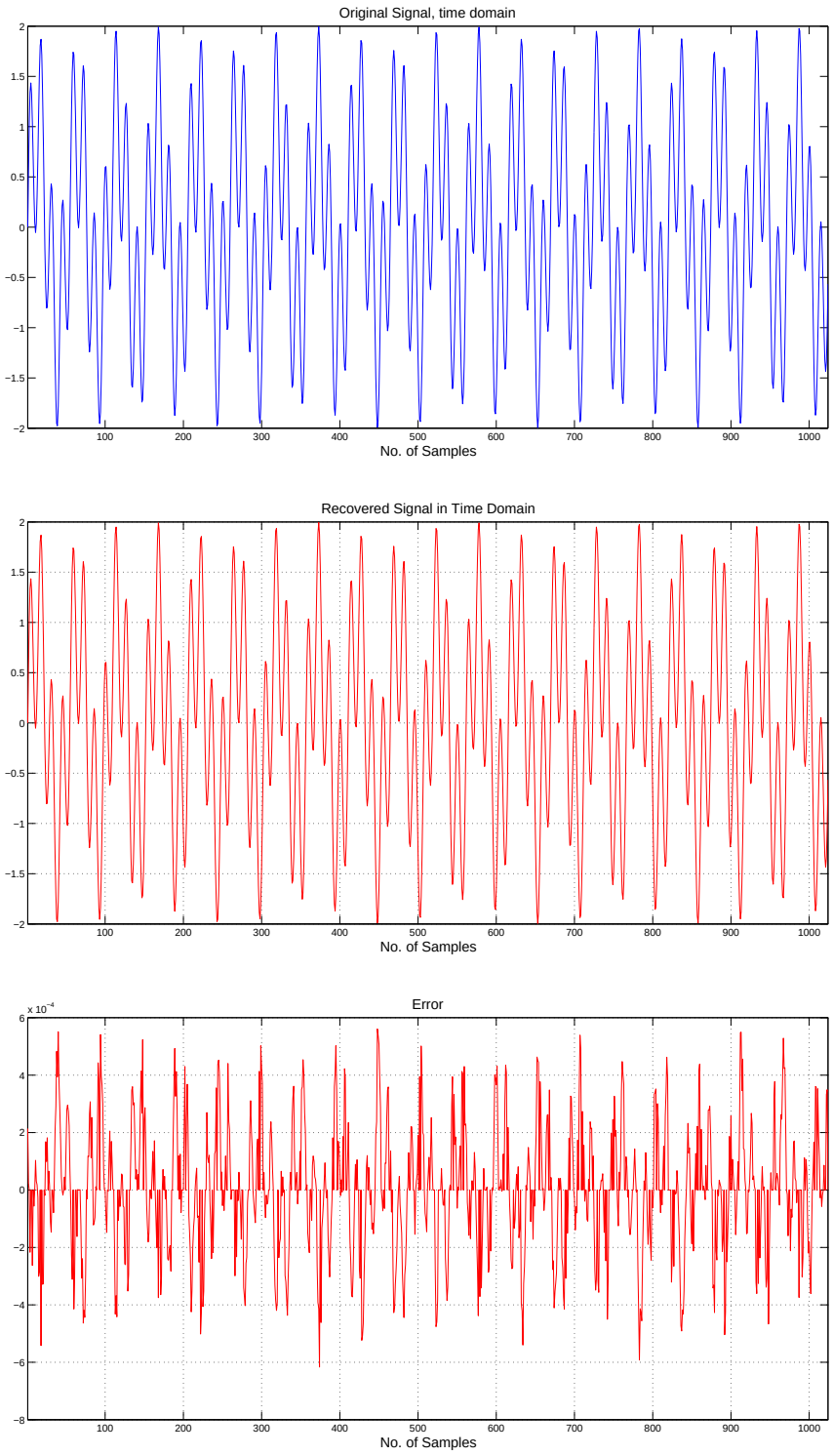

Figure 2.3: Compressive Sensing Example: (a)the original signal after traditional sampling with N=1024, and (b) the recovered signal in time domain after applying compressive sensing with M=256 andt he error between (a) and (b) is plotted in (c)

2.2.3 Compressive Sensing and Seismic Data Processing

Nowadays most of the acquired data is huge in size. Most of the seismic exploration techniques depends upon acquisition of data. The existing acquisition techniques do not utilize the structure of the seismic data. By using compressive sensing, one can make use of the fact that seismic data is sparse in some particular domain. This feature enables a new sampling scheme for which the sampling rate depends upon the sparsity of the data.

The first advancement was the continuous acquisition as instances of compressive sensing and identification of seismic data [31–33]. A lot of progress has been made in the selection of a sparse transform domain and the random sensing schemes for the compressive sensing [65]. Curvelet based seismic data processing was presented in [66]. Seismic data restoration is discussed by Hermann [67] and Cao [34]. Interpolation of seismic data using compressive sensing and curvelet is presented in [68–72] . Model for simultaneous acquisition using compressive sensing is presented in [73]. Separation of multiple using compressive sensing is discussed by Hermann [74]. Compressive sensing can also be used for marine data acquisition as discussed in [75, 76]. Deconvolution problem of seismic data is discussed by Saachi in [77].

As discussed earlier, compressive sensing exploits the fact that all most all the signals are sparse in some particular domain [43]. For example, many captured signals such as seismic data, medical images, photos, music, can be compressed by representing them in appropriate basis. When appropriate basis are used then

most of the coefficients will be zero or almost zero. The biggest challenge is to find an appropriate transform which can transform the seismic data in sparse fashion. For the seismic data curvelets and wave atoms are extensively used [71, 78]. The curvelet transform composes wavefields as superposition of multi scale and highly localized waveforms. Because of this, one can get needle-like curvelets at small scales. It has been shown by [14] that curvelet transform is suitable for compressing the seismic data, due to their near invariance under wave propagation. For oscillatory wave fronts, wave atoms are more suitable [12]. However, they suffer from high computational cost and suboptimal reconstructed seismic signal, as will be shown in the upcoming chapters.

2.3 Radon Transform

2.3.1 Introduction

The Radon transform is named after Johann Karl August Radon. He was an Austrian mathematician who introduced the Radon transform in 1917 [17]. Initially he only introduced the transform pair (forward as well as inverse transform) for straight lines. The Radon transform was also introduced without any practical application. Later Radon also presented the formulas for the transform in three-dimensions [79]. Now, Radon transform has been generalized for higher-dimensional Euclidean spaces [28]. Although initially the Radon transform was introduced without any practical application, the concept of Radon transforms,

however, led to a Nobel-prize in 1979 for the groundbreaking concept of viewing organs from outside the body using Tomography [80]. Mathematical theory of Radon transform was discussed by Deans [81]. Fundamental properties of the Radon transform examined by Durrani Bisset [17].

Radon transform has been used for many applications, including image reconstruction [15],solution of hyperbolic partial differential equations [18] image processing , medical imaging [16, 17], solution of mathematical problems [19] and, finally in the field of seismic data processing [20–24].

2.3.2 The Generalized Radon Transform

The generalized Radon transform integrates the data along any curve. It calculates the projections of an image along specified directions. In the case of a two-dimensional (2-D) function $f(x,t)$, the line integral is considered as the projection [82]. To represent an image, multiple, projections from different angles are recorded in Figure 2.4a. Line integral of 2D function $f(x,t)$ in the vertical direction is known as the projection onto the x-axis. On the other hand, the projection onto the y-axis, is the line integral in the horizontal direction -see Figure 2.4b.

The generalized Radon transform of $f(x,t)$ is defined as [83]

$$\hat{f}(\eta) = \int_{-\infty}^{\infty} f(x, \phi(x;\eta))dx, \tag{2.12}$$

η spans the parameter domain.

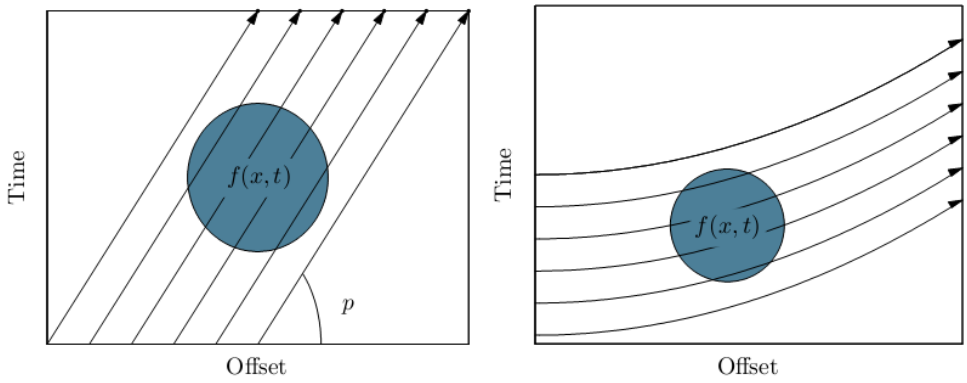

(a) Straight line trajectories. (b) Parabolic trajectories.

(a)

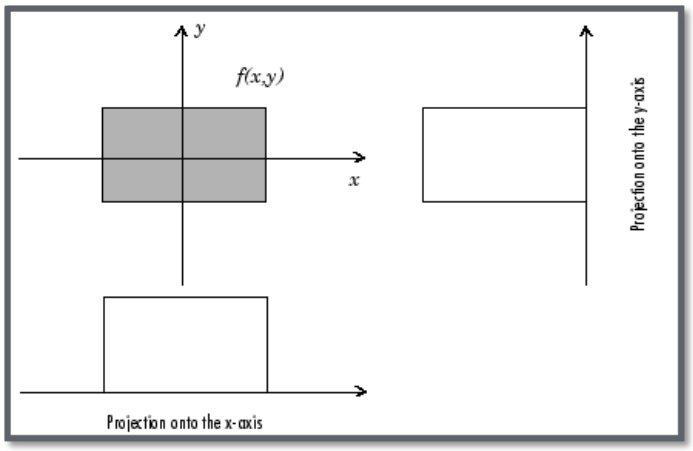

(b)

Figure 2.4: Projection (a) provides the basic concept of projection. Projections along x,y-axis and different trajectories are shown in (b)

In discrete form, Radon transform is represented as:

$$\hat{f}(\Omega) = \sum_{m=0}^{M-1} f(m, \phi(m;\Omega)), \tag{2.13}$$

here Ω spans the parameter domain. Figure 2.5 shows an example of the Radon transform of a square image shown in Figure 2.5a.

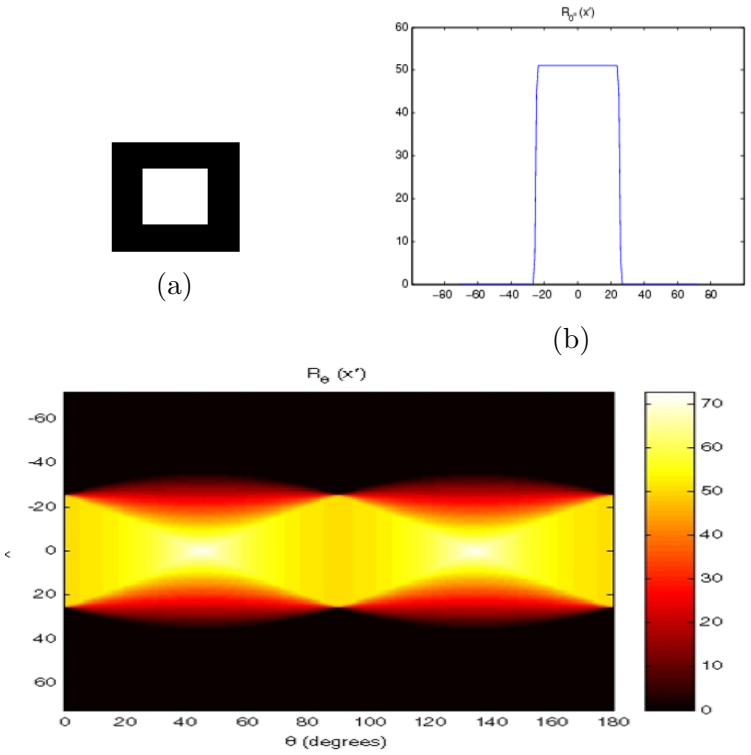

Figure 2.5: Generalized Radon Transform (a) Original Image (b) Projection 0 degree (c) Radon transform

2.3.3 Properties of Radon transform

Some basic properties of the Radon transform are discussed here for the data $g(x,t)$ [27]. For the sake of simplicity let $\eta = \{p, \tau\}$ and $g(x, \phi(x;\eta)) = px + \tau$. So Radon transform equation 2.12 become

$$\hat{g}(p,\tau) = \int_{-\infty}^{\infty} g(x, \phi(x; px+\tau))dx. \tag{2.14}$$

The above equation can also be written in terms of delta function:

$$\hat{g}(p,\tau) = \int_{-\infty}^{\infty}\int_{-\infty}^{\infty} g(x,t)\delta(y - px - \tau))dxdy.$$

Linearity

Radon transform is linear [27]. It means that the Radon transform of sum of function is equal to the sum of Radon transform of individual function. Let $h(x,t)$ be the sum of the function for which one want to evaluate the Radon transform; i.e. :

$$h(x,y) = \sum_i w_i g_i(x,t). \tag{2.15}$$

Taking the Radon transform of the previous equation:

$$\begin{aligned}\hat{h}(p,\tau) &= \sum_i w_i \int_{-\infty}^{\infty}\int_{-\infty}^{\infty} g_i(x,t)\delta(y - px - \tau))dxdt \\ &= \sum_i w_i \hat{g}_i(p,\tau)\end{aligned} \tag{2.16}$$

An example illustrating the linearity of the Radon transform is shown in the Figure 2.6. Figure 2.6 shows the individual Radon transform of $g_1(x,t)$ and $g_2(x,t)$. On the other hand, the Figure 2.6c is the Radon transform of the sum of $g_1(x,t)$ and $g_2(x,t)$. Both Radon transform are same so the linearity property holds for the Radon transform.

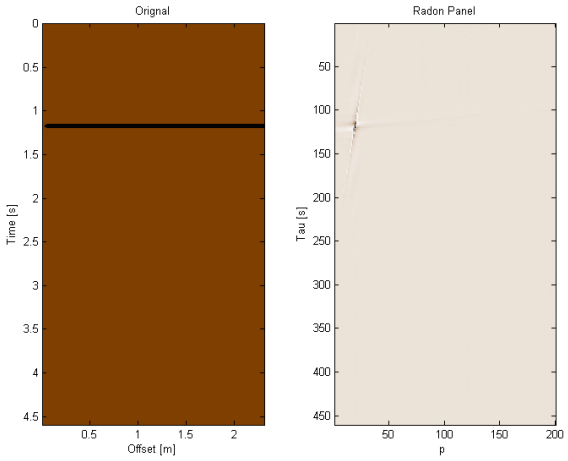

(a)

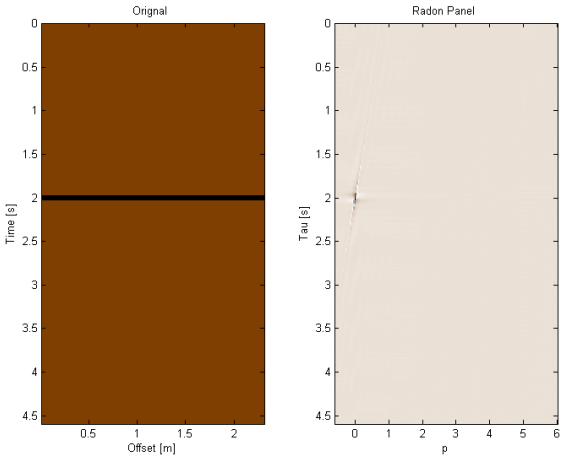

(b)

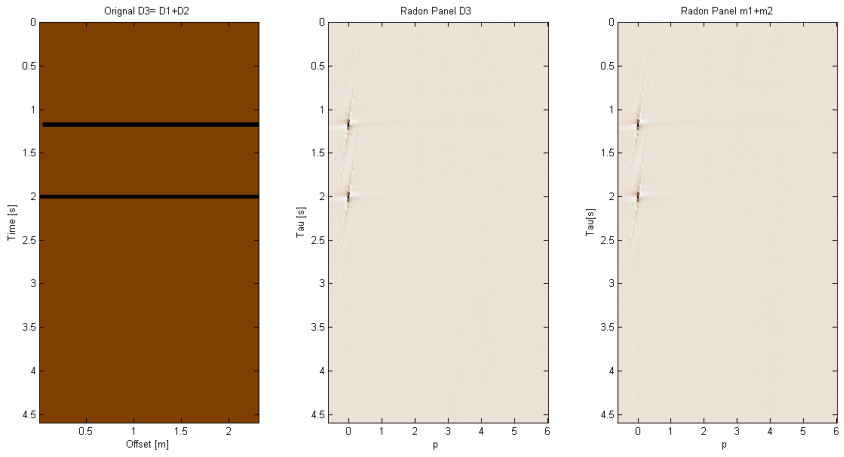

(c)

Figure 2.6: Linearity Property of Radon Transform: Two separate functions $g_1(x,t)$ and $g_2(x,t)$ along with their radon transform are shown in (a) and (b). In (c) Radon transform for $g_3(x,t) = g_1(x,t) + g_2(x,t)$ is plotted

Shift

Also the Radon transform holds the shifting property [27]. The slope of the line cannot be altered by shifting . So in case of shifting a function, the only parameter that is changed in the Radon domain is the offset parameter.

$$h(x,t) = g(x - x^*, t - t^*)$$

$$\begin{aligned} \hat{h}(p,\tau) &= \int_{-\infty}^{\infty} g_i(x - x^*, px + \tau - t^*)dx \\ &= \int_{-\infty}^{\infty} g_i(\tilde{x}, p(\tilde{x} + x^*) + \tau - t^*)d\tilde{x} \\ &= \hat{g}(p, \tau - t^* + px^*) \end{aligned} \tag{2.17}$$

Figure 2.7 shows an example of the data in (a) before shifting and its Radon transform as after causing the line to be shifted by 1 seconds (along with its transform).

Scaling

A compression in the t direction results in a compression in the time intercept parameter of the Radon domain. Similarly scaling of the slope will result scaling in the Radon domain [27].

$$h(x,t) = g(\frac{x}{a}, \frac{t}{b})$$

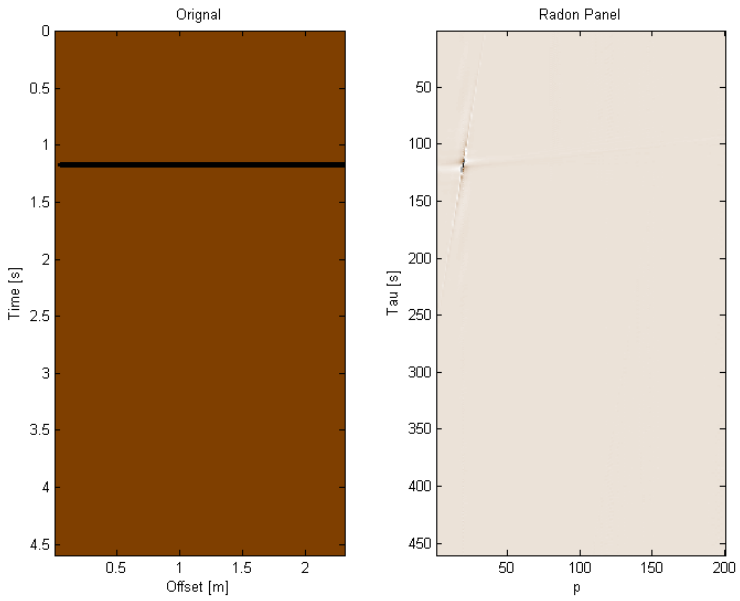

(a)

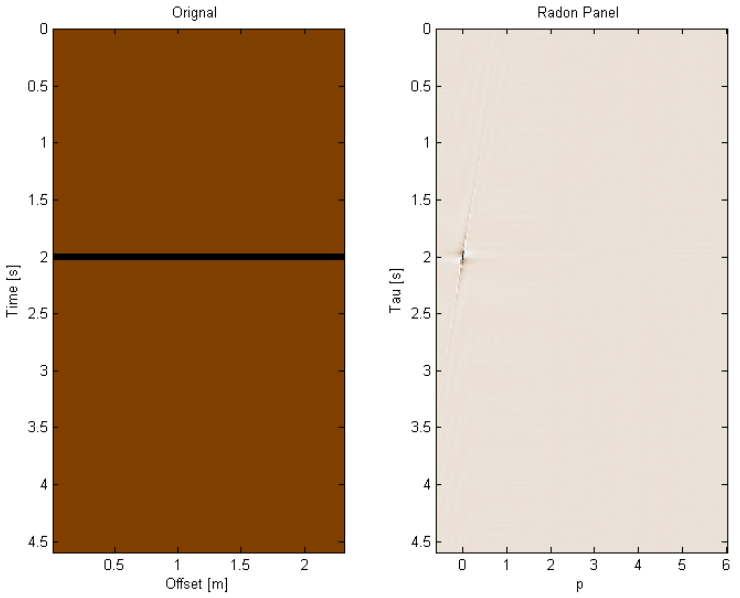

(b)

Figure 2.7: Shifting Property of Radon Transform: (b) is the shifted version of (a)

$$\begin{aligned}\hat{h}(p,\tau) &= \int_{-\infty}^{\infty} g(\frac{x}{a}, \frac{px+\tau}{b})dx \\ &= a\int_{-\infty}^{\infty} g(\tilde{x}, \frac{pa\tilde{x}+\tau}{b})dx \\ &= a\hat{g}(\frac{pa}{b}, \frac{\tau}{b})\end{aligned} \tag{2.18}$$

Figure 2.8 shows an example of the data in (a) before scaling and its Radon transform. Data after scaling is shown in (b) and (c).

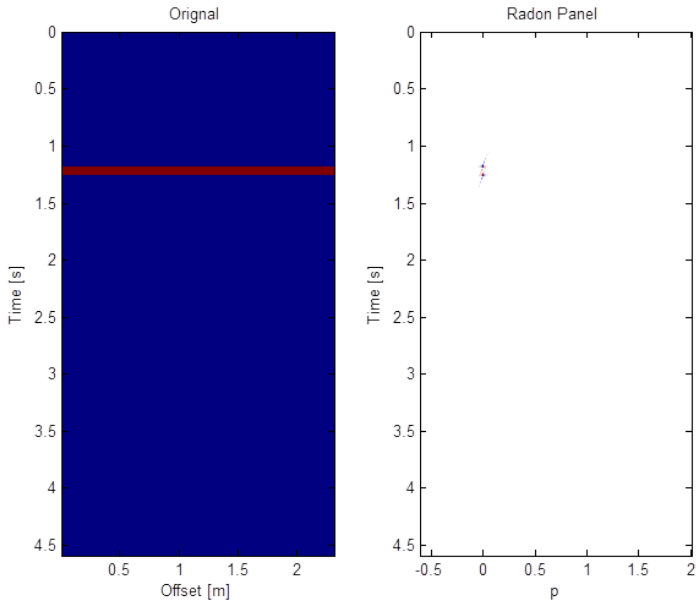

(a)

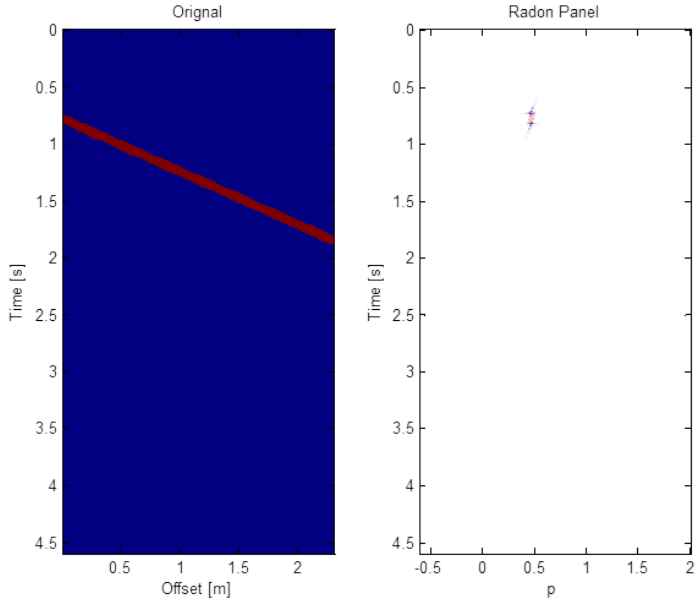

(b)

Figure 2.8: Scaling Property of Radon transform: Unscaled data is presented in (a). The scaled version of (a) are shown in (b)and (c)

2.3.4 Inversion of the Radon transform

Inverse Radon transform is used for the reconstruction of the actual data. The inverse transform can be obtained by several available techniques but the most common inversion techniques are the Fourier Slice Theorem and Filtered Back Projection.

One of the techniques used for the inverse Radon transform is the use of Fourier Slice theorem. The Fourier Slice Theorem shows that the function $g(x,t)$ can be reconstructed by taking the 1-D Fourier transform of the Radon transform which will result in the 2-D Fourier spectrum of $g(x,t)$ [84].

Another technique used for the inverse Radon transform is the filtered back projection. Filtered back algorithm can be divided into two phases, namely, the projection and the filtration.

The projection phase is similar to the forward Radon transform. The only difference is that now the line integrals are projected back onto the plane. As clear from the Figure 2.10 one can see the shapes in the reconstructed image but the resolution is very low and the image is blurred. To reduce the blurriness of the reconstructed image, a high pass filter is applied in the frequency domain. So the complete procedure is to take the 1-D Discrete Fourier Transform(DFT) of the sinogram data for each angle,then multiply the obtained result with the high pass filter, and finally use the inverse DFT to get the original data back from the Radon domain. The simplest form of high pass filter is a ramp. Applying the ramp filter significantly improves the quality of the reconstructed image.This Filtered Back

projection formula for computing the inverse Radon transform implies that the parameter domain is filtered with the absolute frequency in the t-direction for all values of x, on the other hand back projection part integrates up along a line [85].

$$g(x,t) = \int_{-\infty}^{\infty} \bar{\hat{g}}(p, t - px)dp \tag{2.19}$$

Equation (2.19) shows the result of the filtered back projection. Figure 2.9b shows the Radon transform of the -see Fig. 2.9a. Filtered back projection is used to

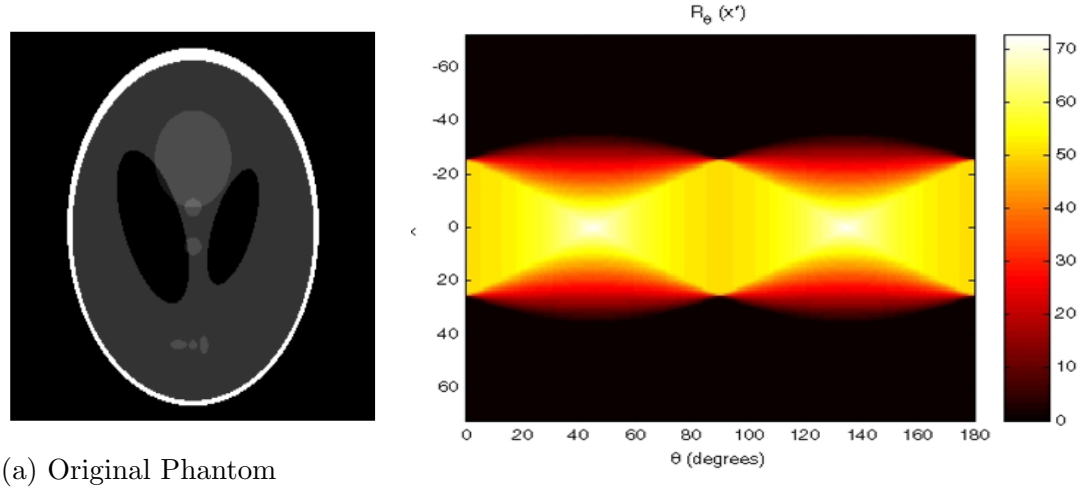

(a) Original Phantom Image

(b) Radon of Phantom

Figure 2.9: Radon Transform

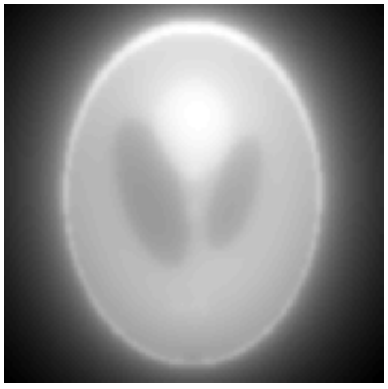

Figure 2.10: Unfiltered Inverse Radon transform of 2.9a

get the original image back. Figure 2.10 shows the unfiltered back projection result. The obtained image is blurred. The Figure 2.11 shows the result after the

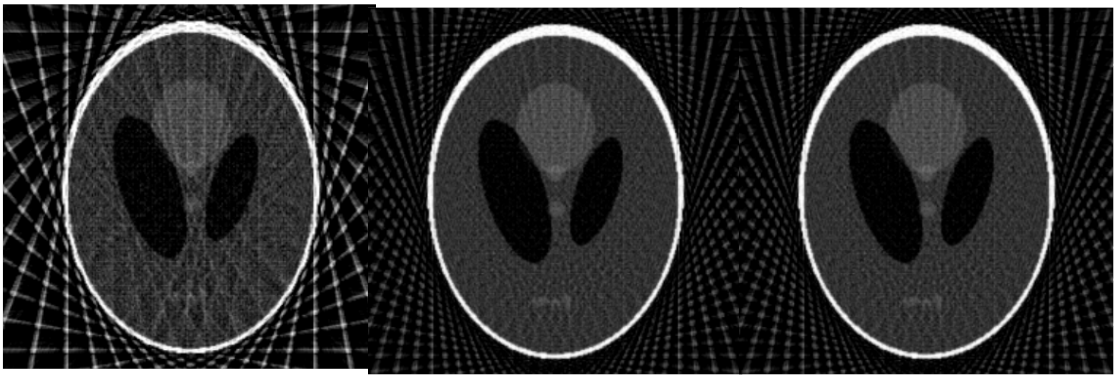

(a) 18 Projections (b) 36 Projections (c) 90 Projections

Figure 2.11: Filtered Inverse Radon transform

filtration and with no of projections 18, 36 ,90 respectively.

2.3.5 Radon transform and Seismic Data Processing

For seismic data processing, different approaches have been proposed and applied including the industry standard Radon transformation, which has attracted the attention of seismic data processing engineers and scientists during the last two decades. For the case of the seismic data, the Radon transform transforms the data from the time-space domain (t, x) to the linear Radon domain $(\tau - p)$ or parabolic Radon domain $(\tau - q)$, where $p = 1/v$ and $q = 1/v^2$, where v is the velocity of the propagation wave , p is called the slowness and q is the curvature of the curve. The transformed data is processed in the transformed domain. After the processing the data is finally transformed back to the $t - x$ domain.

There are three types of Radon transform that are used in the seismic data

processing: linear Radon transformation (slant-stack), the parabolic Radon transform, and the hyperbolic Radon transform. Among these transforms, parabolic Radon transform is mostly used due to its effectiveness (better than the linear Radon Transform) and low computational cost [22]. In the next two chapters linear and parabolic Radon transform will be introduced for the compressive sensing.

Mathematical Model

Let $g(x,t)$ represent the seismic data in offset 'x' and time 't'. Generalized Radon Transform [83] pair for this seismic data $g(x,t)$ is given by eq 2.20 2.21

$$u(q,\tau) = \int_{-\infty}^{\infty} g(x, t = \tau + q\phi(x))dx \tag{2.20}$$

$$\hat{g}(x,t) = \int_{-\infty}^{\infty} u(q, \tau = t - q\phi(x))dq \tag{2.21}$$

where q and τ are representing some parameter of the curve. Similarly, $\phi(x)$ is the function of the offset parameter 'x' and depend on the path of integration. In discrete form these can be represented as

$$u(q,\tau) = \sum_{x} g(x, t = \tau + q\phi(x)) \tag{2.22}$$

$$\hat{g}(x,t) = \sum_{q} u(q, \tau = t - q\phi(x)) \tag{2.23}$$

CHAPTER 3

COMPRESSED LINEAR RADON TRANSFORM AND ITS APPLICATIONS

Radon transform is robust in nature and has attracted the attention of seismic data processing scientists and engineers during the last two decades. It is being used for quite some time in different applications which includes seismic deconvolution [20], multiple removal [23, 24, 26], first arrival picking or enhancement [21]. Radon transform is easier to compute, a well established mathematical theory, and is a part of many seismic data processing work-flows.

There are three types of Radon transform that are used in the seismic data processing: linear Radon transform (slant-stack), the parabolic Radon transform, and the hyperbolic Radon transform. The linear Radon transform, transforms the data from the time-space domain (t, x) to the linear Radon domain $(\tau - p)$,

where $p = 1/v$.

In the first section of this chapter a review of linear Radon transform is presented. Besides basic theory of linear Radon transform, Radon transform of point source, linear and non-linear events is presented. In the second section of the chapter, compressive sensing using linear Radon transform as sparsifying transform is discussed. The proposed setup is used to find the missing linear events of the seismic data. Using the proposed setup a new technique for first arrival picking is presented. Furthermore, deconvolution and seismic events classifications are also discussed. All these applications are presented with detailed simulation results and comparison.

3.1 Linear Radon Transform

3.1.1 Introduction

The linear Radon transform integrates the data along planar surfaces. It transforms linear events to a single points in the transformed $\tau - p$ domain. Linear seismic events are periodic in linear Radon domain (Slant stack) and we can use the deconvolution in Radon domain to attenuate these multiples. Taner(1980) suggested that the multiples are periodic in time for all p traces in the $\tau - p$ domain. Forward linear Radon transform was developed by Beylkin (1987) he also applied the filter in the inverse Radon transform domain [86]. Kostov (1990) used Toeplitiz structure for least squares solution of the Radon transform [28]. Zhou

and Greenhalgh (1994) showed that applying the rho filter in the forward Radon transform rather than the inverse transform could give better resolution [87].

Linear Radon transform is obtained by replacing $\phi(x) = x$ and $q = p$ in generalized Radon transform equation (2.20). The linear Radon transform equations in continuous domain are:

$$u(p,\tau) = \int_{-\infty}^{\infty} g(x, t = \tau + px)dx \tag{3.1}$$

$$\hat{g}(x,t) = \int_{-\infty}^{\infty} u(p, \tau = t - px)dp \tag{3.2}$$

Similarly, the discrete form of these equations is obtained from (2.22).

$$u(p,\tau) = \sum_{x} g(x, t = \tau + px) \tag{3.3}$$

$$\hat{g}(x,t) = \sum_{p} u(p, \tau = t - px) \tag{3.4}$$

here x is the offset, $g(x,t)$ is representing the seismic data$p = \frac{\sin\theta}{v} = \frac{\Delta t}{\Delta x}$ and $u(p,\tau)$ linear Radon domain.

In frequency domain the linear Radon transform can be represented as

$$U(p,\omega) = \int_{-\infty}^{\infty} G(x,\omega)e^{i\omega px}dx \tag{3.5}$$

$$\hat{G}(x,\omega) = \int_{-\infty}^{\infty} U(p,\omega)e^{-i\omega px}dp \tag{3.6}$$

3.1.2 Types of Linear Radon Transform

The linear Radon Transform, can be sub-divided into two types.

- Forward Slant Stack
- Inverse Slant Stack

Forward Slant Stack

The first type of Radon transform is known as Forward Slant Stack. It can be obtained by substituting frequency domain equation of the inverse Radon transform (3.6) into forward Radon transform equation(3.5).

$$\hat{G}(x,\omega) = \int_{-\infty}^{\infty}\int_{-\infty}^{\infty} G(\acute{x},\omega)e^{i\omega p\acute{x}}d\acute{x}e^{-i\omega px}dp$$

The above equations can be simplified as shown below:

$$\begin{aligned}\hat{G}(x,\omega) &= \int_{-\infty}^{\infty}\int_{-\infty}^{\infty} G(\acute{x},\omega)e^{i\omega p(\acute{x}-x)}d\acute{x}dp \\ &= \int_{-\infty}^{\infty} d\acute{x}G(\acute{x},\omega)\int_{-\infty}^{\infty} e^{i\omega p(\acute{x}-x)}dp\end{aligned}$$

Let rho ρ be a filter given by 3.7.

$$\rho(x,\omega) = \int_{-\infty}^{\infty} e^{-\omega px}dp = \frac{2\pi}{|\omega|}\delta(x) \tag{3.7}$$

Replacing the ρ filter in the previous equation, a convolution equation is obtained [3.8]. Further simplifying convolution model eq 3.10 is obtained.

$$\begin{aligned}\hat{G}(x,\omega) &= \int_{-\infty}^{\infty} G(\acute{x},\omega)\rho(x-\acute{x},\omega)d\acute{x} \\ &= G(x,\omega) * \rho(x,\omega)\end{aligned} \tag{3.8}$$

$$\hat{G}(x,\omega) = F(x,\omega) * \rho(x,\omega) = \frac{2\pi}{|\omega|} D(x,\omega) \tag{3.9}$$

$$G(x,\omega) = \frac{|\omega|}{2\pi}\hat{G}(x,\omega) \tag{3.10}$$

The final Radon transform equations for the Forward Slant stack Radon transform, as follow:

$$U(p,\omega) = \int_{-\infty}^{\infty} G(x,\omega)e^{i\omega px}dx \tag{3.11}$$

$$G(x,\omega) = \frac{|\omega|}{2\pi}\int_{-\infty}^{\infty} U(p,\omega)e^{-i\omega px}dp \tag{3.12}$$

But in practice, one don't have infinite p. For the finite p case, rho filter becomes

$$\rho(x,\omega) = \int_{P_{min}}^{P_{max}} e^{-\omega px}dp = \begin{cases} \frac{1}{i\omega x}(e^{-i\omega P_{min}x} - e^{i\omega P_{max}x}) & \omega x \neq 0 \\ P_{max} - P_{min} & \omega x = 0 \end{cases} \tag{3.13}$$

$$\rho(x,\omega) = \begin{cases} 2P_{max}\frac{\sin(\omega P_{max}x)}{\omega P_{max}x} & \omega x \neq 0 \\ 2P_{max} & \omega x = 0 \end{cases} \tag{3.14}$$

Inverse Slant stack

Inverse Slant Stack Operator was introduced by Zhou and Greenhalgh (1994). In the case of inverse slant stack transform first the inverse τ-p transform is applied then for the proper inversion of the slant-stack forward transform is performed. Inverse slant stack using the same procedure as for Forward slant stack , is given by

$$U(p,\omega) = \frac{|\omega|}{2\pi} \int_{-\infty}^{\infty} G(x,\omega) e^{i\omega p x} dx \tag{3.15}$$

$$G(x,\omega) = \int_{-\infty}^{\infty} U(p,\omega) e^{-i\omega p x} dp \tag{3.16}$$

Comparison

There is not much difference between the forward Slant stack Radon transform and the inverse Slant stack Radon transform. Deconvolution procedure is required in both cases. But direction of the deconvolution is different in both the cases. In the case of Forward slant stack transform, the deconvolution is required to recover the data from the tau-p space and it is performed on the inverse transform that is in x-direction. On the other hand, in the inverse slant stack operator, The deconvolution process is required to estimate the tau-p space and is performed on the forward transform that is in p-direction. So to increase the resolution of tau p domain inverse slant stack transform should be used.

3.2 Linear Radon Transform of Different Curves

3.2.1 Point Source

A point source is modeled as a product of two delta functions. Initially the point source is placed in the origin of the coordinate system

$$g(x,t) = \delta(x)\delta(t) \tag{3.17}$$

$$u(p,\tau) = \int_{-\infty}^{\infty} \delta(x)\delta(px+\tau)dx = \delta(\tau) \tag{3.18}$$

By using the shifting property , above equation cans be rewritten as

$$g(x,t) = \delta(x-\acute{x})\delta(t-\acute{t}) \tag{3.19}$$

$$u(p,\tau) = \delta(\tau-\acute{t}+p\acute{x}) \tag{3.20}$$

$$g(x,t) = \int_{-\infty}^{\infty}\int_{-\infty}^{\infty} d(\acute{x},\acute{t})\delta(x-\acute{x})\delta(t-\acute{t})d\acute{x}d\acute{t} \tag{3.21}$$

By taking the Radon transform of the shifted point source, we get

$$\begin{aligned} u(p,\tau) &= \int_{-\infty}^{\infty}\int_{-\infty}^{\infty}\int_{-\infty}^{\infty} d(\acute{x},\acute{t})\delta(x-\acute{x})\delta(\tau-\acute{t}+px)d\acute{x}d\acute{t}dx \\ &= \int_{-\infty}^{\infty}\int_{-\infty}^{\infty} d(\acute{x},\acute{t})\delta(\acute{t}-\tau-p\acute{x})d\acute{x}d\acute{t} \end{aligned} \tag{3.22}$$

This result shows that the point in t-x domain will transform into an infinite line in the linear Radon domain (-see Fig3.1).

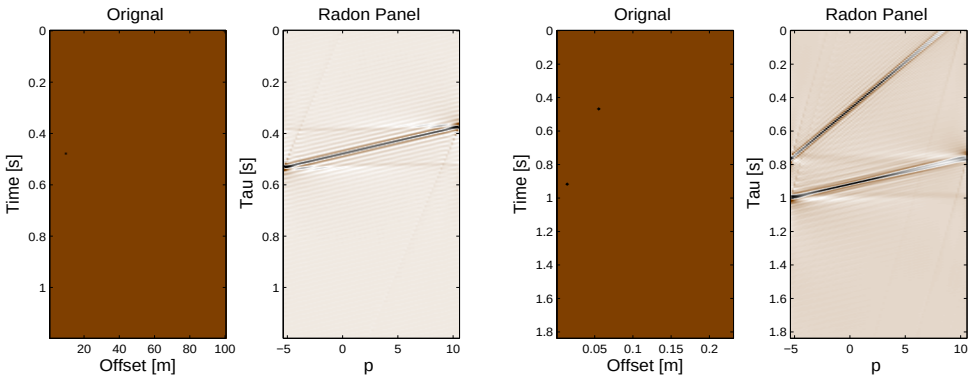

(a) (b)

Figure 3.1: Linear Radon Transform of Point Source

3.2.2 Line

A line in terms of the δ can be represented by the following equation

$$g(x,t) = \delta(t - \acute{p}x - \acute{\tau}) \tag{3.23}$$

The linear Radon transform of the line is given by

$$\begin{aligned} u(p,\tau) &= \int_{-\infty}^{\infty}\int_{-\infty}^{\infty} \delta(t - \acute{p}x - \acute{\tau})\delta(t - px - \tau)dxdy \\ &= \int_{-\infty}^{\infty} \delta((p - \acute{p})x + \tau - \acute{\tau})dx \\ &= \begin{cases} \frac{1}{|p-\acute{p}|} & for\ p \neq \acute{p} \\ 0 & for\ p = \acute{p}\ and\ \tau \neq \acute{\tau} \end{cases} \end{aligned} \tag{3.24}$$

the results shows that the Radon transform of a straight line will produce a single point in the $\tau - p$ domain. These results are confirmed by the following matlab simulation (Figure 3.2)

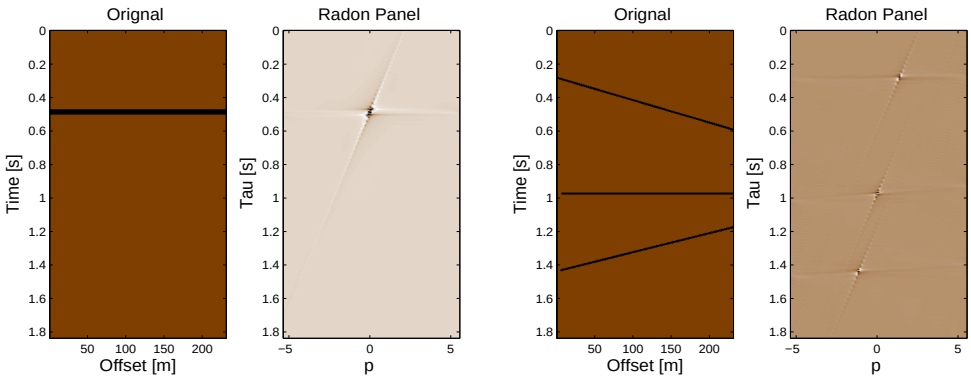

(a) (b)

Figure 3.2: Linear Radon Transform of Line

3.2.3 Curve

For a given curve (3.25), the curvature can be found by using the following equations (3.26)

$$\tau = t - \phi(x) \tag{3.25}$$

$$\psi(p, \tau; x) = t(x) - \phi(x) - \tau = 0 \tag{3.26}$$

$$\frac{\partial \psi(p, \tau; x)}{\partial x} = \frac{dt}{dx} - \frac{(d\phi(x)}{dx} = 0 \tag{3.27}$$

Travel time curves are mostly hyperbolic or parabolic in nature. Let the travel time curve be represented by

$$t^2(x) = a + bx^2 \tag{3.28}$$

Taking the derivative of the above equation and using the equations (3.26),

$$\frac{dt}{dx} = p = \frac{bx}{t} \tag{3.29}$$

$$\psi(p,\tau;x) = \sqrt{a+bx^2} - px - \tau = 0 \tag{3.30}$$

$$\frac{\partial\psi(p,\tau;x)}{\partial x} = \frac{bx}{t} - p = 0 \tag{3.31}$$

Now our aim is to eliminate the x and τ. To achieve this goal square the τ and substituting t form the (3.28)

$$\tau^2 = t^2 - 2ptx + p^2x^2 \tag{3.32}$$

$$\tau^2 = a + bx^2 + p^2x^2 \tag{3.33}$$

in the similar way x can be eliminated by

$$p = \frac{dt}{dx} = \frac{bx}{\sqrt{a+bx^2}} \tag{3.34}$$

$$bx^2 = p^2(a+bx) \tag{3.35}$$

$$-p^2\frac{a}{b} = x^2(p^2-b) \tag{3.36}$$

Substituting this in (3.33) will give us

$$\frac{\tau^2}{a} + \frac{p^2}{b} = 1 \tag{3.37}$$

The above equation represents an eclipse. So an hyperbolic event in $t-x$ domain will transform in the eclipse int the $\tau - p$ domain. The results are shown in the figure 3.3

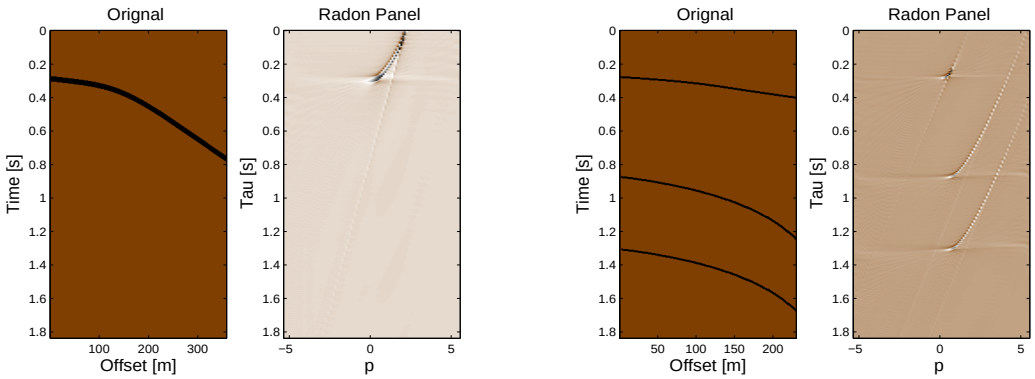

Figure 3.3: Linear Radon Transform of Hyperbolic Curve

Seismic Example

Here is an example for the case of synthetic seismic data without compressive sensing is presented. Figure 3.4 shows the Radon transform of the synthetic data. As it is evident from the results that the $\tau - p$ domain is not sparse in this case so we will have to look for other means (Parabolic RT) to obtain a sparse representation(see Chapter 4).

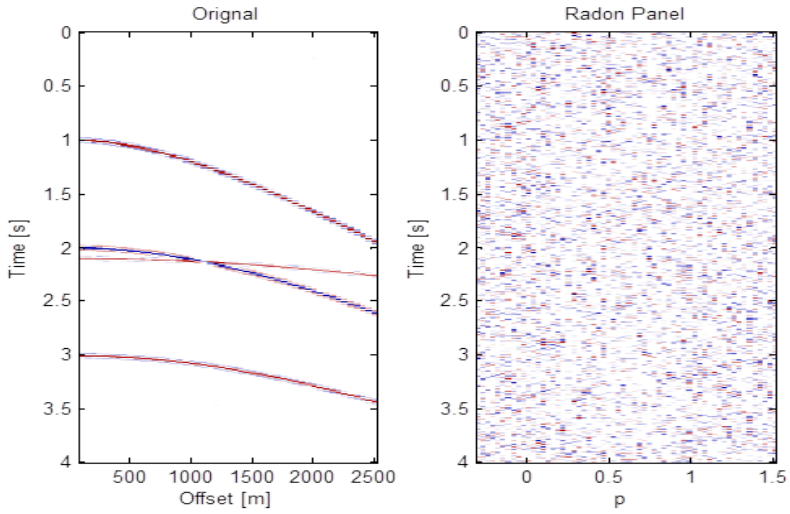

Figure 3.4: Linear Radon Transform of Synthetic Data

3.3 Compressive Sensing with Linear Radon Transform

In this section, use of linear Radon transform as a sparsifying transform for compressive sensing, is presented.

Let $g(n)$ be the sampled, acquired seismic data, vector with size N. This signal can be expanded in terms of orthonormal basis matrix $\boldsymbol{\psi}$ as follows:

$$g(n) = \sum_{i=1}^{N} x_i \psi_i(t), \tag{3.38}$$

where x_i are the coefficients sequence of $g(t)$. To make the formulation easier the signal $g(n)$ in terms of matrix as follows:

$$\boldsymbol{g} = \boldsymbol{\psi}\boldsymbol{x}. \tag{3.39}$$

Here, $\boldsymbol{\psi}$ has dimension $N \times N$. Also assume that the number of non zero entries in $\boldsymbol{g}$ are K. In other words, $\boldsymbol{g}$ is a K sparse vector with length N, when represented in basis $\boldsymbol{\psi}$.

In the case of linear Radon transform the entries of the $\boldsymbol{\psi}$ contains the following:

$$\psi_n = e^{i\omega_n \boldsymbol{p}\boldsymbol{x}^{\boldsymbol{T}}}, \tag{3.40}$$

where $\boldsymbol{p}$ and $\boldsymbol{x}$ are vectors of size N. In matrix form, for particular value of ω, $\boldsymbol{\psi}$

can be expanded as

$$\boldsymbol{\psi} = \begin{bmatrix} e^{i\omega p_1 x_1} & e^{i\omega p_2 x_1} & e^{i\omega p_3 x_1} & \dots & e^{i\omega p_n x_1} \\ e^{i\omega p_1 x_2} & e^{i\omega p_2 x_2} & e^{i\omega p_3 x_2} & \dots & e^{i\omega p_n x_2} \\ \vdots & \vdots & \vdots & \vdots & \vdots \\ e^{i\omega p_1 x_n} & e^{i\omega p_2 x_n} & e^{i\omega p_3 x_n} & \dots & e^{i\omega p_n x_n} \end{bmatrix} \tag{3.41}$$

As $\boldsymbol{g}$ is K sparse vector, compressive sensing can be used to acquire the data with much less sample than suggested by the Shannon Nyquist theorem. So instead of sampling all the elements of $\boldsymbol{g}$, the signal can be recovered by less number of samples. Let $\boldsymbol{\phi}$ be another basis matrix, known as sensing matrix, with size $M \times N$, where $M \ll N$. The sampled signal $\boldsymbol{g}$ can be represented in terms of new basis $\boldsymbol{\phi}$, as follows:

$$\boldsymbol{y} = \boldsymbol{\phi g} \tag{3.42}$$

$$\boldsymbol{y} = \boldsymbol{\phi \psi x} \tag{3.43}$$

Let $\boldsymbol{A} = \boldsymbol{\phi \psi}$,measurement matrix, with dimension $M \times N$. The (3.43) simplifies to

$$\boldsymbol{y} = \boldsymbol{Ax} \tag{3.44}$$

To recover the original signal we have to find the coefficient vector $\hat{\boldsymbol{x}}$ by solving the following relation

$$\boldsymbol{A}\hat{\boldsymbol{x}} = \boldsymbol{b} \tag{3.45}$$

where

$$\boldsymbol{b} = \boldsymbol{\phi g} \tag{3.46}$$

Here $\boldsymbol{A}$, is a rectangular matrix, with less rows than the columns. So $\boldsymbol{A}$ is an under-determined system of linear, number of unknowns are greater than the number of equations. Restricted isometric property(RIP) can be utilized for the perfect reconstruction of the under-sampled data [63]. The RIP is a sufficient a sufficient condition for many sparsifying recovery theorem. Besides RIP the sensing matrix and representation matrix should have incoherence [41].

If the RIP and incoherence is satisfied then one way to solve compressive sensing problem is by using the l_1-norm for the reconstruction, the following model is obtained:

$$\min \|\boldsymbol{x}\|_1 \text{subject to } \boldsymbol{Ax} = \boldsymbol{b} \tag{3.47}$$

Once the coefficients are estimated by l_1-norm then the original signal can be recovered by using the following relation

$$g = \boldsymbol{\psi}\hat{x} \tag{3.48}$$

Because most of the practical problems may involve a large measurement matrix, finding an appropriate measurement matrix $\boldsymbol{\phi}$ is significant challenge. Fortunately, there are number of techniques have been suggested for easier selection of the measurement matrix. One of the suggested approaches is to randomly choose N unit vectors in K-dimensional space. Or, randomly choose K rows from an

$N \times N$ orthogonal matrix and normalize the columns for the measurement matrix [41]. Another frequently seen approach is to form a matrix with randomly chosen Gaussian entries [88]. All these techniques work for Compressive sensing as long the following relation is satisfied

$$M \geq cK \log(N/K), \tag{3.49}$$

3.4 Applications of Compressive Sensing and Linear Radon Transform

In the remaining part of this chapter, different application of seismic data processing using compressive sensing and linear Radon transform are discussed. The applications that are discussed

- Interpolation of linear missing seismic traces
- Classification of linear seismic events
- Deconvolution of linear seismic events
- First arrival picking of the seismic refraction data

3.5 Interpolation of Missing Linear Seismic Events

Interpolation/ reconstruction of missing seismic traces is one of the most key pre-processing step, in which the resolution of the data is increased. During the last few years the demand for denser seismic traces has increased a lot. In most cases, and due to the certain limitations of hardware, budgets, computing power it is not possible to acquire a lot of seismic traces(samples). Sometimes even due to the topological structures of the earth surface or the conditions, it is not possible to place seismic sensors(geophones), and, hence, there are some missing traces in the acquired data. Thus, reducing the amount of acquired data as well as effective reconstruction of complete seismic data from acquired incomplete seismic data are very important issues.

Most famous methods are based on transformation of seismic data into sparse domain by using transforms like wavelet, Radon, curvelet as discussed in [89–91]. Similarly there are some techniques based on filters as discussed in [92]. Low rank based interpolation is presented in [93]. Energy of the primary reflections can also be used for the interpolation as discussed in [94]. Same energy concept is extended in [95]. Interferometric interpolation of missing seismic data is discussed in [96]. Compressive sensing based interpolation using the curvelet transform are presented in [97, 98]. Recently a new technique based on the weighted L_1-norm minimization is proposed in [99]

By using the proposed model (-see sec 3.3), here a new technique for the in-

terpolation of missing seismic traces, based on compressive sensing where Radon transform being the sparsifying domain, is presented. Once the data is acquired in compressed fashion via compressive sensing, a certain feature of the compressed signal in Radon domain is used for the interpolation. Finally, the data is converted back from the Radon domain to time space(t-x) domain, which contains the interpolated data.

Algorithm

Given a seismic record, the proposed compressive sensing with $\tau - p$ method for interpolation of missing seismic traces is stated as follows:

1. Use the compressive sensing to acquire the seismic data in the compressed fashion as described previously in this section.

2. Use the following facts for binary thresholding:

   (a) The curves are converted to single points in the $\tau - p$ domain.

   (b) These points have higher value than the points corresponding to the noise or irrelevant curves.

3. Apply the inverse linear Radon transform to the previous step result.

Overall algorithm is presented in the Figure 3.5.

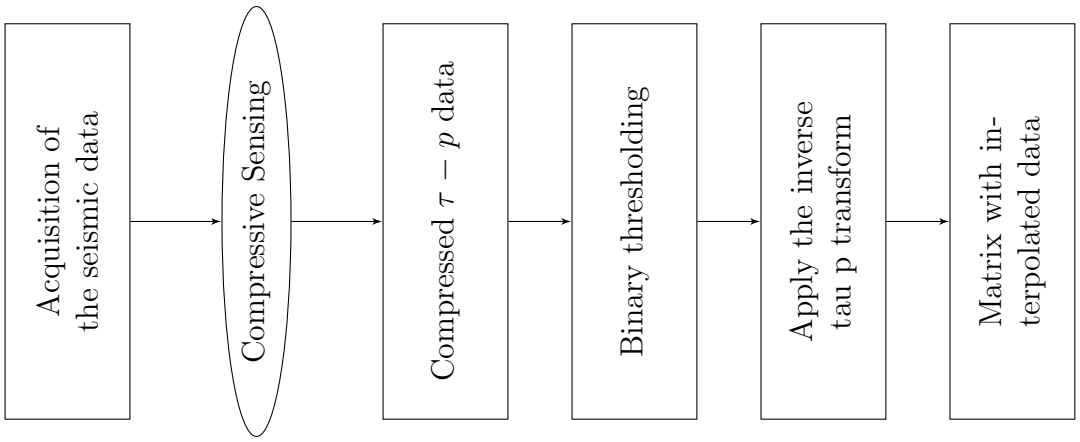

Figure 3.5: Workflow of the proposed technique for interpolation of linear events

3.5.1 Simulation Result

The parameters of the synthetic seismic shot gather are presented in [21]. The data contains ground-roll, head waves and three reflectors as shown in Figure 3.6a. The total number of traces in the data are 120(N=120) with spatial sampling interval 25m and sampling interval 4m/s. Among these 40 traces are randomly missing. Compressive sensing with linear Radon transform is used for the interpolation of missing seismic traces. Figure 3.6b shows the compressed $\tau - p$ domain with M=100. Now based on the second step of the algorithm the the result after the thresholding is presented in the Figure 3.6c. Finally the results after the application of the inverse $\tau - p$ transform are presented in Figure 3.6d. The resulted image contains the interpolated data.Besides 40 missing traces (33%), with the help of compressive sensing, an additional 17% compression is achieved.

Figure 3.7 shows the linear missing traces estimation with 50% compression (M=60). To show how well compressive sensing works, results for the 83% compression (M=20) are presented in the Figure 3.8.As expected the linear Radon

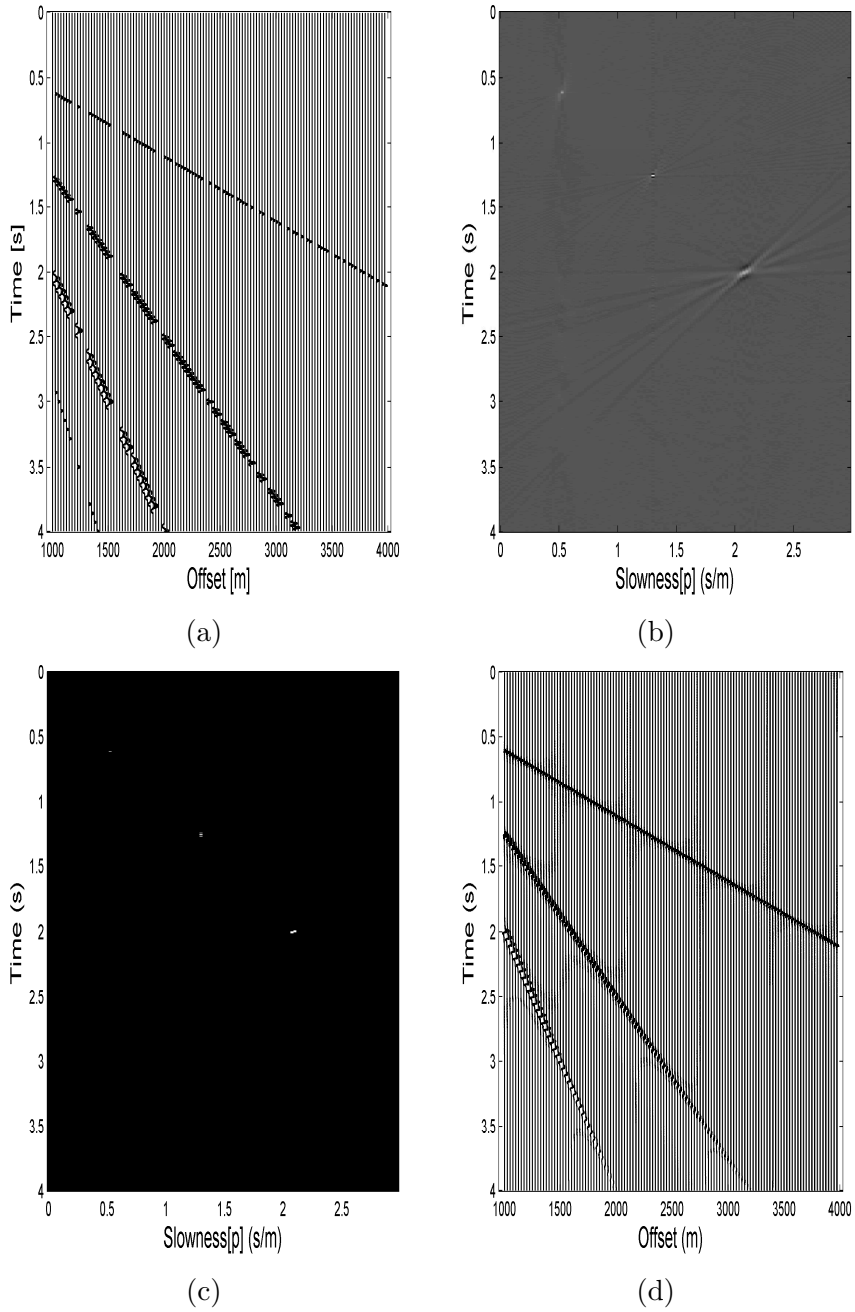

Figure 3.6: (a) The synthetic seismic reflected data. (b) The compressed $\tau - p$ transform of (a) , after the acquisition in compressed fashion with M=100 (17% compression). (c) The produced binary mask (white stands for one and black for zero) of (b). (d) The interpolated data after applying the inverse $\tau - p$ transform on (c).

transform work flawlessly for the interpolation of the linear events present in the data.

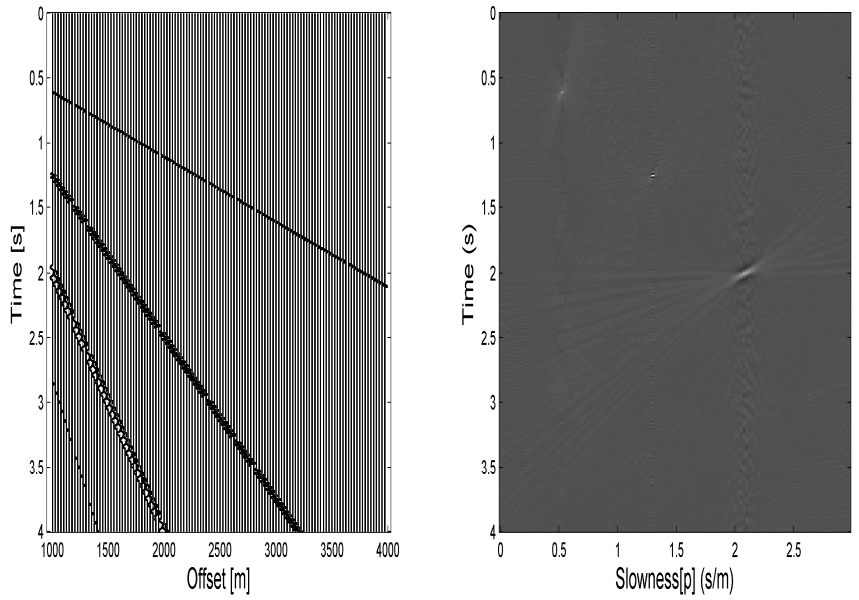

(a) (b)

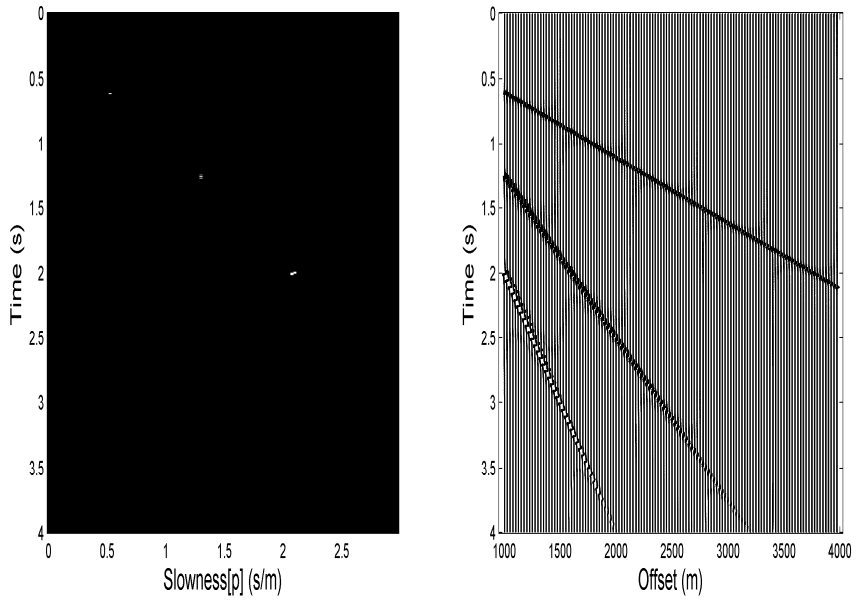

(c) (d)

Figure 3.7: (a) The synthetic seismic refracted data. (b) The compressed $\tau - p$ transform of (a) , after the acquisition in compressed fashion with M=60 (50% compression). (c) The produced binary mask (white stands for one and black for zero) of (b). (d) The interpolated data after applying the inverse $\tau - p$ transform on (c).

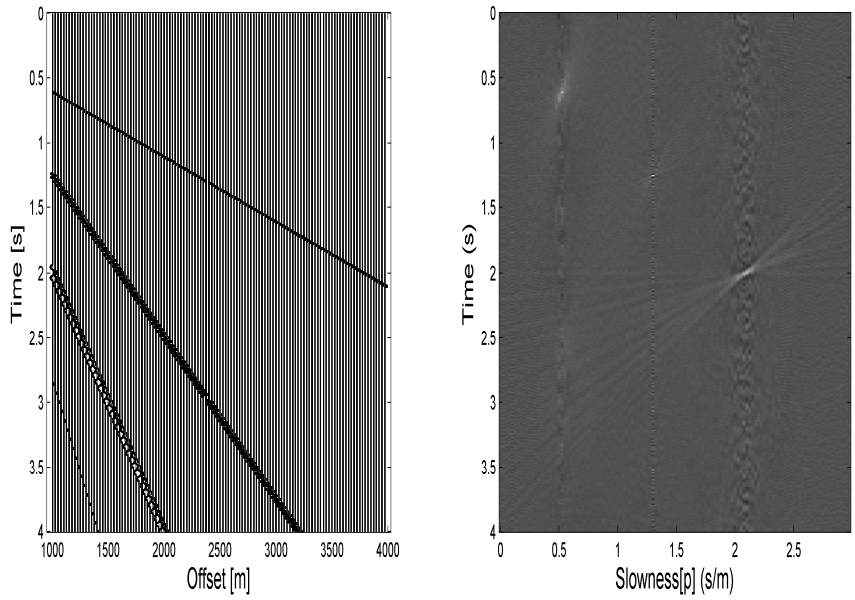

(a) (b)

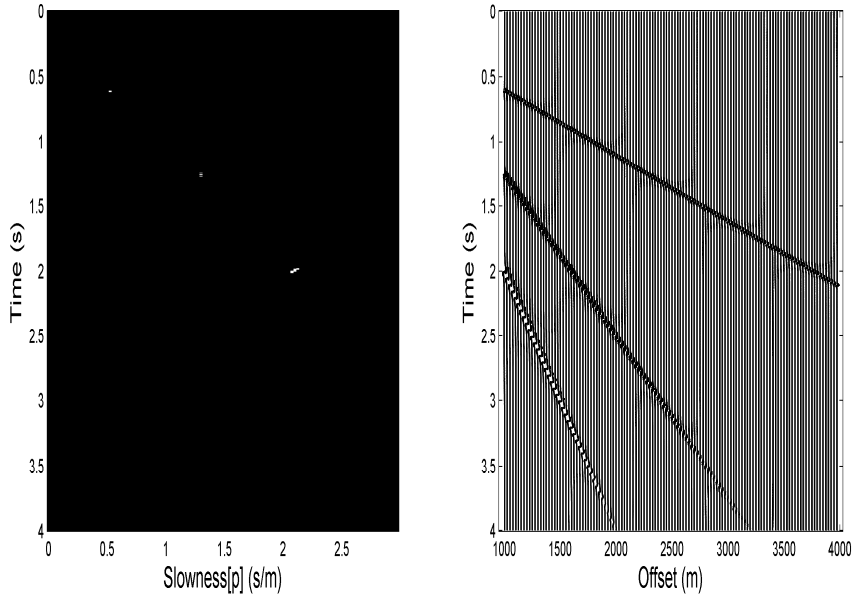

(c) (d)

Figure 3.8: (a) The synthetic seismic refracted data. (b) The compressed $\tau - p$ transform of (a) , after the acquisition in compressed fashion with M=20 (83% compression). (c) The produced binary mask (white stands for one and black for zero) of (b). (d) The interpolated data after applying the inverse $\tau - p$ transform on (c).

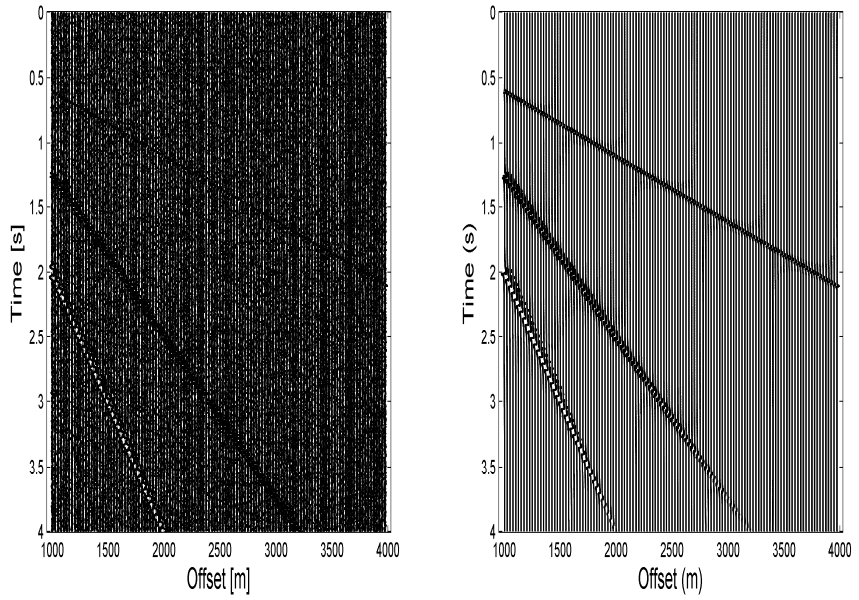

(a) (b)

Figure 3.9: (a) The synthetic seismic refracted data with 10% random Gaussian noise. (b) The interpolated data after taking the inverse $\tau - p$ transform and M=40 (67% compression).

To test the robustness of the proposed setup, data with different noise level is tested. Total number of traces and number of missing traces remains same. The results after the addition of the noise with 0.1 standard deviation and 67% compression are presented in Figure 3.9.

Similar comparison after the addition of white noise with standard deviation 0.2 and 0.4 are presented in the Figure 3.10 and Figure 3.11 respectively. With this high level of noise, the linear events are completely missing from Figure 3.11a, which makes manual interpolation it virtually impossible. However, the linear interpolated events are fairly clear in Figure 3.11b, which presents the results after the interpolation using compressive sensing and linear Radon transform.

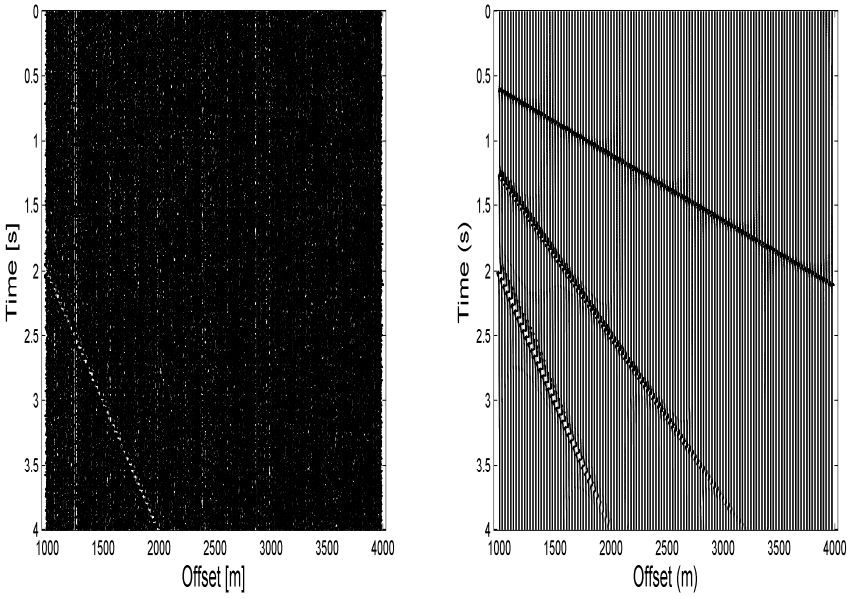

(a) (b)

Figure 3.10: (a) The synthetic seismic refracted data with 20% random Gaussian noise. (b) The interpolated data after taking the inverse $\tau - p$ transform and M=20 (83% compression).

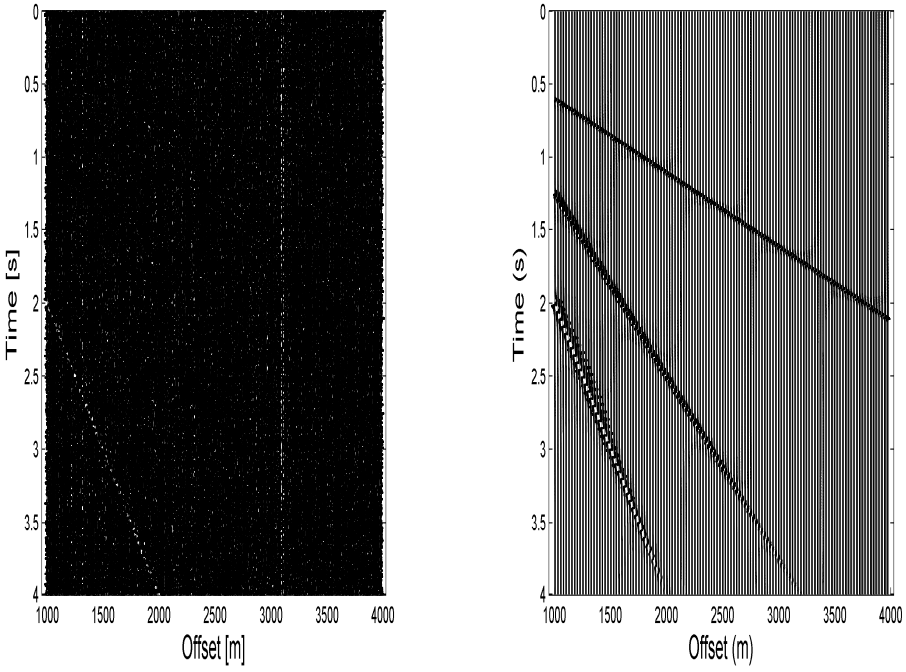

(a) (b)

Figure 3.11: (a) The synthetic seismic refracted data with 40% random Gaussian noise. (b) The interpolated data after taking the inverse $\tau - p$ transform and M=20 (83% compression).

Comparison Linear Radon vs Curvelet

In this section comparison with curvelet is presented. Hermann has used the curvelet with compressive sensing in [97,98]. For the simulation curve-lab toolbox is used [100]. For the fair comparison same machine (Intel Core i7) with same number of iterations is used. Results for same data with different noise level using curvelet is presented in Figure 3.12 - 3.15.

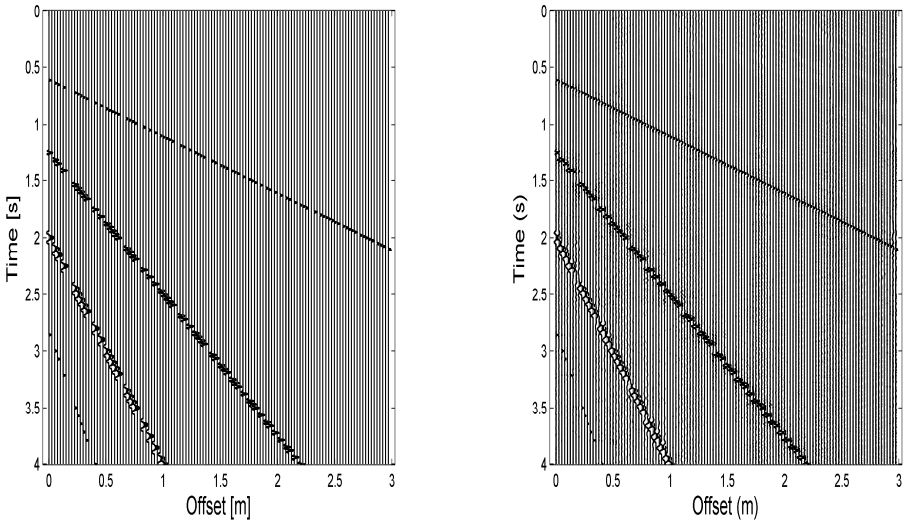

(a) (b)

Figure 3.12: Figure (a) gives the data with missing traces the interpolation of the synthetic data using curvelet transform as the sparsifying transform for the compressive sensing without noise is presented in (b).

From the simulation results for the curvelet transform, it is evident that curvelet transform is not robust as compared to the proposed Radon transform model. Linear Radon transform, interpolates the missing traces even for high noise levels and low compression levels. On the other hand, curvelet transform does not perform well when SNR is low. Besides the performance issue a major difference between the curvelet and the proposed setup is the computation time.

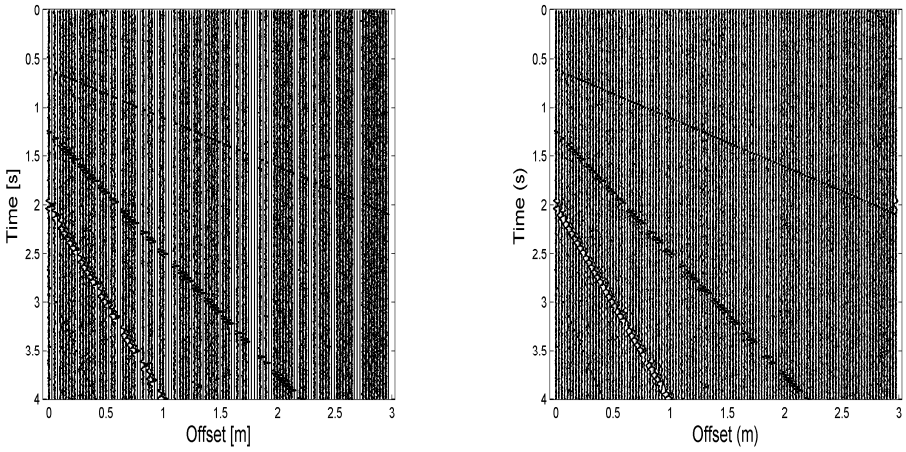

(a) (b)

Figure 3.13: Figure (a) gives the data with missing traces and 10 % noise. The interpolation of the synthetic data using curvelet transform as the sparsifying transform for the compressive sensing is presented in (b).

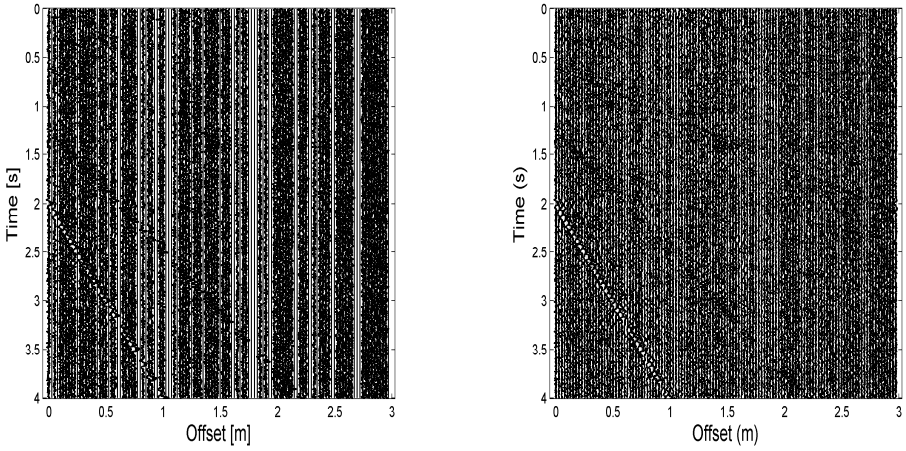

(a) (b)

Figure 3.14: Figure (a) gives the data with missing traces and 20 % noise. The interpolation of the synthetic data using curvelet transform as the sparsifying transform for the compressive sensing is presented in (b).

Table 3.1 and 3.2 shows the run time for different level of compression for proposed setup and curvelet transform. The comparison for different noise level is presented in table 3.2. From the results it is evident that proposed algorithm is about 25 times faster than the curvelet transform.

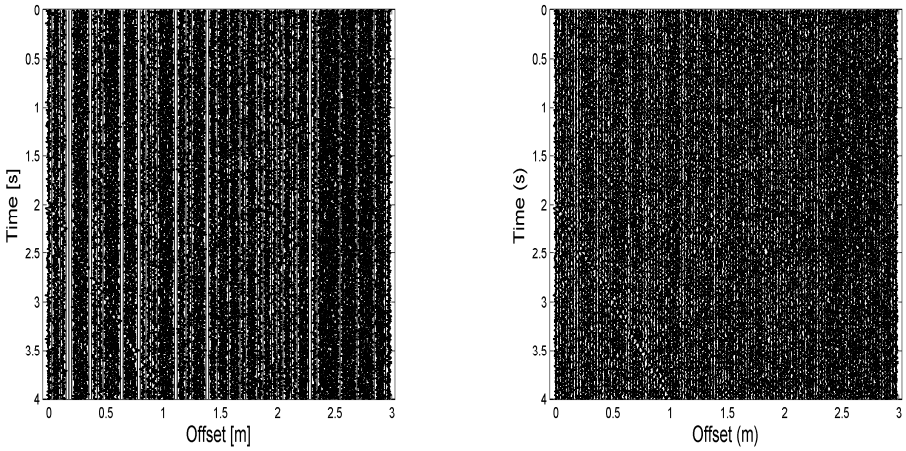

(a) (b)

Figure 3.15: Figure (a) gives the data with missing traces and 40 % noise. The interpolation of the synthetic data using curvelet transform as the sparsifying transform for the compressive sensing is presented in (b).

Transform Type	Compression	Time
Radon Transform	17%	2.58 seconds
Radon Transform	33%	2.55 seconds
Radon Transform	50%	2.60 seconds
Radon Transform	67%	2.54 seconds
Radon Transform	83%	2.57 seconds
Curvlet Transform	-	51.55 seconds

Table 3.1: Time comparison: Linear Radon transform vs Curvelet transform, Noise-less case

Noise	Time Radon	Time Curvlet
0 %	2.53 seconds	51.55 seconds
10%	2.53 seconds	53.01 seconds
20%	2.56 seconds	55.36 seconds
30%	2.59 seconds	60.54 seconds
40%	2.59 seconds	60.64 seconds

Table 3.2: Time comparison: Linear Radon transform vs Curvelet transform

3.6 Classification: Separation Of Linear Seismic Events

Linear Radon transform can also be used for the extraction of linear events, like first arrival refractions and ground rolls, from the seismic data. By combining linear Radon transform and compressive sensing, the linear events can be separated at the time of acquisition. Basic model remains the same as discussed in the case of interpolation. For the separation of linear events, the fact that linear event will be mapped to single point in $\tau - p$ domain is used. On the other hand the non-linear events will be spread out in $\tau - p$ domain. Spread out events will have lower value than the non-linear events, hence these events can be muted by doing some thresholding.

3.6.1 Simulation Result

For the simulation, synthetic data(3.16a) is used. The data contain total 7 events, out of these 7 events 4 are linear and 3 are non-linear events. The results after applying the linear Radon transform along with the compressive sensing are presented with different compression level in figure 3.16. To test the robustness of the proposed method result, after the addition of the 10% and 30% random noise, are presented in Figure 3.17 and Figure 3.18.

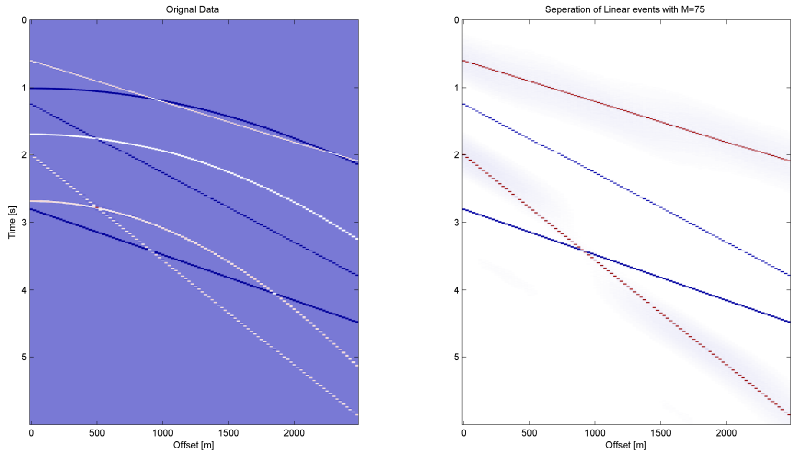

(a)

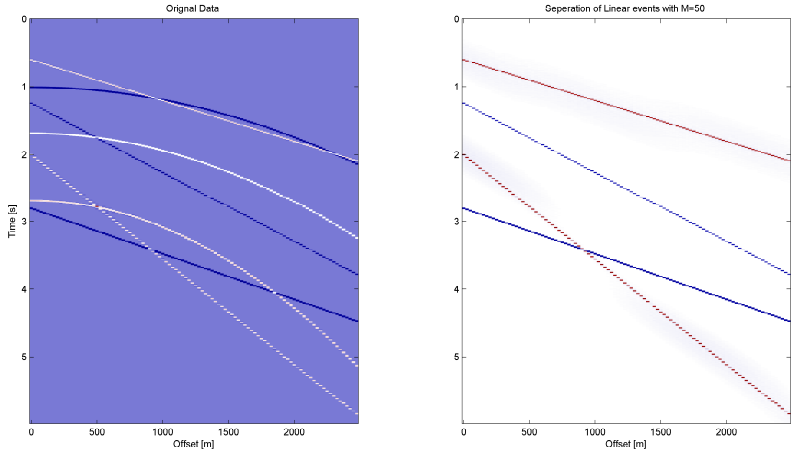

(b)

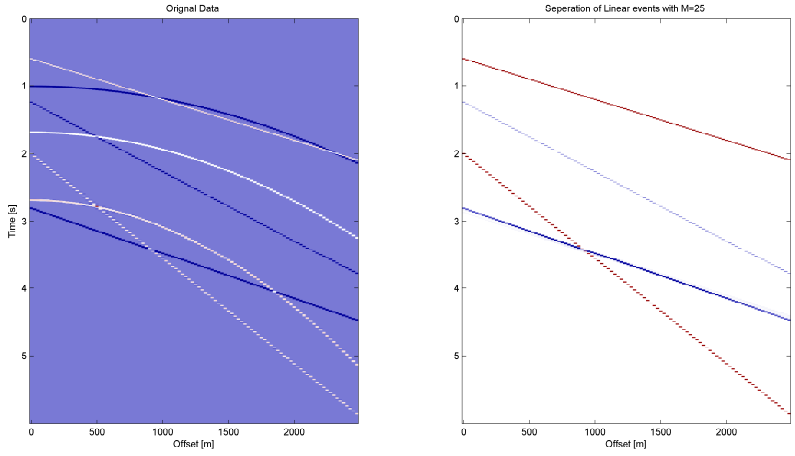

(c)

Figure 3.16: Separation of Linear Seismic events. Figure (a) shows the result of the application of proposed method for the classification of linear seismic events, with N=100, M=75(25% Compression). (b) and (c) provides the result after the application of the proposed method with 50% and 75% compression respectively.

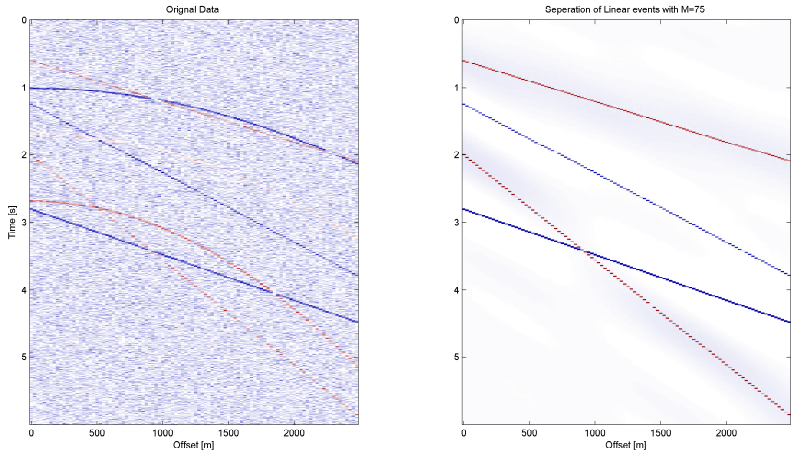

(a)

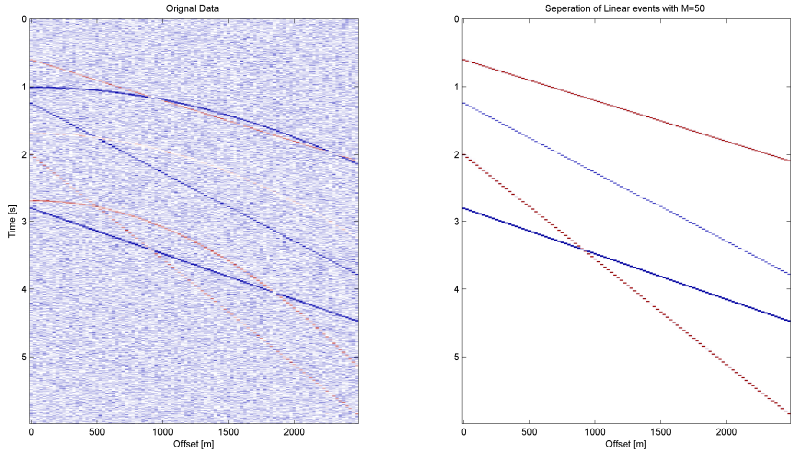

(b)

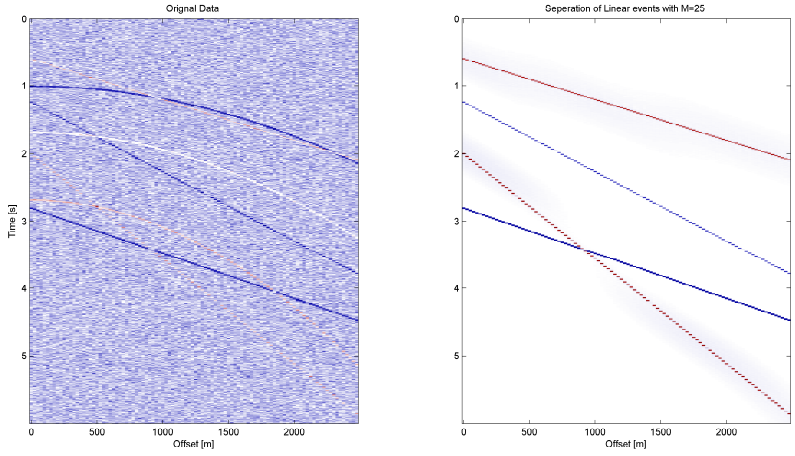

(c)

Figure 3.17: (a)Synthetic data with 10% random Gaussian noise and the result of the application of proposed method for the classification of linear seismic events, with N=100, M=75(25% Compression). (b) and (c) provides the result after the application of the proposed method with 50% and 75% compression respectively.

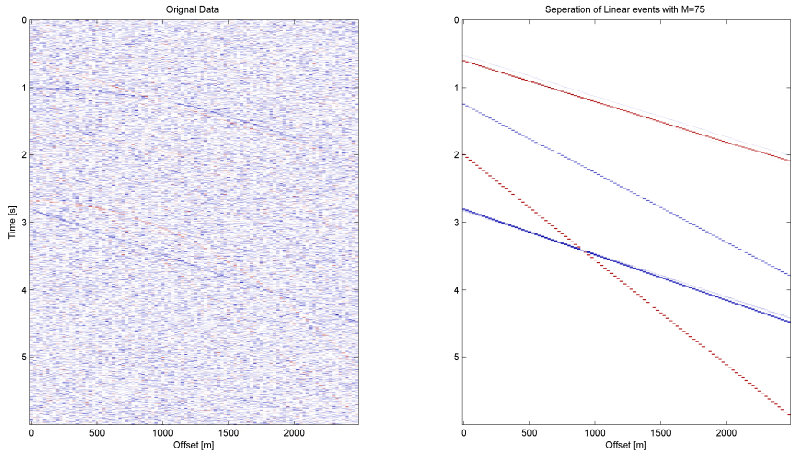

(a)

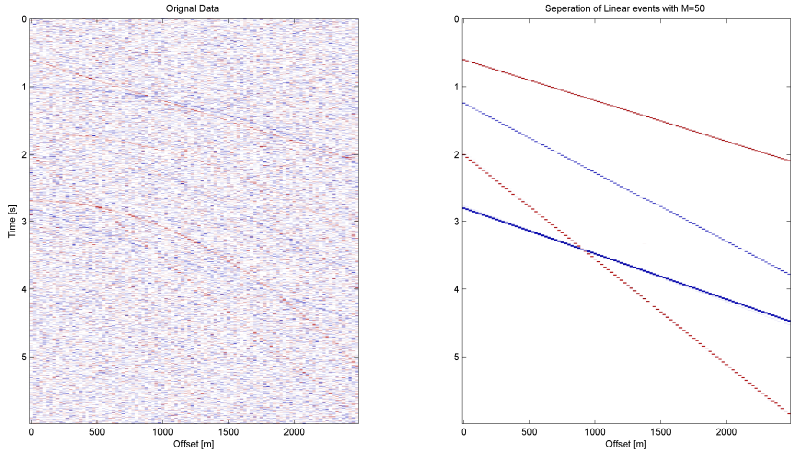

(b)

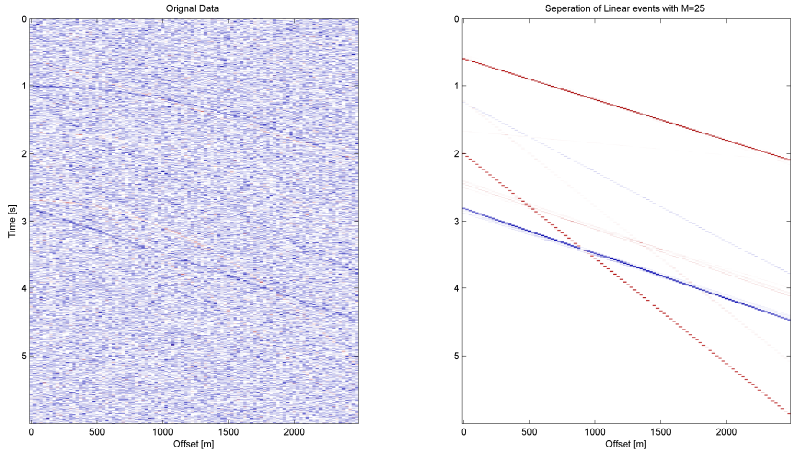

(c)

Figure 3.18: (a)Synthetic data with 30% random Gaussian noise and the result of the application of proposed method for the classification of linear seismic events, with N=100, M=75(25% Compression). (b) and (c) provides the result after the application of the proposed method with 50% and 75% compression respectively.

3.7 Deconvolution

Deconvolution is used to retrieve the reflectivity from the seismic data. It is a filtering process in which wavelet is removed from the captured seismic data. Most common way of deconvolution is the use of Weiner filter, transferring one wavelet into another in least square sense. There are many deconvolution techniques has been proposed for seismic data such as predictive.

Maximum entropy based entropy was introduced by Burg (1967) [101–103]. This effective technique is known as spiking deconvolution but it is sensitive to noise variance. To minimize the effect of noise a consistent relative entropy method is discussed in [104–106]. Deconvolution based on zero-lag is presented in [107, 108]. The most famous type of deconvolution is predictive deconvolution [109, 110]. Predictive deconvolution is independent of the lag value and uses the relative entropy concept. It removes the multiples and even increase the resolution. Commercially a combination of deterministic and predictive deconvolution is used.

In this section a new technique for the seismic deconvolution, based on Radon transform compressive sensing, is presented.

Algorithm

Given a seismic record, the proposed compressive sensing with Radon transform method for seismic deconvolution is stated as follows:

1. Use the compressive sensing to acquire the seismic data in the compressed

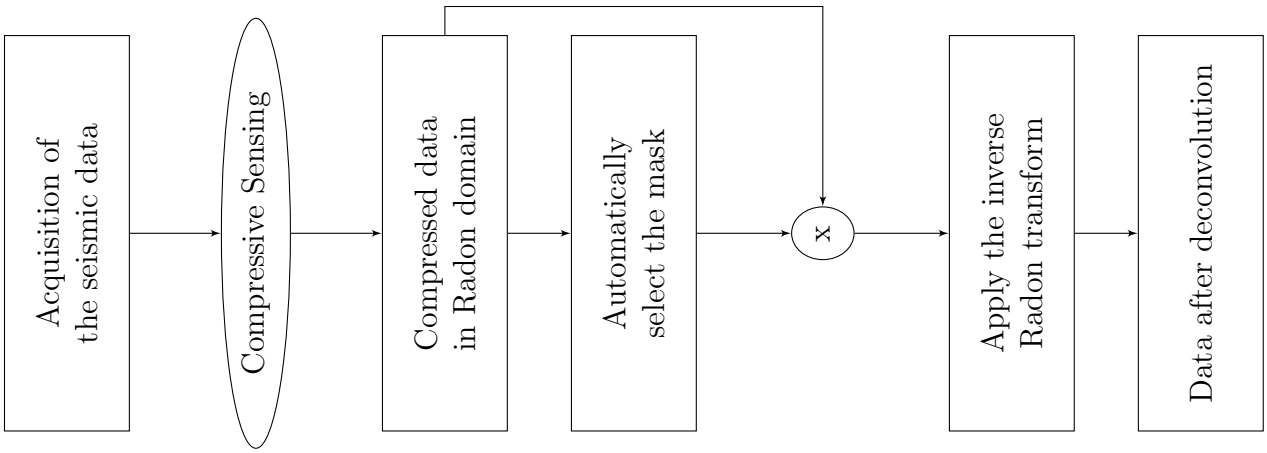

Figure 3.19: Workflow of the proposed technique for Deconvolution

fashion as described in the previous section.

2. Use the following facts to generate an automatic mask:

   (a) The curves are converted to single points in the Radon domain.

   (b) These points have higher value than the points corresponding to the noise or irrelevant curves.

3. Multiply the mask with the compressed Radon domain. This will leave only the curves in the Radon domain.

4. Apply the inverse linear radon transform to the previous step result.

Overall algorithm is presented in the Figure 3.19.

3.7.1 Simulation Results

The synthetic data contains four reflections as shown in Figure 4.21a. The total number of traces in the data are 50(N=50) with spatial sampling interval 25m and sampling interval 4m/s. Figure 4.21b shows the compressed $\tau - q$ domain

with M=40. Now based on the third step of the proposed algorithm the Radon domain after muting of the non-significant part is presented in the Figure 4.21b. Finally the results after the application of the inverse parabolic Radon transform are presented in Figure 4.21d, which shows the deconvolution results with 20% compression. The estimated noise is presented in Figure 4.21e.

Seismic deconvolution results for 40% and 80% compression are presented in Figure 3.21 and 3.22.

It is evident from the results, the proposed deconvolution algorithm provides reasonable good results even for high compression level. One of the most common technique of seismic deconvolution is the fx-deconvolution. Figure 3.23 provides the deconvolution results with fx-deconvolution.

As evident from the results, the proposed algorithm provides better results than the fx-deconvolution. Computationally the comparison between the both technique is presented in the table 3.1 and 3.3. Both algorithm were tested on Intel Core i7 processor. The proposed algorithm is faster than the fx-deconvolution but the major difference is in the number of samples needed for the both technique.

Transform Type	Compression	Time
Radon Transform	80%	0.121122 seconds
Radon Transform	60%	0.120375 seconds
Radon Transform	40%	0.120143 seconds
Radon Transform	20%	0.117257 seconds
Fx deconvolution	-	0.185387 seconds

Table 3.3: Time comparison: Linear Radon transform vs FX-deconvolution

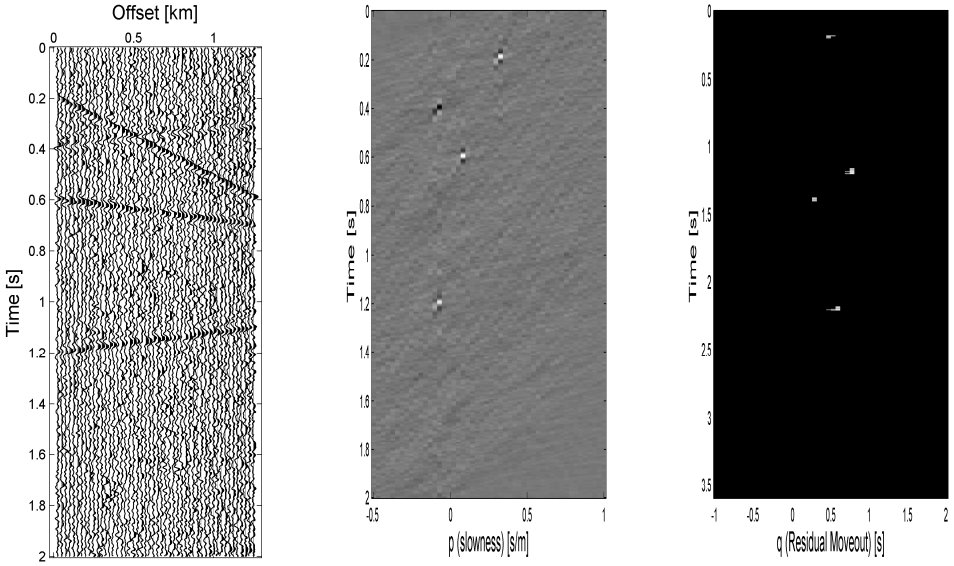

(a) (b) (c)

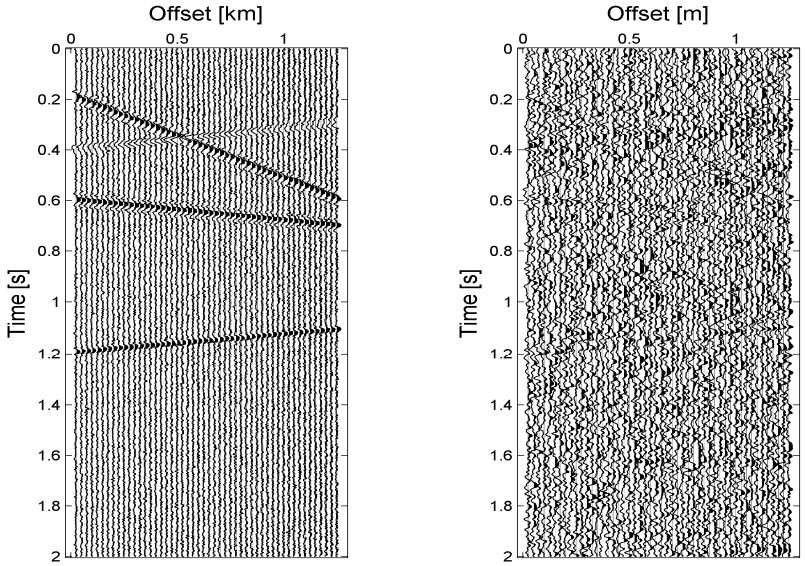

(d) (e)

Figure 3.20: Deconvolution of seismic data using Compressive sensing With N=50 (a) The synthetic data used for the deconvolution. (b) The compressed $\tau - p$ transform of (a), after the acquisition in compressed fashion with M=40 (20% compression). (c) The $\tau - p$ domain after the muting of the non-significant data. (d) The seismic data after taking the inverse parabolic Radon transform, of the (c). The estimated noise is shown in (e).

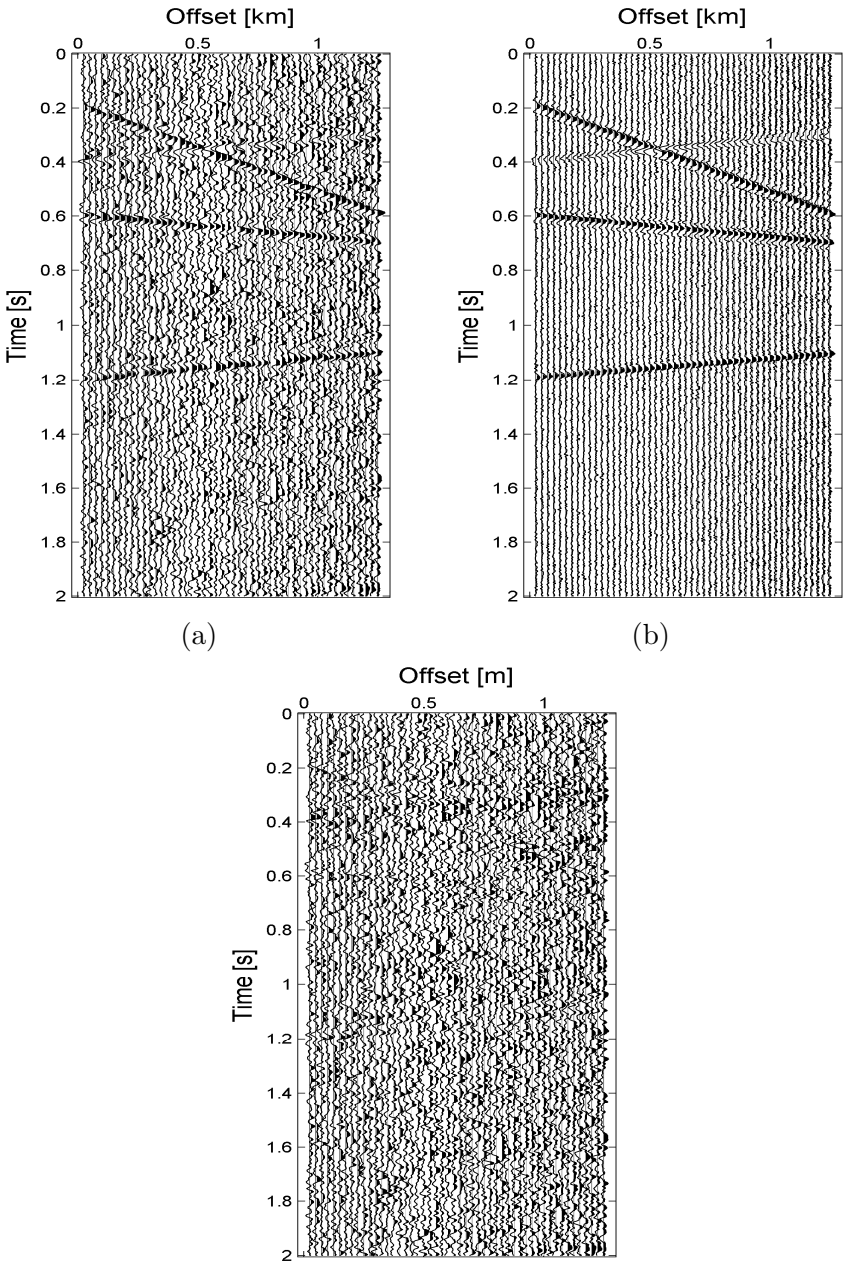

Figure 3.21: Deconvolution of seismic data using Compressive sensing With N=50 (a) The synthetic data used for the deconvolution. (b) The seismic data after deconvolution with M=30 (40% compression). The estimated noise is shown in (c).

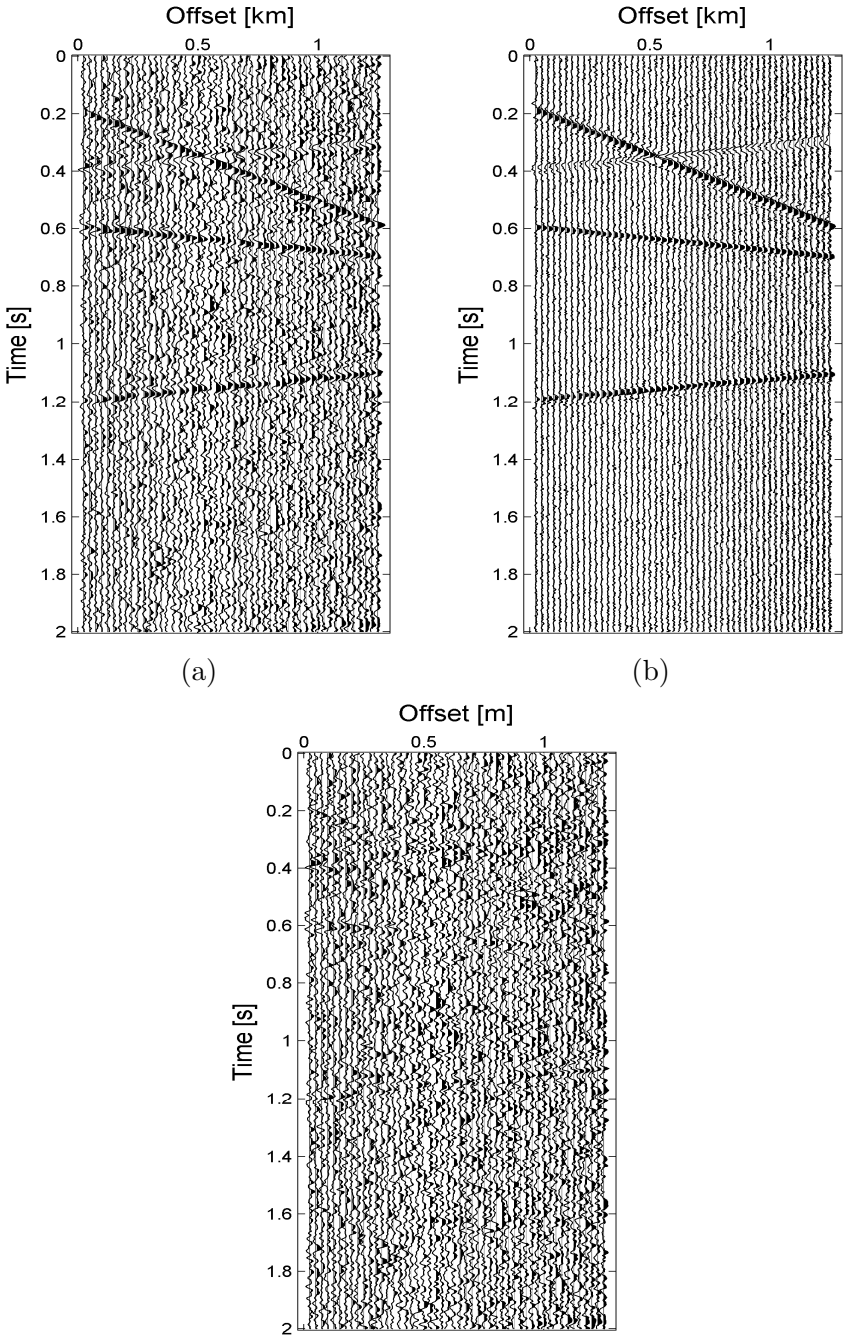

Figure 3.22: Deconvolution of seismic data using Compressive sensing With N=50 (a) The synthetic data used for the deconvolution. (b) The seismic data after deconvolution with M=10 (80% compression). The estimated noise is shown in (c).

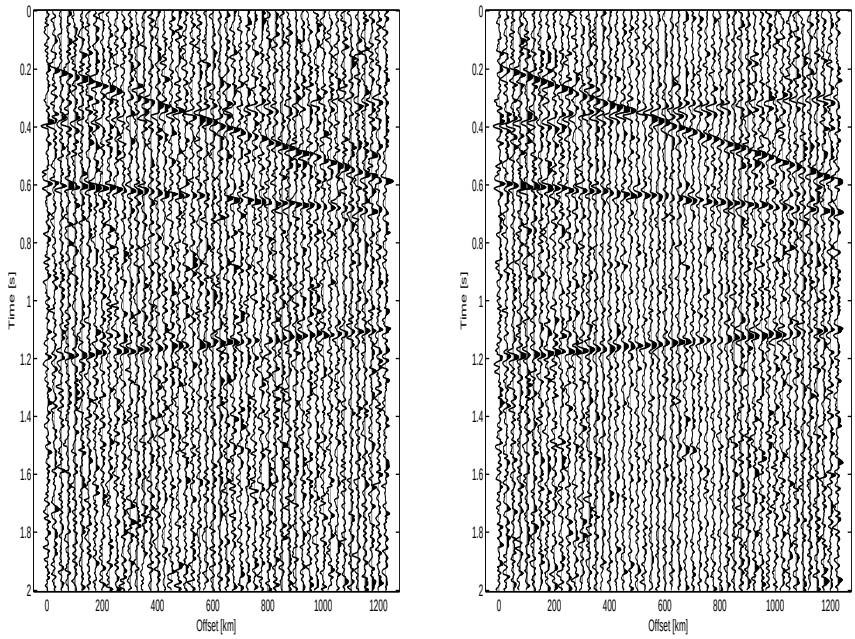

(a)

(b)

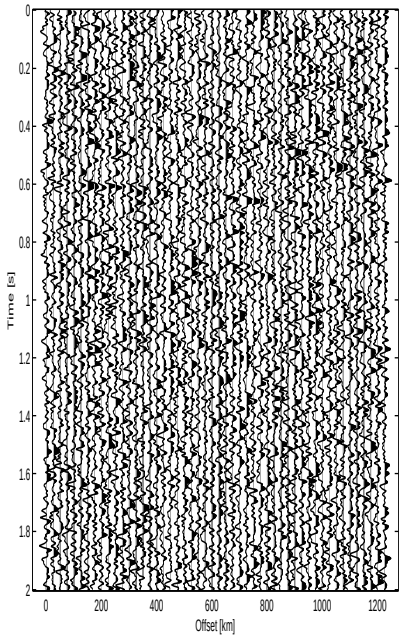

(c)

Figure 3.23: Deconvolution of seismic data using fx deconvolution (a) The synthetic data used for the deconvolution. (b) The seismic data after deconvolution . The estimated noise is shown in (c).

3.8 First Arrival Picking

In near-surface modeling the most important part is the analysis of the refraction data. For given seismic traces, the first arrival picking is the task of finding the onsets of the first signal breaks. One of the fundamental stage of seismic processing is the static correction. Accurate calculation of the first arrival time is required for the static correction [111]. The quality of the first arrival is depend on the type of source used, near surface structure, and signal to noise ratio.

First arrival/break picking is of two types: manual and automatic [112]. Manual picking techniques are the traditional techniques of first arrival picking and as the name suggests, in manual techniques, humans after inspecting the amplitude and waveform changes picks the first arrivals. Manual picking techniques are subjected to human and not much accurate. As one have to check all the traces therefore manual picking is quite time consuming. On the other hand, automatic techniques involves software and computers to detect the first arrival by following some specific criteria. They are more efficient and faster than the traditional technique but can be prune to inaccurate picking. Still computer based picking takes time and we need faster algorithm and softwares for fast first arrival picking.

Nowadays, semi-automatic techniques are used in which first autonomic picking is used, then visual inspection is done. Sometimes for complex geological surfaces whole process is repeated. Due to the large amount and poor quality of data, the picking can take up to 15 - 30% of the total processing time.

There are many well-known first arrival picking techniques. Peraldi and

Clement introduces the cross correlation based method for first arrival picking [113]. They uses the cross correlation of the adjacent traces for the first arrival picking. The technique does not work well as the shape of the adjacent traces do not remain same. Statistical based algorithm for the first arrival picks is introduced by [114]. Gelchinsky uses both correlation and statistical properties of the traces for the first arrival pick [115]. Energy based techniques have been quite famous. First such technique is presented by Coppens [116]. The algorithm proposed by Coppens is quite robust. Spagnolini (1991) presents his adaptive picking method which detects the abrupt changes in the energy and uses it for the first arrival picking [117]. Neural Networks based algorithm is presented in [118]. This method requires a lot of time for adequate training so this method is quite slow. Methods based on high order statistics [119], fractal-dimension analysis [120, 121] , and wavelet transform [122] has been presented. But all these methods have limitation especially when the SNR is low.

Here a new technique for the first arrival picking based on $\tau - p$ transform and compressive is presented. Basic Model is same as presented for the interpolation case.

Algorithm

Given a seismic refracted record, the proposed compressive sensing with $\tau - p$ method for automatic first arrivals is stated as follows:

1. Use the compressive sensing to acquire the seismic data in the compressed fashion as described in the previous section.

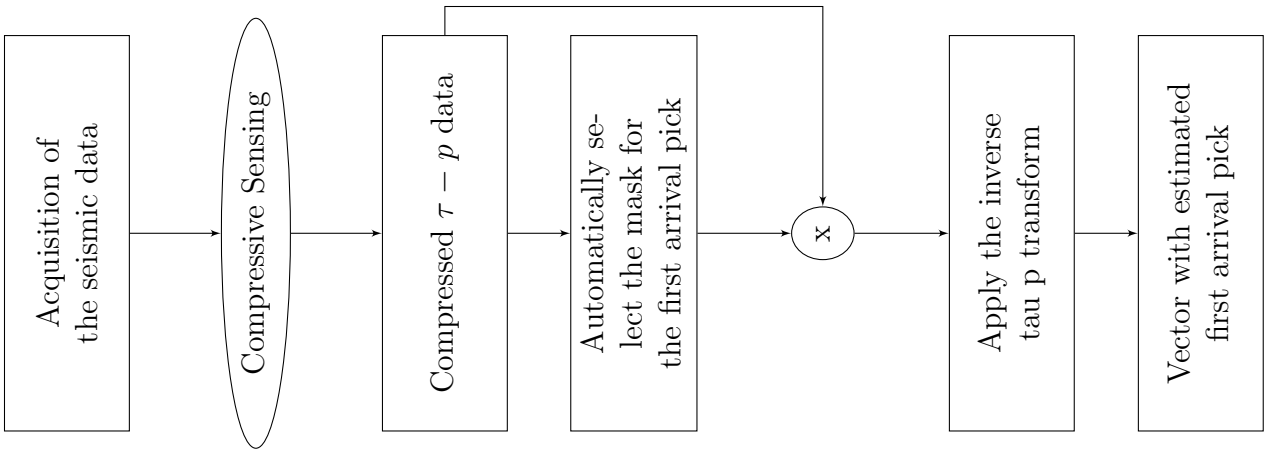

Figure 3.24: Workflow for first-arrival picking

2. Use the following facts to generate an automatic mask (one for the first arrival region , zero for otherwise):

   (a) Usually the first point in the compressed $\tau - p$ domain, is the point corresponding to the first arrival.

   (b) Compressive sensing produces a straight line parallel to τ-axis in the $\tau - p$ domain as shown in Figure 3.25.

3. Multiply the mask with the compressed $\tau - p$ domain. This will leave only the first arrival point in the $\tau - p$ domain.

4. Apply the inverse linear Radon transform to the previous step result.

3.8.1 Simulation Results

The parameters of the synthetic seismic shot gather are presented in [21]. The data contains ground-roll, head waves and three reflectors as shown in Figure 3.25. The total number of traces in the data are 120(N=120) with spatial sampling interval

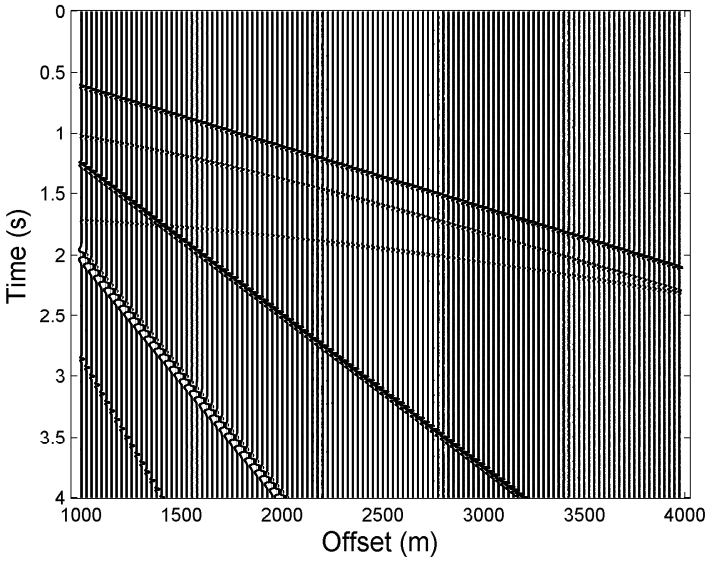

Figure 3.25: First Arrival Picking: Original Data, $\tau - p$ domain

25m and sampling interval 4m/s. Figure 3.26b shows the compressed $\tau - p$ domain with M=90. Now based on the third step of the proposed algorithm the generated mask is presented in the Figure 3.26c. Finally the results after the application of the inverse $\tau - p$ transform are presented in Figure 3.26d. The resulted image contains the first arrival picks. The comparison with the manual picks and the picks calculated using the proposed method are presented in the Figure 3.26e. Estimated picks are very close to the actual picks of the model, a comparison with the $\tau - p$ energy ratio method [21], is shown in Figure 3.26f.

Figure 3.27 shows the same comparison with 60% compression (M=50). The figure 3.27e provides the comparison with the manual picking. There is not much difference in the actual picks and the estimated picks. To show how well compressive sensing works, results for the 80% compression (M=25) are presented in the Figure 3.28.

To show the robustness of the proposed algorithm random Gaussian noise was

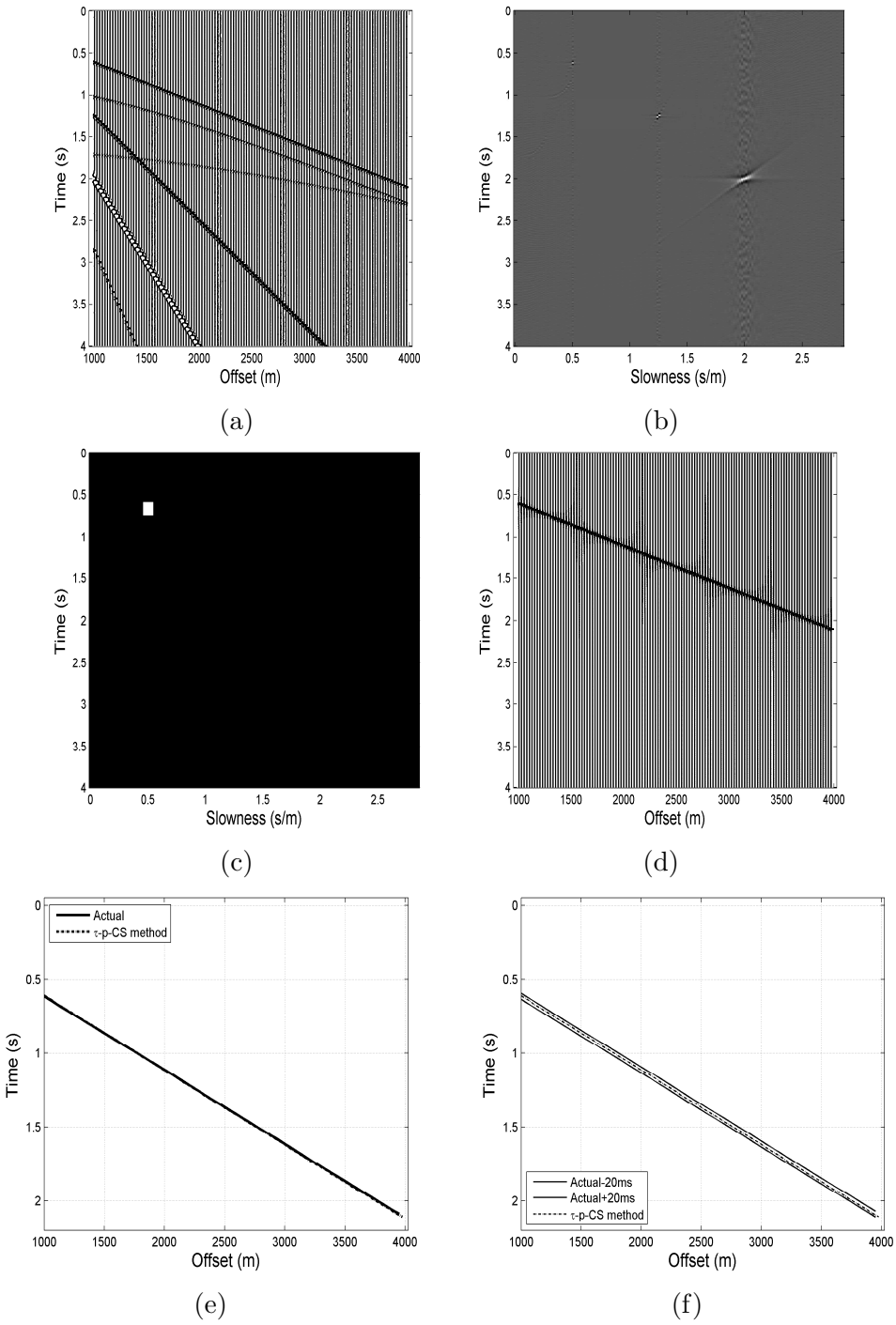

Figure 3.26: (a) The synthetic seismic refracted data. (b) The compressed $\tau - p$ transform of (a) , after the acquisition in compressed fashion with M=90 (25% compression). (c) The produced binary mask (white stands for one and black for zero) for the automatic selected region of first arrivals of (b). (d) The estimated first arrival picks after taking the inverse $\tau - p$ transform, of the multiplied $\tau - p$ domain of (b) with the mask of (c). The estimated first-arrival picks of (a) compared with the actual picks and and $\tau - p$ ER method in (e) and (f).

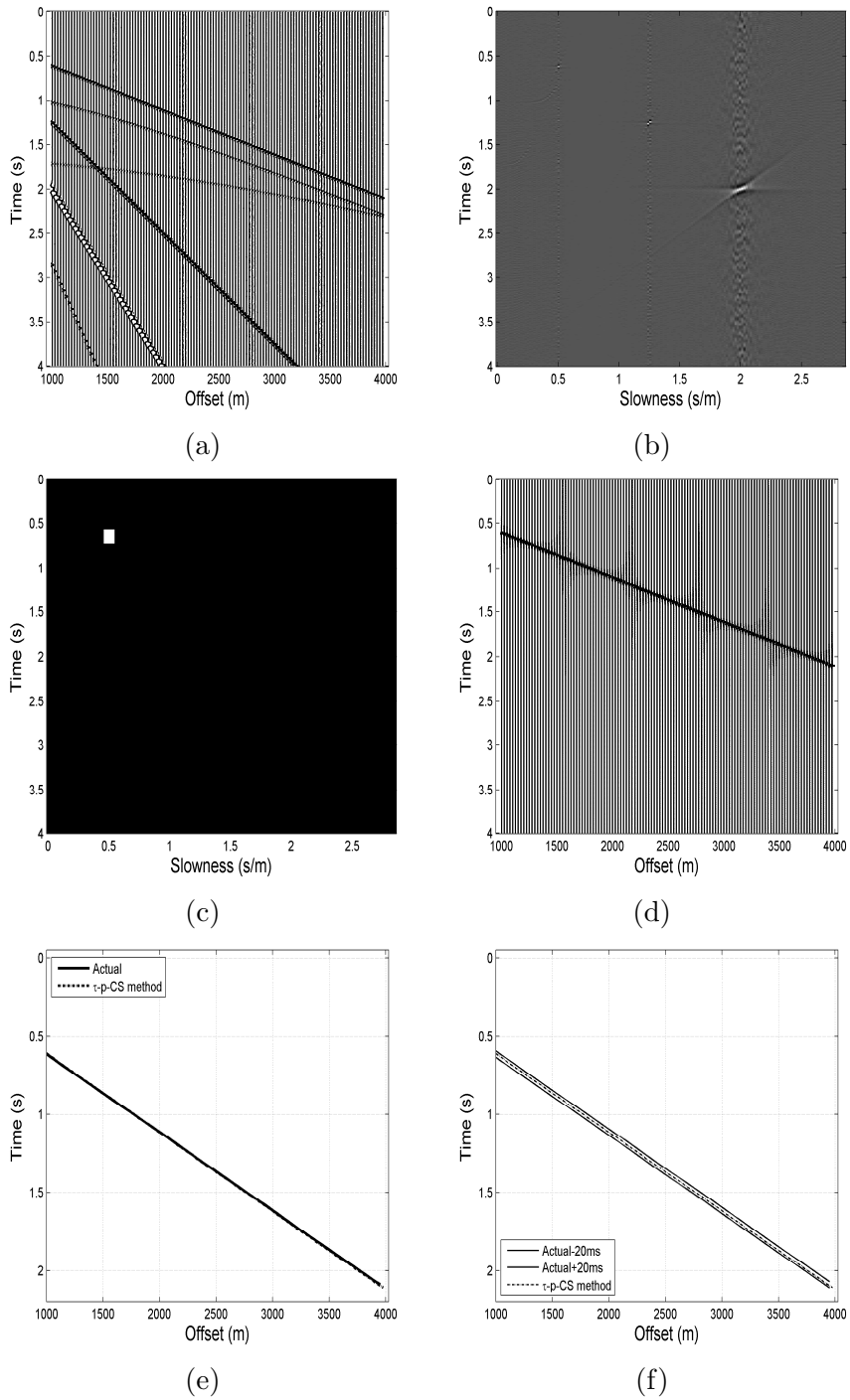

Figure 3.27: (a) The synthetic seismic refracted data. (b) The compressed $\tau - p$ transform of (a) , after the acquisition in compressed fashion with M=50 (60% compression). (c) The produced binary mask (white stands for one and black for zero) for the automatic selected region of first arrivals of (b). (d) The estimated first arrival picks after taking the inverse $\tau - p$ transform, of the multiplied $\tau - p$ domain of (b) with the mask of (c). The estimated first-arrival picks of (a) compared with the actual picks and and $\tau - p$ ER method in (e) and (f).

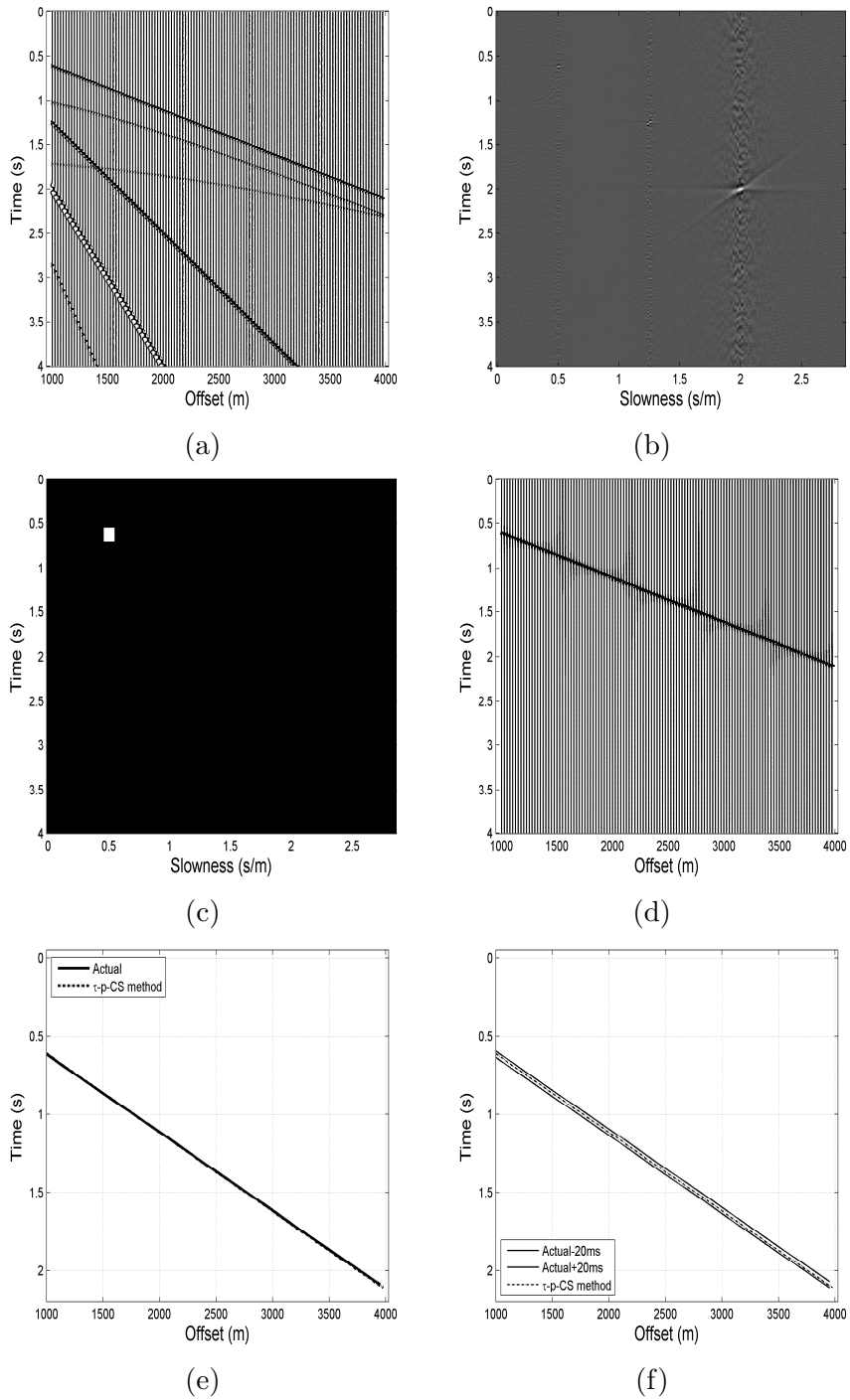

Figure 3.28: (a) The synthetic seismic refracted data. (b) The compressed $\tau - p$ transform of (a) , after the acquisition in compressed fashion with M=25 (80% compression). (c) The produced binary mask (white stands for one and black for zero) for the automatic selected region of first arrivals of (b). (d) The estimated first arrival picks after taking the inverse $\tau - p$ transform, of the multiplied $\tau - p$ domain of (b) with the mask of (c). The estimated first-arrival picks of (a) compared with the actual picks and and $\tau - p$ ER method in (e) and (f).

added to the original synthetic data. The comparison after the addition of the noise with 0.1 standard deviation and 80% compression are presented in Figure 3.29. Figure 3.30c shows also that there is essentially not much difference between the estimated and manual picks. Similar comparison after the addition of white noise with standard deviation 0.2 and 0.4 are presented in the figure and Figure respectively. With this high level of noise, the first-arrival event is completely missing from Figure, which makes picking it virtually impossible. However, the first-arrival event is fairly clear on Figure, which represents the compressed $\tau - p$ transform. Figure shows that the first-arrival event picked using the proposed method compares well to the actual (true) picks.

To test the performance of the proposed algorithm in the presence of multiple first-arrival events, we use the model parameters of previous synthetic data but with a wider offset range to include the direct and refraction arrivals from all layer interfaces as shown in Figure 3.32a . Our existing algorithm will not perform well for this kind of data set, therefore a little modification as described below is needed. Run the proposed algorithm multiple times after dividing the whole data into small segments. The overall steps are provided in the Figure .

The comparison with the actual picking and the estimated picking for the different compression levels (20, 40, 60%) are presented in the figure respectively. From the Figure 3.32, 3.33 and 3.34 it is evident that a large part of the estimated picks lies in the $\pm$220 ms range of the actual picking.

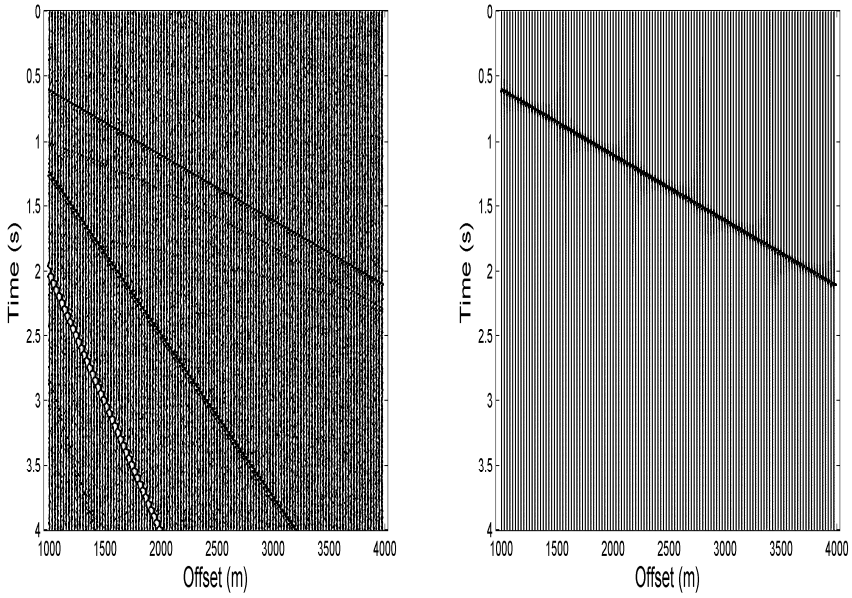

(a) (b)

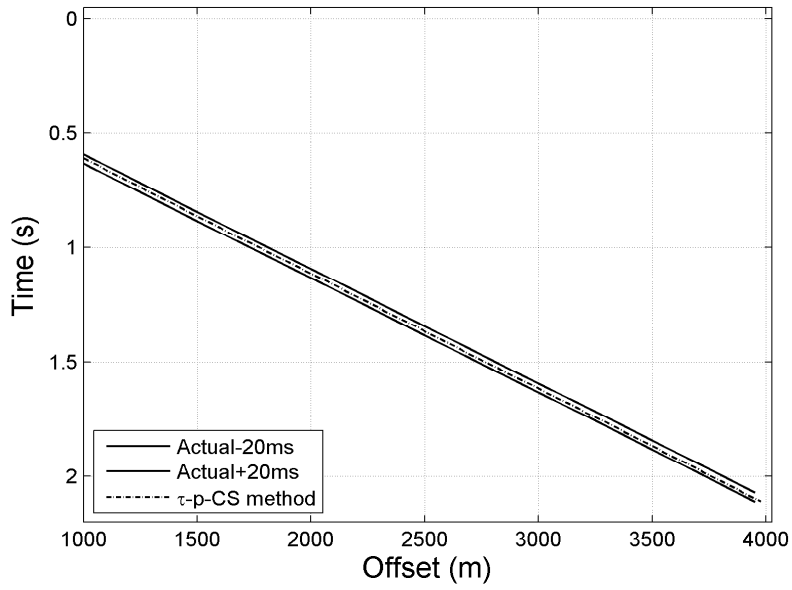

(c)

Figure 3.29: (a) The synthetic seismic refracted data with 10% Gaussian noise. (b) The estimated first arrival picks with M=25 (80% compression). (c) The estimated first-arrival picks is compared with the actual picks and $\tau - p$ ER method.

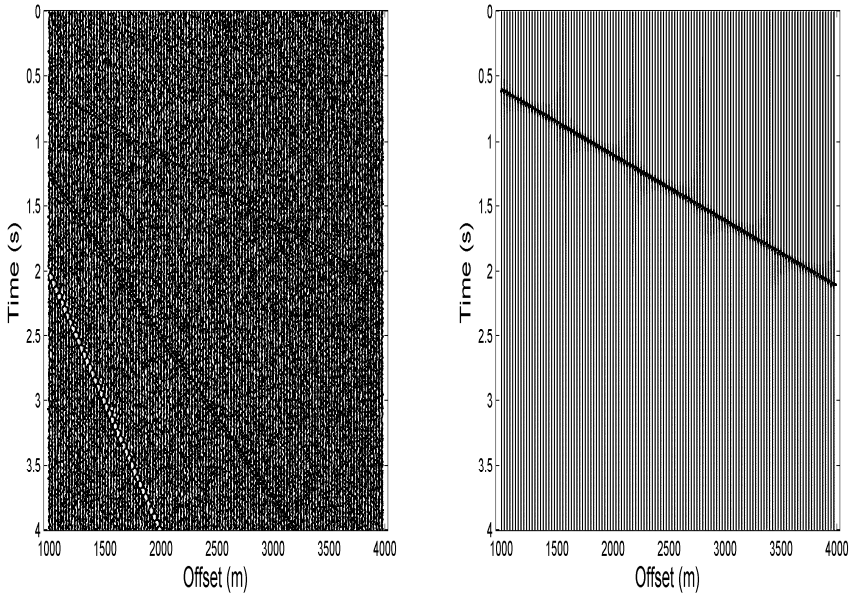

(a) (b)

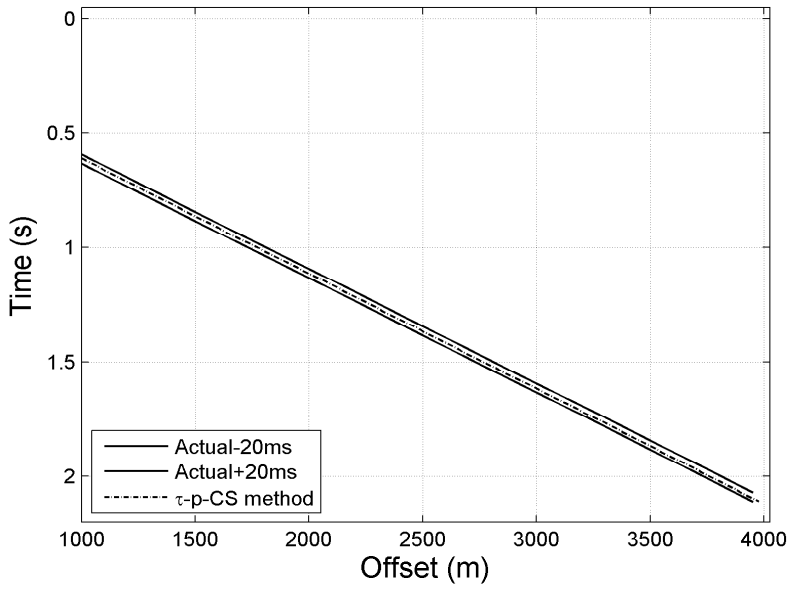

(c)

Figure 3.30: (a) The synthetic seismic refracted data with 20% Gaussian noise. (b) The estimated first arrival picks with M=25 (80% compression). (c) The estimated first-arrival picks is compared with the actual picks and $\tau - p$ ER method.

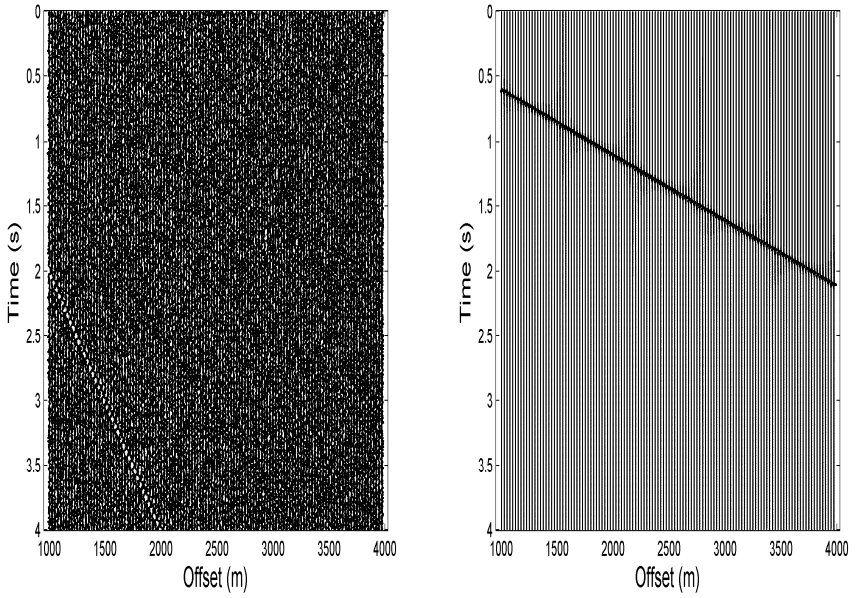

(a) (b)

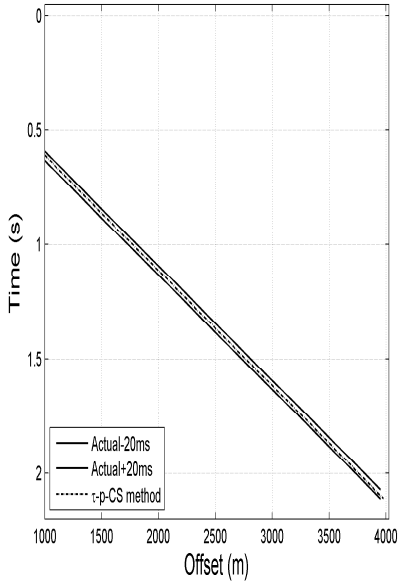

(c)

Figure 3.31: (a) The synthetic seismic refracted data with 30% Gaussian noise. (b) The estimated first arrival picks with M=25 (80% compression). (c) The estimated first-arrival picks is compared with the actual picks and $\tau - p$ ER method.

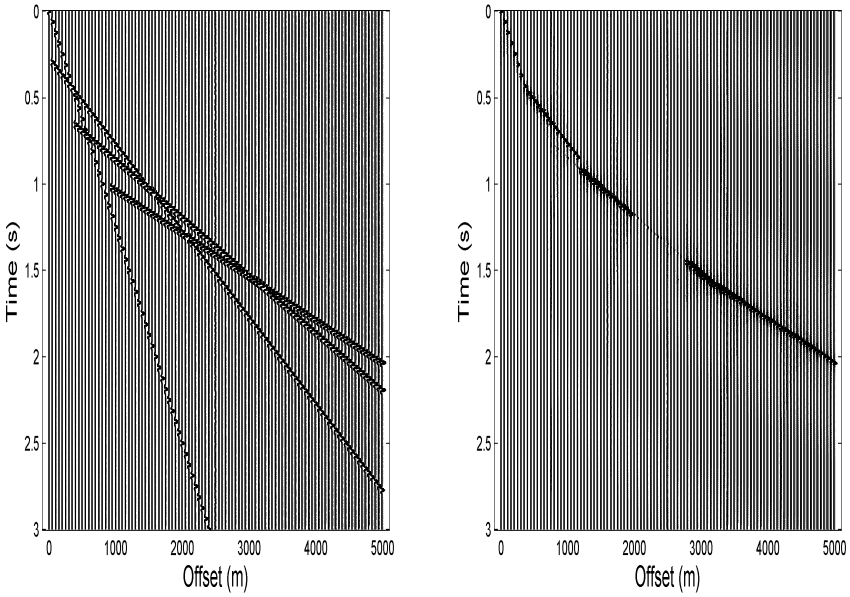

(a) (b)

Figure 3.32: (a) The synthetic seismic refracted data with multiple first arrivals. (b) The estimated first arrival picks with M=80 (20% compression). The estimated first-arrival picks is compared with the actual picks and and $\tau - p$ ER method of the actual picks in (c) and (d).

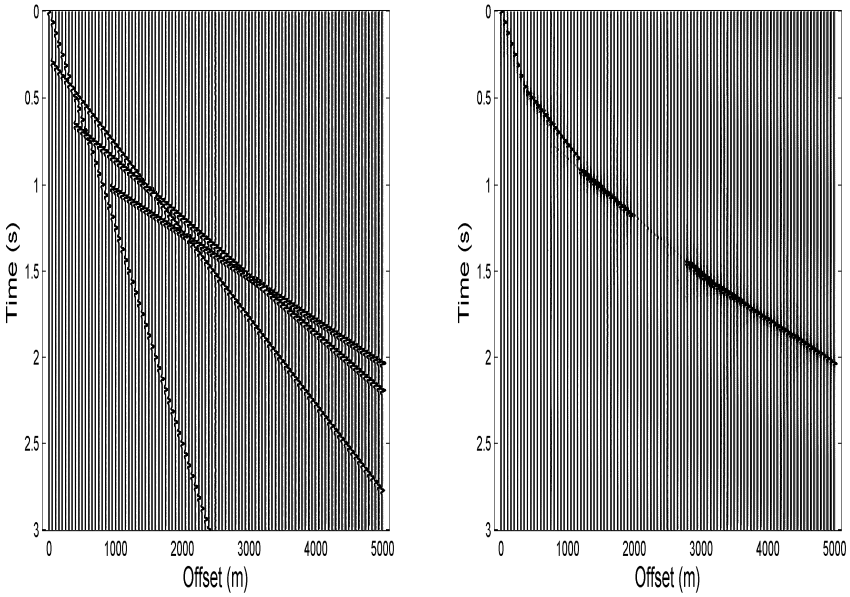

(a) (b)

Figure 3.33: (a) The synthetic seismic refracted data with multiple first arrivals. (b) The estimated first arrival picks with M=60 (40% compression). The estimated first-arrival picks is compared with the actual picks and and $\tau - p$ ER method of the actual picks in (c) and (d).

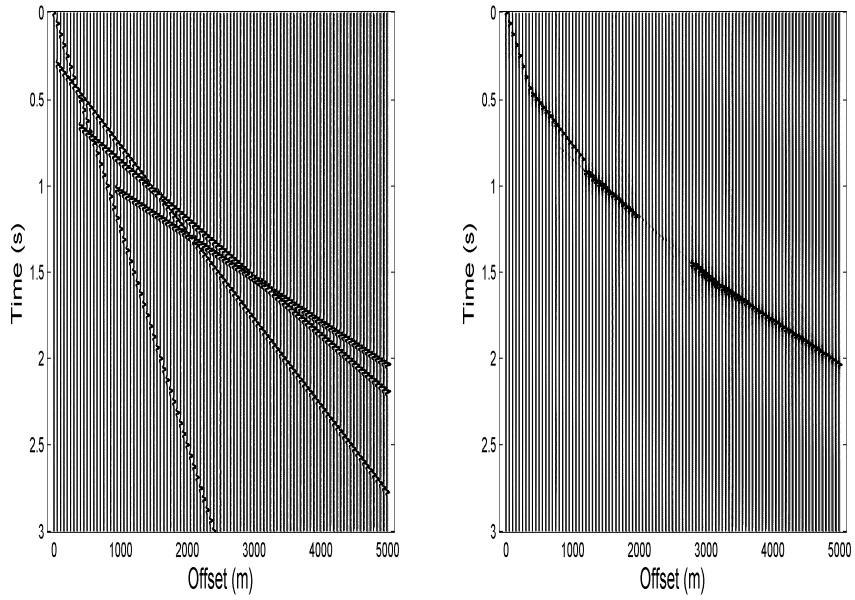

(a) (b)

Figure 3.34: (a) The synthetic seismic refracted data with with multiple first arrivals. (b) The estimated first arrival picks with M=40 (60% compression). The estimated first-arrival picks is compared with the actual picks and and $\tau - p$ ER method of the actual picks in (c) and (d).

Real Data

We applied our proposed method on the following data sets from Yilmaz (2001): 1) Shot gather 6 (Figure14a), which consists of 48 traces with sampling time 4 ms and spacing 100m. 2) Shot gather 23 (Figure16a), which consists of 48 traces with sampling time 2ms and spacing 67 m with a vibroseis source and is located in San Juaquin.

The comparison for shot gather 6 with 20% compression is shown in the Figure 3.35 . The Figure 3.35c presents the comparison with the actual pick and the estimated pick. In Figure a comparison of the proposed algorithm with the famous Coppens method is presented3.35d. For the dynamite shot gather in Figure3.35d , the proposed method outperformed the Coppens method. The extreme case

with 80% compression is shown in Figure 3.36. The figure 3.36d justifies the use of compressive sensing by comparing the actual picks with the estimated and the Coppens picks.

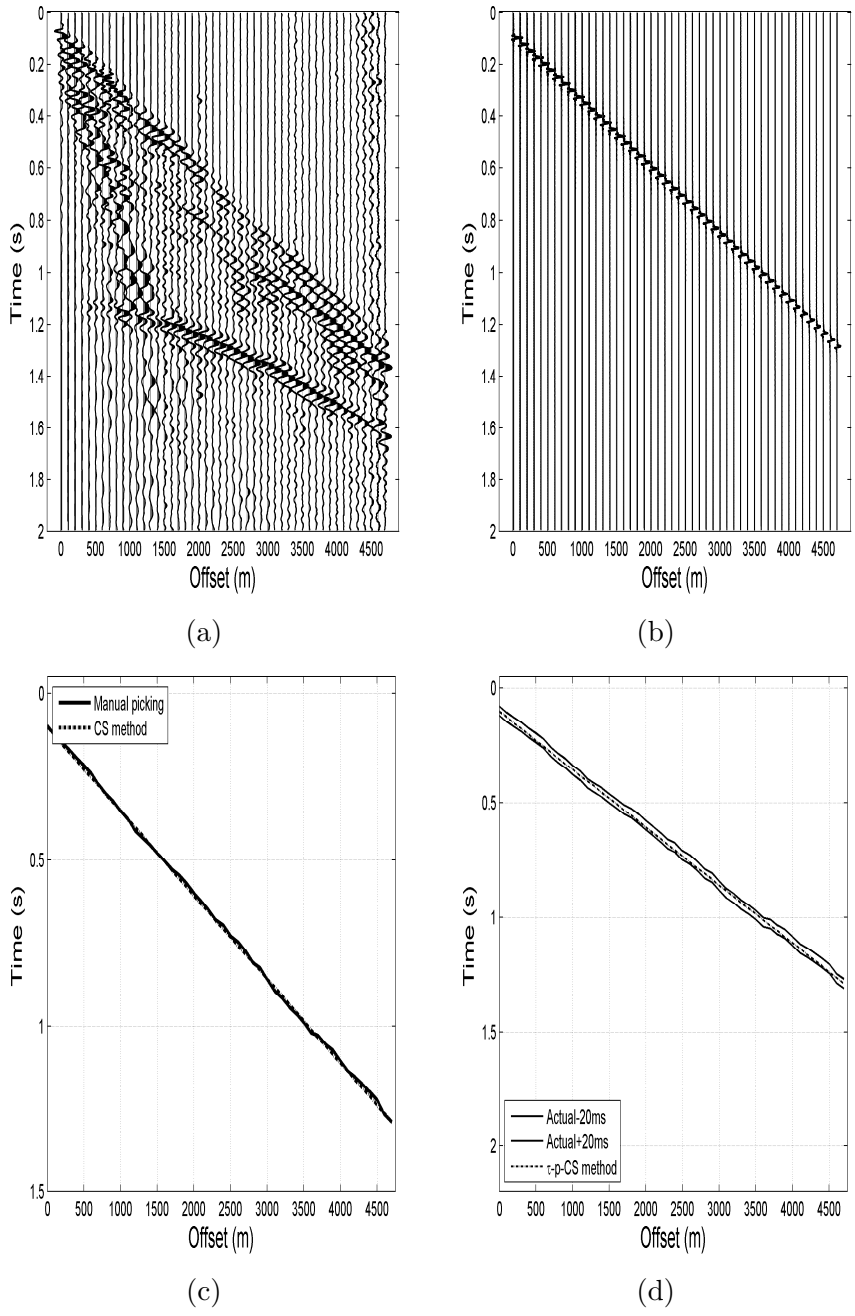

Figure 3.35: (a) The real seismic refracted data for shot gather 6. (b) The estimated first arrival picks with M=40 (20% compression). The estimated first-arrival picks is compared with the actual picks and and $\tau - p$ ER method of the actual picks in (c) and (d).

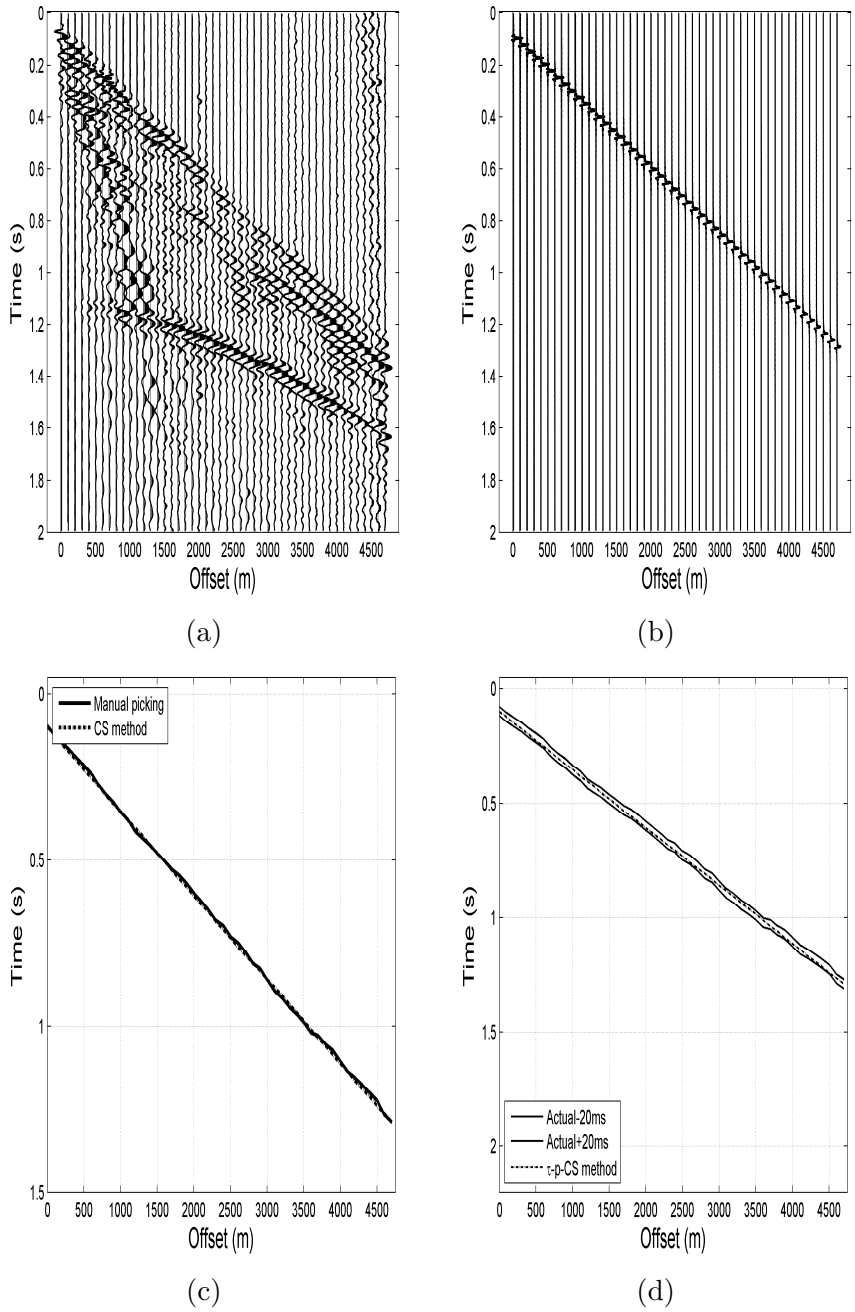

Figure 3.36: (a) The real seismic refracted data for shot gather 6. (b) The estimated first arrival picks with M=20 (60% compression). The estimated first-arrival picks is compared with the actual picks and and $\tau - p$ ER method of the actual picks in (c) and (d).

The results for the shot gather 23 is shown in the Figure 3.37 and 3.38. Figure 3.37d provides the comparison with the Coppens and estimated picks. Most of the

estimated picks lies between the 20ms range of the actual picks. 60% compression results are presented in the figure 3.38.

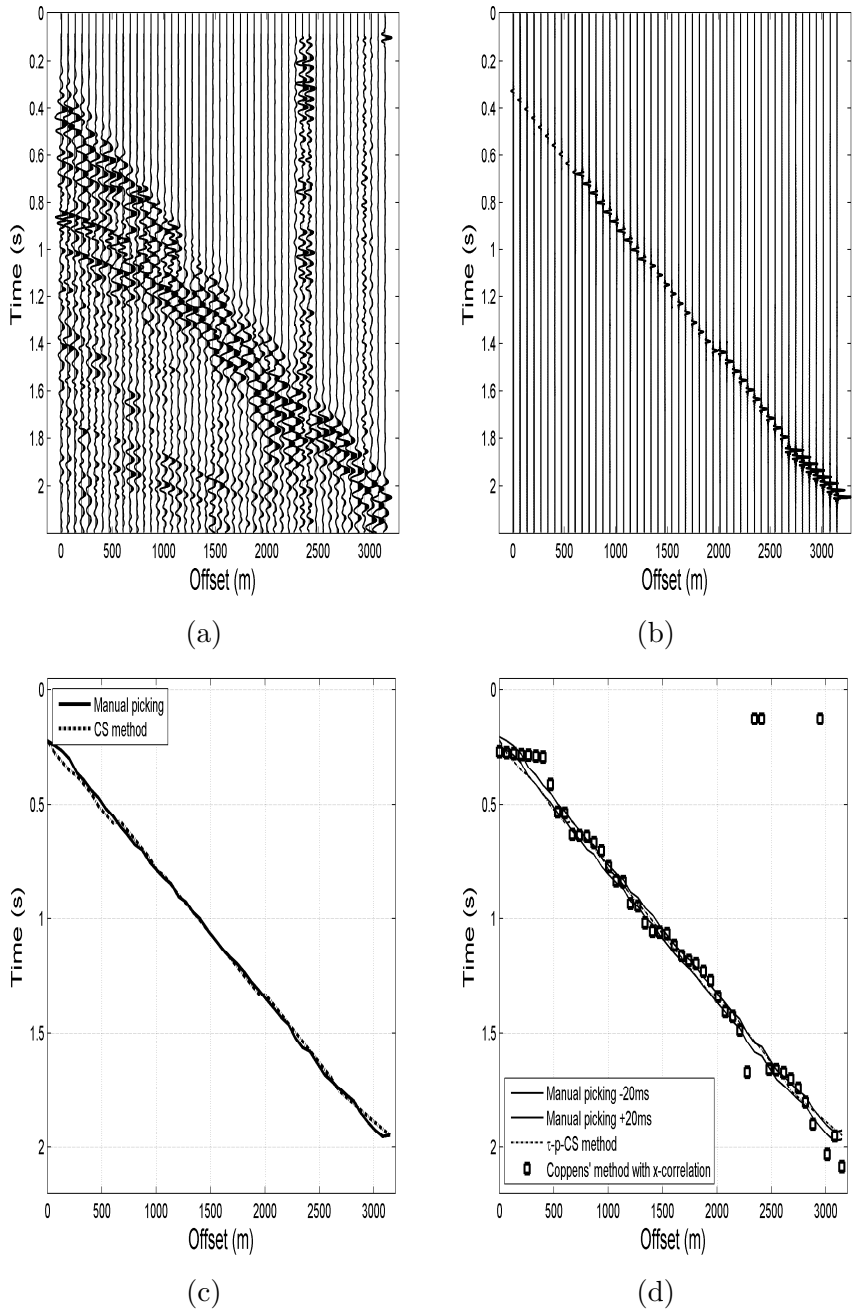

Figure 3.37: (a) The real seismic refracted data for shot gather 23. (b) The estimated first arrival picks with M=40 (20% compression). The estimated first-arrival picks is compared with the actual picks and and $\tau - p$ ER method of the actual picks in (c) and (d).

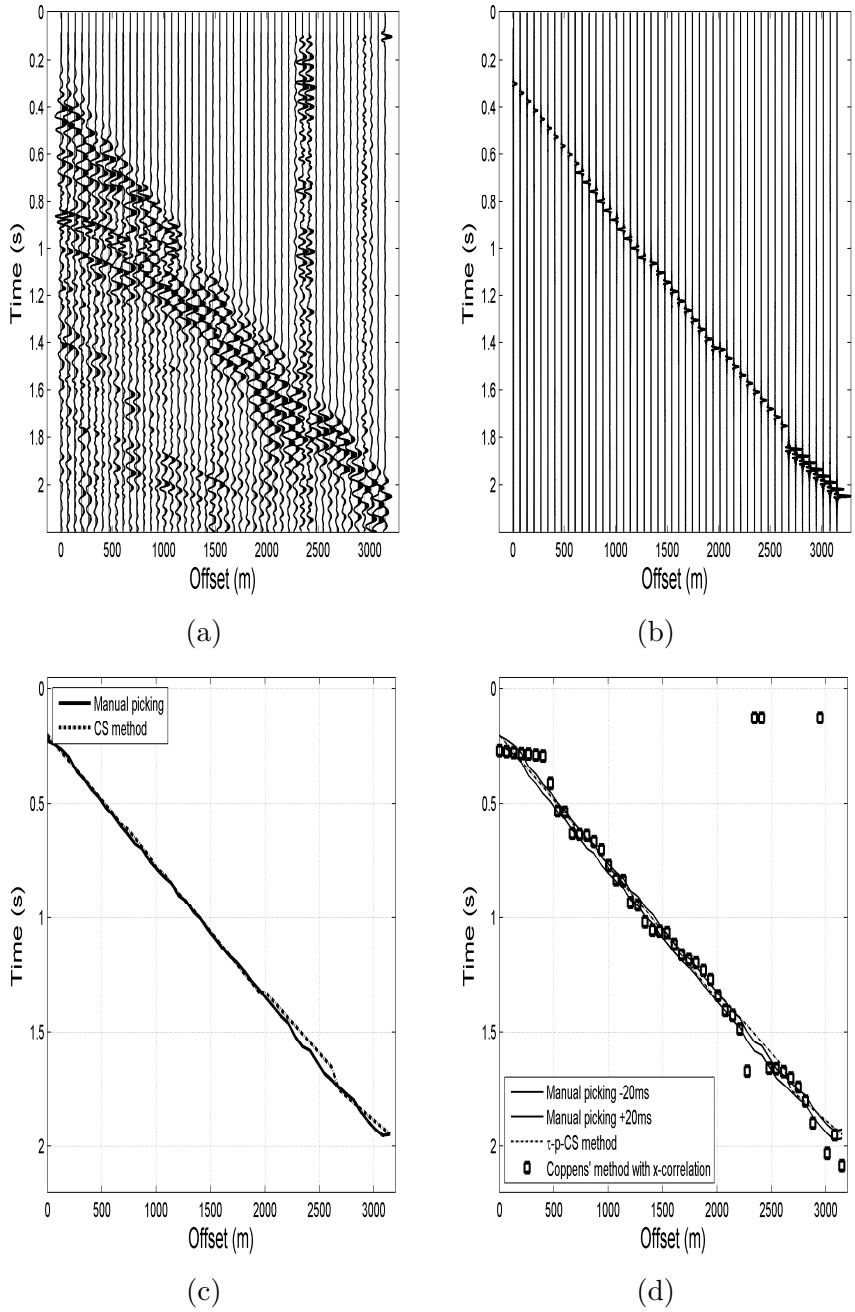

Figure 3.38: (a) The real seismic refracted data for shot gather 23. (b) The estimated first arrival picks with M=20 (60% compression). The estimated first-arrival picks is compared with the actual picks and and $\tau - p$ ER method of the actual picks in (c) and (d).

3.9 Conclusion

In the first section of this chapter a brief review of linear Radon transform is presented. Linear Radon transform and its types are discussed. Besides basic theory of linear Radon transform, Radon transform of point source, linear and non-linear events is presented.

In the second part of the chapter, compressive sensing using linear Radon transform as sparsifying transform is presented. The proposed algorithm is used for the interpolation of missing traces. From the comparison with the curvelet transform, it became evident that Radon is much faster than the curvelet transform. Moreover Radon transform is robust and works for low SNR signals as well.

Compressive sensing with linear Radon transform as a sparsifying transform can be used to separate the linear events from the non-linear Radon transform at the time of acquisition.

At the end of this chapter, first break problem is tackled using the proposed algorithm. From the detailed simulation results, it is clear that Radon transform with compressive sensing, not only reduce the number of measurements but it is also quite robust and provides accurate detection of the first arrival. The algorithm is modified for the multiple first arrival picking and at the end results for the real field data are presented with different compression level.

CHAPTER 4

COMPRESSED PARABOLIC RADON TRANSFORM AND ITS APPLICATIONS

Instead of linear Radon transform, Parabolic Radon transform is mostly used due to its effectiveness (better than the linear Radon Transform) and low computational cost [22]. Parabolic Radon transform is robust in nature and has attracted the attention of seismic data processing scientists and engineers during the last two decades. It is being used for quite some time in different applications which includes seismic deconvolution [20], multiple removal [23, 24, 26].

In the first section of this chapter a brief review of parabolic Radon transform is presented. Besides basic theory of parabolic Radon transform, parabolic Radon transform of point source, linear and non-linear events is presented. In the second section of the chapter, compressive sensing using parabolic Radon transform as

sparsifying transform is discussed. The proposed setup is used to find the missing non-linear events of the seismic data. Using the proposed setup a new techniques for deconvolution, classification and multiple removal, are presented. All these applications are discussed with simulation results for different synthetic and real data sets.

4.1 Parabolic Radon Transform

4.1.1 Introduction

In parabolic Radon transform, a parabolic curve in time domain will be mapped to a single point in the $\tau - q$ or Radon domain.In case of the parabolic Radon transform the integral is taken along a parabolic curve. On common shot point gathers, seismic events are not linear in nature but they are parabolic or hyperbolic in nature. Refractions and direct waves are linear, reflections and diffractions are hyperbolic. The hyperbolic Radon transform maps the hyperbolic events of the CMP gathers to points in the Radon domain. But Direct hyperbolic transform are too expensive to realize due to their complexity. Therefore hyperbolic Radon transform are not used in practice and faster method are sought. One of the method that can represent the reflected seismic events in sparse domain is parabolic Radon transform.

Hampson (1986) proposed an efficient frequency domain least-squares

parabolic transform method. The time domain semblance weighted Gauss-Seidel parabolic Radon transform was proposed by Bradshaw and Ng (1987). The t^2-stretching of the time axis was proposed by Yilmaz (1989).The Hampsonś frequency method was improved by Sacchi [123–125]. They incorporated the priori information for the formulation of High resolution parabolic Radon transform. Cary introduced the robust high-resolution parabolic Radon transform by posing the problem in the TX domain [29]. Sacchi and Porsani proposed a method to achieve an effective high-resolution Radon solution, by means of conjugate gradients. Trad proposed the robust high-resolution parabolic Radon by posing the problem in the FX domain [22, 126]. Some variant of weighted Parabolic Radon transforms are discussed in [17, 24, 127, 128].

Mathematically, parabolic Radon transform can be obtained by substituting $\phi(x) = x^2$ in the generalized Radon transform equation (2.20). The forward and inverse parabolic Radon transform becomes

$$u(q, \tau) = \sum_x d(x, t = \tau + qx^2) \tag{4.1}$$

$$\hat{d}(x, t) = \sum_q u(q, \tau = t - qx^2)) \tag{4.2}$$

here x is the offset and $q = 1/v^2$ represent the curvature of the curve.

4.1.2 Types of Parabolic Radon transform

Different types of parabolic Radon transform are discussed in this section.

Hampson Parabolic Radon transform

In general, seismic events are hyperbolic in nature but we can approximate small portions of these events as parabolas. On the NMO-corrected data, the parabolic Radon transform was performed by Hampson. Following equation gives the hyperbolic move out of the NMO-corrected input data:

$$t_n = \sqrt{t^2 - \frac{x^2}{{v_n}^2}} \tag{4.3}$$

Here v_n is the corrected velocity, t is the recorded time, t_n is the corrected time. The resulting events can be approximated by parabolas. Squaring both sides of the above equation, we obtain the following equation:

$$t^2 = {t_0}^2 + \frac{x^2}{v^2} \tag{4.4}$$

$${t_{err}}^2 = {t_0}^2 + \frac{x^2}{{v_{err}}^2} \tag{4.5}$$

$${t_{err}}^2 = t^2 + \frac{x^2}{{v_{err}}^2} - \frac{x^2}{v^2} \tag{4.6}$$

$$\frac{{t_{err}}^2}{t^2} = 1 + \frac{x^2}{t^2}(\frac{1}{{v_{err}}^2} + \frac{1}{v^2}) \tag{4.7}$$

$$\frac{t_{err}}{t} = \sqrt{1 + \frac{x^2}{t^2}(\frac{1}{{v_{err}}^2} + \frac{1}{v^2})} \tag{4.8}$$

$$\frac{t_{err}}{t} \approx 1 + \frac{x^2}{2t^2}(\frac{1}{{v_{err}}^2} + \frac{1}{v^2}) \tag{4.9}$$

$$t = \tau + qx^2 \tag{4.10}$$

t_{err} is approximately parabolic,

$$t^2 = \tau^2 + \frac{x^2}{v^2} \tag{4.11}$$

Parabolic Radon transform t^2 Stretched input data

Yilmaz proposed that after application of the t^2-stretch all the hyperbolic events in the offset domain can be transformed to exact parabolas. Events on the CMP gather have hyperbolic travel times defined by

$$t^2 = \tau^2 + \frac{x^2}{v^2} \tag{4.12}$$

Applying $\tilde{t} = t^2$ and $\tilde{\tau} = \tau^2$

$$\tilde{t} = \tilde{\tau} + \frac{x^2}{v^2} \tag{4.13}$$

Transformed equation is parabolic and can be defined as:

$$u(q, \tilde{\tau}) = \int_{-\infty}^{\infty} d(x, \tilde{t} = \tilde{\tau} + qx^2)dx \tag{4.14}$$

$$\hat{d}(x, \tilde{t}) = \int_{-\infty}^{\infty} u(q, \tilde{\tau} = \tilde{t} - qx^2)dq \tag{4.15}$$

Or in discrete form,

$$u(q, \tilde{\tau}) = \sum_{x} d(x, \tilde{t} = \tilde{\tau} + qx^2)) \tag{4.16}$$

$$\hat{d}(x, \tilde{t}) = \sum_{q} u(q, \tilde{\tau} = \tilde{t} - qx^2) \tag{4.17}$$

4.1.3 Inverse Parabolic Radon

In the frequency domain, Parabolic Radon transform can be represented as:

$$D(x,\omega) = \int_{-\infty}^{\infty} U(q,\omega) e^{-i\omega q x^2} dq \tag{4.18}$$

$$\hat{U}(q,\omega) = \int_{-\infty}^{\infty} D(x,\omega) e^{i\omega q x^2} dx \tag{4.19}$$

Replacing forward Radon transform into inverse Radon transform following equation is obtained:

$$\hat{U}(q,\omega) = \int_{-\infty}^{\infty}\int_{-\infty}^{\infty} U(\acute{q},\omega) e^{-i\omega \acute{q} x^2} d\acute{q} e^{-i\omega q x^2} dx \tag{4.20}$$

The above relation can be further simplified,

$$\hat{U}(q,\omega) = \int_{-\infty}^{\infty}\int_{-\infty}^{\infty} U(\acute{q},\omega) e^{i\omega x^2 (q-\acute{q})} d\acute{q} dx = \int_{-\infty}^{\infty} d\acute{q} U(\acute{q},\omega) \int_{-\infty}^{\infty} e^{i\omega x^2 (q-\acute{q})} dx \tag{4.21}$$

Let $\sigma(q,\omega)$ be equal to $\int_{-\infty}^{\infty} e^{\omega q x^2}$. Replacing the value of $\sigma(q,\omega)$ in above equation, following convolution equations are obtained.

$$\hat{U}(q,\omega) = U(q,\omega) * \sigma(q,\omega) \tag{4.22}$$

$$U(k_q,\omega) = \frac{\hat{U}(k_q,\omega)}{\sigma(k_q,\omega)} = \frac{\sqrt{\omega}\hat{U}(k_q,\omega)}{\acute{\sigma}(k_q)} \tag{4.23}$$

$\sigma(q,\omega)$ can be simplified as:

$$\sigma(q,\omega) = [1 + isign(q)]\sqrt{\frac{\pi}{2\omega|q|}} \tag{4.24}$$

$$U(k_q,\omega) = \frac{\sqrt{\omega k_p}\hat{U}(k_q,\omega)}{2\pi)} \tag{4.25}$$

4.1.4 Velocity-stack Representation

Parabolic Radon transform in the velocity domain was introduced by Yilmaz, 1989.

$$u(v,\tau) = \sum_x d(x, t = \tau + 4\frac{x^2}{v^2}) \tag{4.26}$$

$$\hat{d}(x,t) = \sum_q u(v, \tau = t - 4\frac{x^2}{v^2})) \tag{4.27}$$

4.2 Parabolic Radon Transform of Different Curves

In this section different events and their parabolic Radon transform are presented. For the derivation, the following set of equations are solved.

$$\psi(p,\tau;x) = t(x) - \phi(x) - \tau = 0 \tag{4.28}$$

$$\frac{\partial\psi(p,\tau;x)}{\partial x} = \frac{dt}{dx} - \frac{(d\phi(x)}{dx} = 0 \tag{4.29}$$

For Parabola $\phi(x) = qx^2$.

4.2.1 Point Source

Consider Linear curve

$$t(x) = \beta x \tag{4.30}$$

$$\frac{dt}{dx} = \beta \tag{4.31}$$

So a single point on C is represented as a line in the transform domain (-see Fig. 4.1).

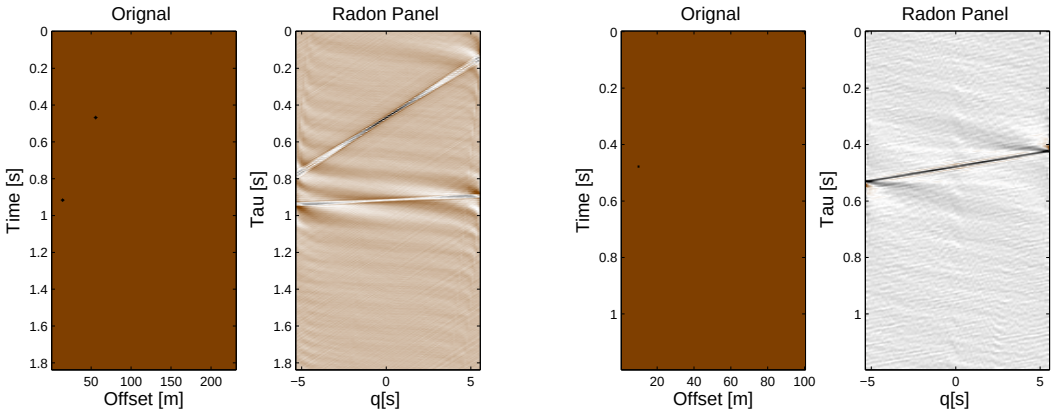

(a) (b)

Figure 4.1: Parabolic Radon Transform of Point

4.2.2 Parabolic Curve

Consider a parabolic curve 'q'. The curvature can be found by solving the eq. 4.28

$$q = \frac{\beta}{2x} \tag{4.32}$$

$$\tau = \frac{\beta x}{2} \tag{4.33}$$

Eliminating x, the following relation is obtained:

$$q\tau = \frac{\beta^2}{4} \tag{4.34}$$

the parabolic Radon transform of typical hyperbolic seismic events

$$t^2(x) = a + bx^2 \tag{4.35}$$

using previous equations,

$$q(x) = \frac{b}{2t(x)} \tag{4.36}$$

$$\tau(x) = \frac{t(x)}{2} + \frac{a}{2t(x)} \tag{4.37}$$

eliminating t(x)

$$\tau = \frac{b}{4q} + \frac{aq}{b} \tag{4.38}$$

Let $a = \frac{2h}{c}$ and $b = \frac{1}{c^2}$, we get

$$ct^2 = x^2 + 2h^2 \tag{4.39}$$

$$\tau = \frac{1}{2c^2 q} q + 2h^2 q \tag{4.40}$$

Curvature of the hyperbolic event

$$k(x) = \frac{\partial^2 t/\partial x^2}{\left(1 + \left(\partial t/\partial x\right)^2\right)^{3/2}} = \frac{dp(x)/dx}{1 + p^2(x)^{3/2}} \tag{4.41}$$

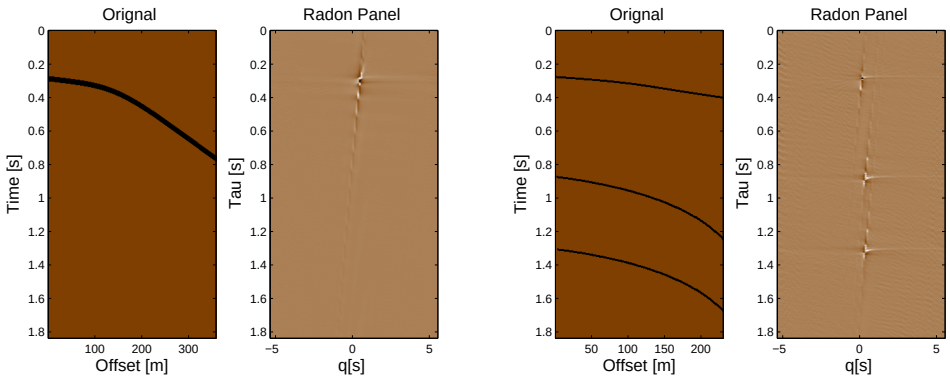

(a) (b)

Figure 4.2: Parabolic Radon Transform of curve

$$dt/dx = p(x) = 2xq \tag{4.42}$$

Moreover, $p(0) = 0$,$k(0) = dp(0)/dx$,$q(0) = k(0)/2$

$$q_a = \frac{b}{2\sqrt{a}} \tag{4.43}$$

$$\tau_a = \sqrt{a} \tag{4.44}$$

$$K_a = \frac{d^2\tau}{dq^2|_a} = \frac{b}{2{q_a}^3} = \frac{\tau_a}{{q_a}^2} = \frac{4t(0)}{K^2(0)} \tag{4.45}$$

So a parabolic curve C is represented as a point in the transform domain -see Fig. 4.2

4.3 Compressive Sensing using Parabolic Radon Transform

In this section, use of Parabolic Radon transform as a sparsifying transform for compressive sensing, is presented.

Let $g(n)$ be the sampled, acquired seismic data, vector with size N. This signal can be expanded in terms of orthonormal basis matrix $\boldsymbol{\psi}$ as follows:

$$g(n) = \sum_{i=1}^{N} x_i \psi_i(t), \tag{4.46}$$

where x_i are the coefficients sequence of $g(t)$. To make the formulation easier the signal $g(n)$ in terms of matrix as follows:

$$\boldsymbol{g} = \boldsymbol{\psi}\boldsymbol{x}. \tag{4.47}$$

Here, $\boldsymbol{\psi}$ has dimension $N \times N$. Also assume that the number of non zero entries in $\boldsymbol{g}$ are K. In other words, $\boldsymbol{g}$ is a K sparse vector with length N, when represented in basis $\boldsymbol{\psi}$. For the parabolic Radon transform $\psi_n = e^{i\omega_n \boldsymbol{q}\boldsymbol{x}^{\boldsymbol{2}\boldsymbol{T}}}$ or in matrix form

$$\boldsymbol{\psi} = \begin{bmatrix} e^{i\omega q_1 x_1^2} & e^{i\omega q_2 x_1^2} & e^{i\omega q_3 x_1^2} & \dots & e^{i\omega q_n x_1^2} \\ e^{i\omega q_1 x_2^2} & e^{i\omega q_2 x_2^2} & e^{i\omega q_3 x_2^2} & \dots & e^{i\omega q_n x_2^2} \\ \vdots & \vdots & \vdots & \vdots & \vdots \\ e^{i\omega q_1 x_n^2} & e^{i\omega q_2 x_n^2} & e^{i\omega q_3 x_n^2} & \dots & e^{i\omega q_n x_n^2} \end{bmatrix} \tag{4.48}$$

As $\boldsymbol{g}$ is K sparse vector, compressive sensing can be used to acquire the data with much less sample than suggested by the Shannon Nyquist theorem. So instead of sampling all the elements of $\boldsymbol{g}$, the signal can be recovered by less number of samples. Let $\boldsymbol{\phi}$ be another basis matrix, known as sensing matrix, with size $M \times N$, where $M \ll N$. The sampled signal $\boldsymbol{g}$ can be represented in terms of new basis $\boldsymbol{\phi}$, as follows:

$$\boldsymbol{y} = \boldsymbol{\phi g} \tag{4.49}$$

$$\boldsymbol{y} = \boldsymbol{\phi \psi x} \tag{4.50}$$

Let $\boldsymbol{A} = \boldsymbol{\phi \psi}$,measurement matrix, with dimension $M \times N$. The (4.50) simplifies to

$$\boldsymbol{y} = \boldsymbol{Ax} \tag{4.51}$$

To recover the original signal we have to find the coefficient vector $\hat{\boldsymbol{x}}$ by solving the following relation

$$\boldsymbol{A}\hat{\boldsymbol{x}} = \boldsymbol{b} \tag{4.52}$$

where

$$\boldsymbol{b} = \boldsymbol{\phi g} \tag{4.53}$$

Here $\boldsymbol{A}$, is a rectangular matrix, with less rows than the columns. So $\boldsymbol{A}$ is an under-determined system of linear, number of unknowns are greater than the number of equations. Restricted isometric property(RIP) can be utilized for the perfect reconstruction of the under-sampled data [63]. The RIP is a sufficient

a sufficient condition for many sparsifying recovery theorem. Besides RIP the sensing matrix and representation matrix should have incoherence [41]. If the RIP and incoherence is satisfied then one way to solve compressive sensing problem is by using the l_1-norm for the reconstruction, the following model is obtained:

$$\min \|\boldsymbol{x}\|_1 \text{subject to } \boldsymbol{A}\boldsymbol{x} = \boldsymbol{b} \tag{4.54}$$

Once the coefficients are estimated by l_1-norm then the original signal can be recovered by using the following relation

$$g = \boldsymbol{\psi}\hat{x} \tag{4.55}$$

Because of the fact that most of the practical problems may involve large measurement matrix, finding an appropriate measurement matrix $\boldsymbol{\phi}$ is big challenge. Fortunately there are number of techniques have been suggested for easier selection of the measurement matrix. One of the suggested approach is to randomly choose N unit vectors in K-dimensional space. Or randomly choose K rows from an $N \times N$ orthogonal matrix and normalize the columns for the measurement matrix [41]. One other approach that is used a lot is to form a matrix with randomly chosen Gaussian entries [88]. All these techniques work for Compressive sensing as long the following relation is satisfied

$$M \geq cK \log(N/K), \tag{4.56}$$

4.4 Applications of Compressive Sensing and Parabolic Radon Transform

In the remaining part of this chapter, different application of seismic data processing using compressive sensing and parabolic Radon transform are discussed. The applications that are discussed

- Interpolation of non-linear missing seismic traces
- Classification of non-linear seismic events
- Deconvolution of seismic data
- Multiple reflection removal from seismic data

4.5 Interpolation of Missing Non-Linear Seismic Events

During the last few years the demand for denser seismic traces has increased a lot. Most famous methods are based on transformation of seismic data into another domain like wavelet, Radon, curvlet. Transform based methods are discussed in [89–91]. Similarly there are some techniques based on filters as discussed in [92]. Berkhout and Verschuur uses the primary reflection energy for the interpolation [94]. Same energy concept is extended in Curry and Shan (2006). Interferometric interpolation of missing seismic data is discussed in [96]. Hermann has used the curvlet with compressive sensing in [97, 98].

Here, a new technique for the interpolation of missing seismic traces, based on compressive sensing where Radon transform being the sparsifying domain, is presented. Once the data is acquired in compressed fashion via compressive sensing, a certain feature of the compressed signal in Radon domain is used for the interpolation. Finally, the data is converted back from the Radon domain to time space(t-x) domain, which contains the interpolated data.

Algorithm

Given a seismic record, the proposed compressive sensing with parabolic Radon transform $\tau - q$ method for interpolation of missing seismic traces is stated as follows:

1. Use the compressive sensing to acquire the seismic data in the compressed fashion as described in the section.
2. Use the following facts for the thresholding:
   (a) The curves are converted to single points in the $\tau - q$ domain.
   (b) These points have higher value than the points corresponding to the noise or irrelevant curves.
3. Apply the inverse parabolic Radon transform to the previous step result.

Overall algorithm is presented in the Figure 4.3.

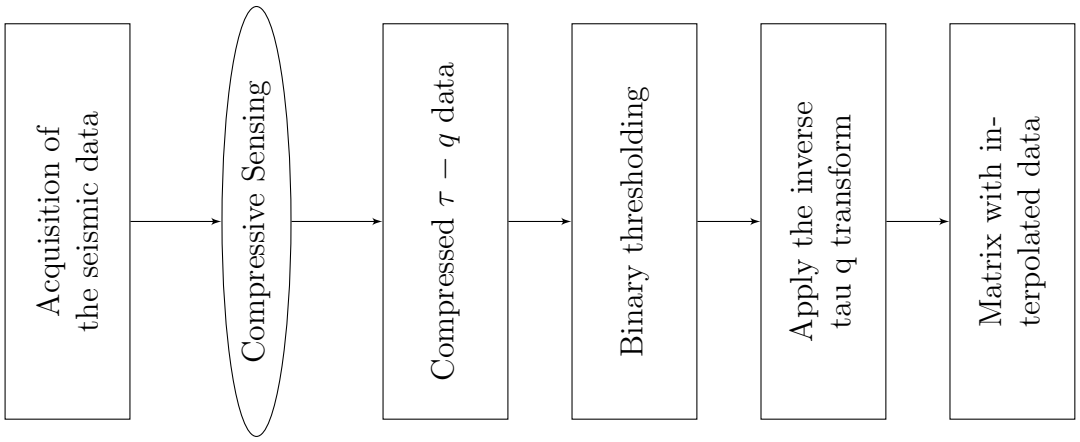

Figure 4.3: Workflow of the proposed technique for interpolation of hyperbolic and parabolic events

4.5.1 Simulation Result

Total number of traces in the seismic data are 50 (N=50). Out of which 19 are missing. For the sparsifying transform parabolic Radon transform is used which interpolates the non linear events. Compressive sensing with parabolic Radon transform is used for the interpolation of missing seismic traces. Figure 4.4b shows the compressed $\tau - q$ domain with M=10. Now based on the second step of the proposed algorithm the binary image is presented in the Figure 4.4c. Finally the results after the application of the inverse $\tau - q$ transform are presented in Figure 4.4d. Besides 18 missing traces (33%), with the help of compressive sensing, additional 80% compression is achieved.

To test the robustness of the proposed setup, data with different noise level was tested. Total number of traces and number of missing traces are same as for the noiseless case. The results after the addition of the noise with 0.1 standard deviation and 80% compression are presented in Figure 4.5.

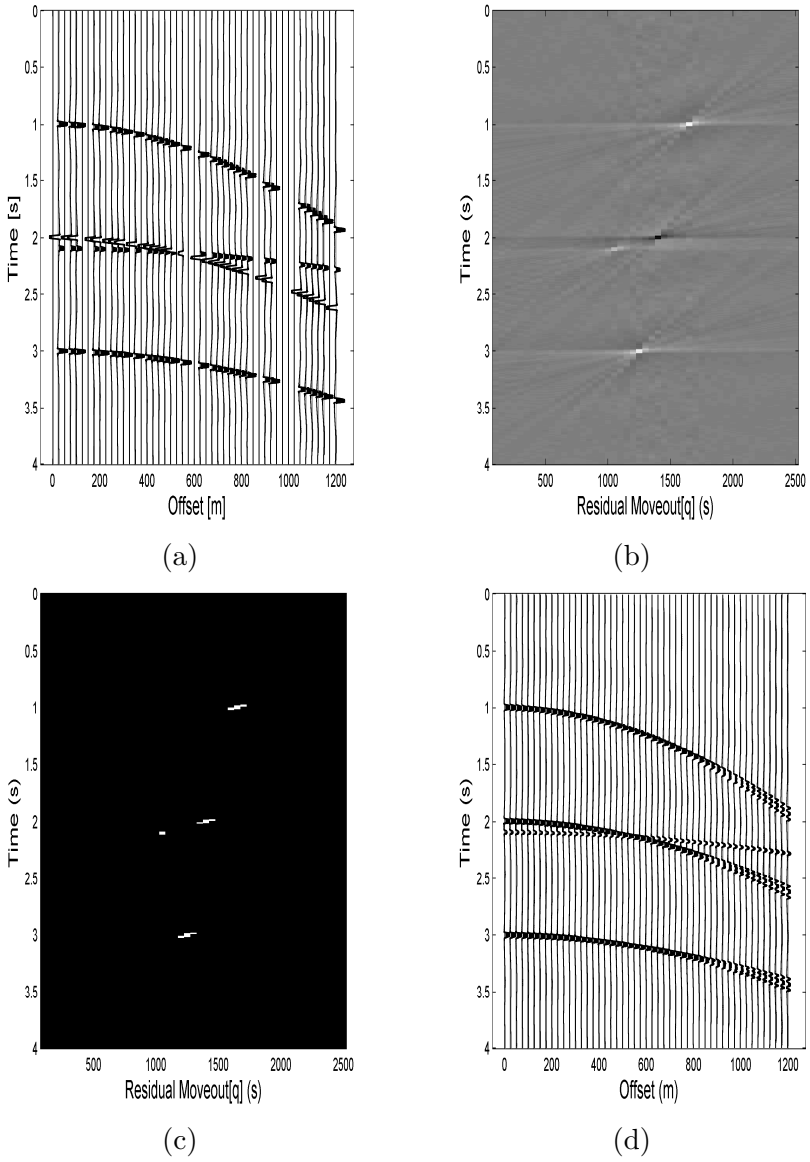

(a) (b) (c) (d)

Figure 4.4: (a) The synthetic seismic reflected data. (b) The compressed $\tau - q$ transform of (a), after the acquisition in compressed fashion with M=10 (80%compression). (c) The produced binary mask (white stands for one and black for zero) of (b). (d) The interpolated data after taking the inverse $\tau - q$ transform to the (c).

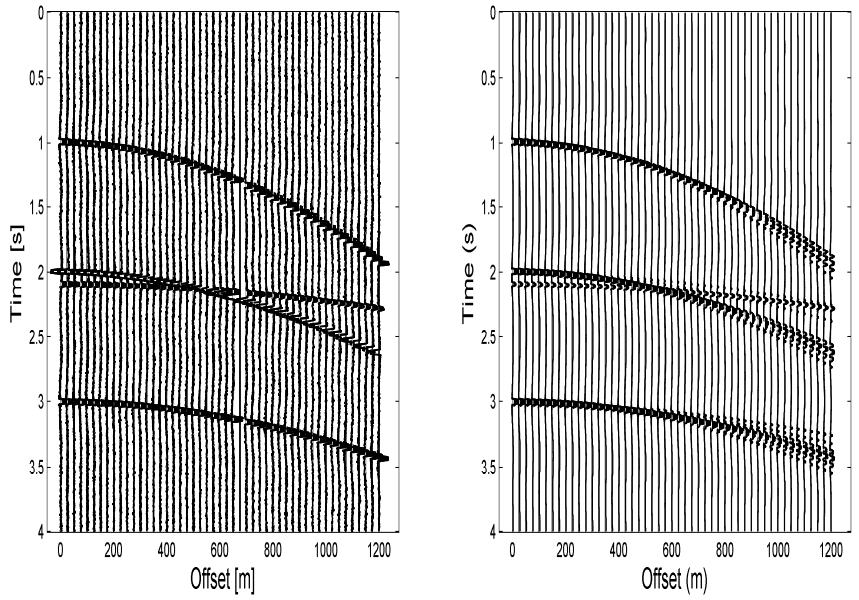

(a) (b)

Figure 4.5: (a) The synthetic seismic reflected data with 10% random Gaussian noise. (b) The interpolated data after taking the inverse $\tau - q$ transform and M=10 (80%compression).

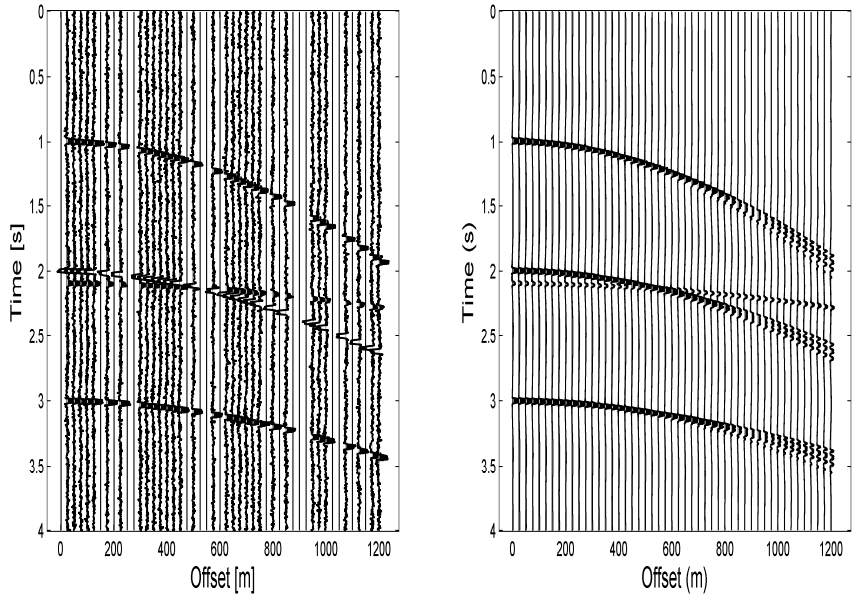

(a) (b)

Figure 4.6: (a) The synthetic seismic reflected data with 20% random Gaussian noise. (b) The interpolated data after taking the inverse $\tau - q$ transform and M=10 (80%compression).

Similar comparison after the addition of white noise with standard deviation 0.2 and 0.4 are presented in the Figure 4.6 and 4.7 respectively.

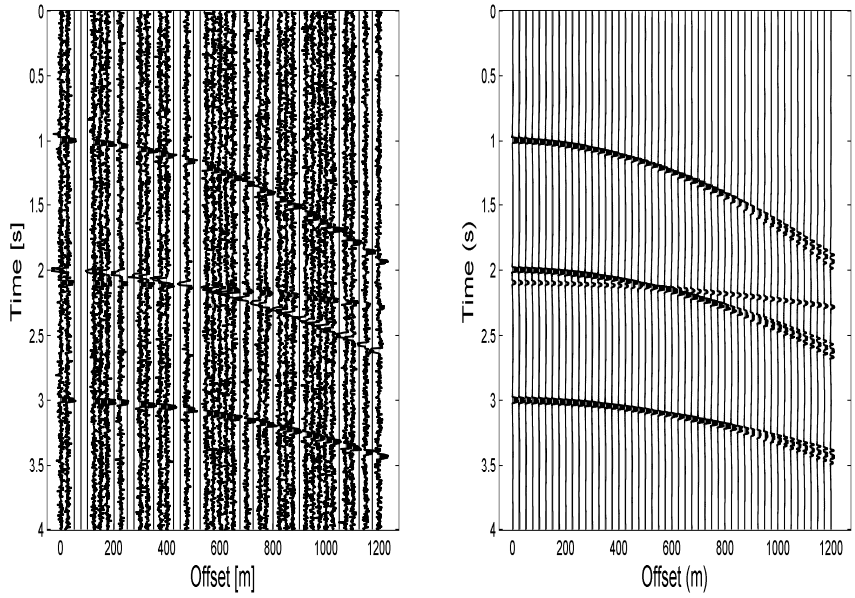

(a) (b)

Figure 4.7: (a) The synthetic seismic reflected data with 40% random Gaussian noise.(b) The interpolated data after taking the inverse $\tau - q$ transform and M=10 (80%compression) .

The proposed formulation, of compressive sensing using parabolic Radon transform, was tested on the data [129] as shown in the Figure 4.8a.

Total number of traces in the data are 481. Out of these 481 traces 161 traces are missing. Figure 4.8a shows the result of the proposed algorithm without any compression. From the interpolated data, it can be deduced that besides the interpolation the resolution of the curves has also increased. The results with different compressions are presented in figure 4.9.

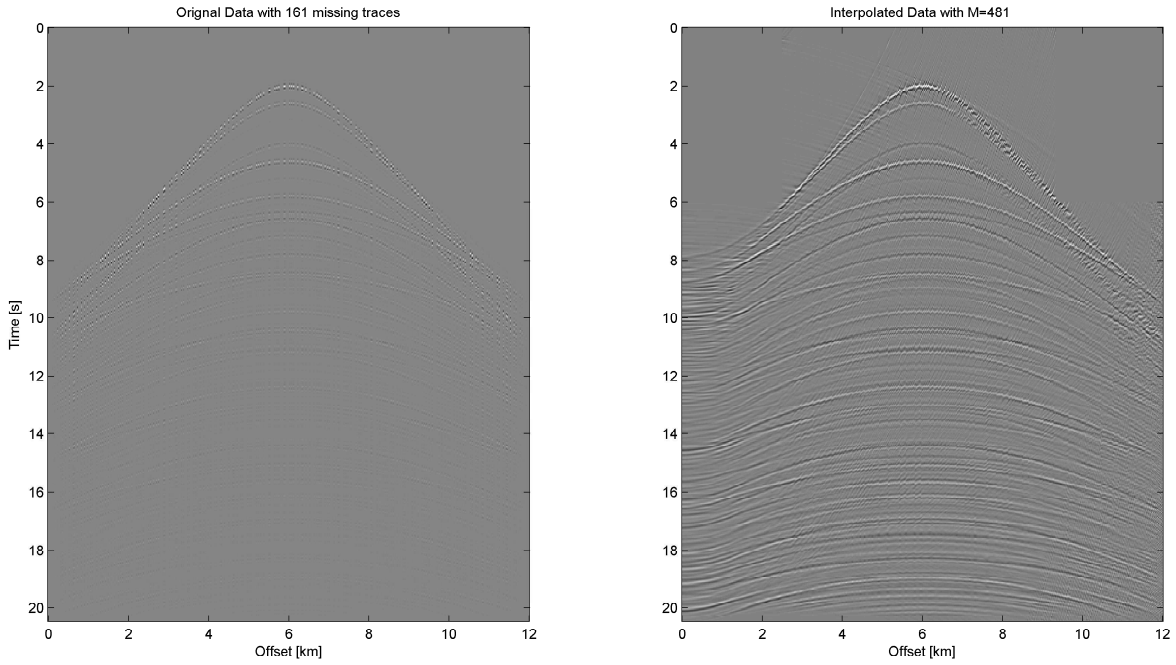

(a)

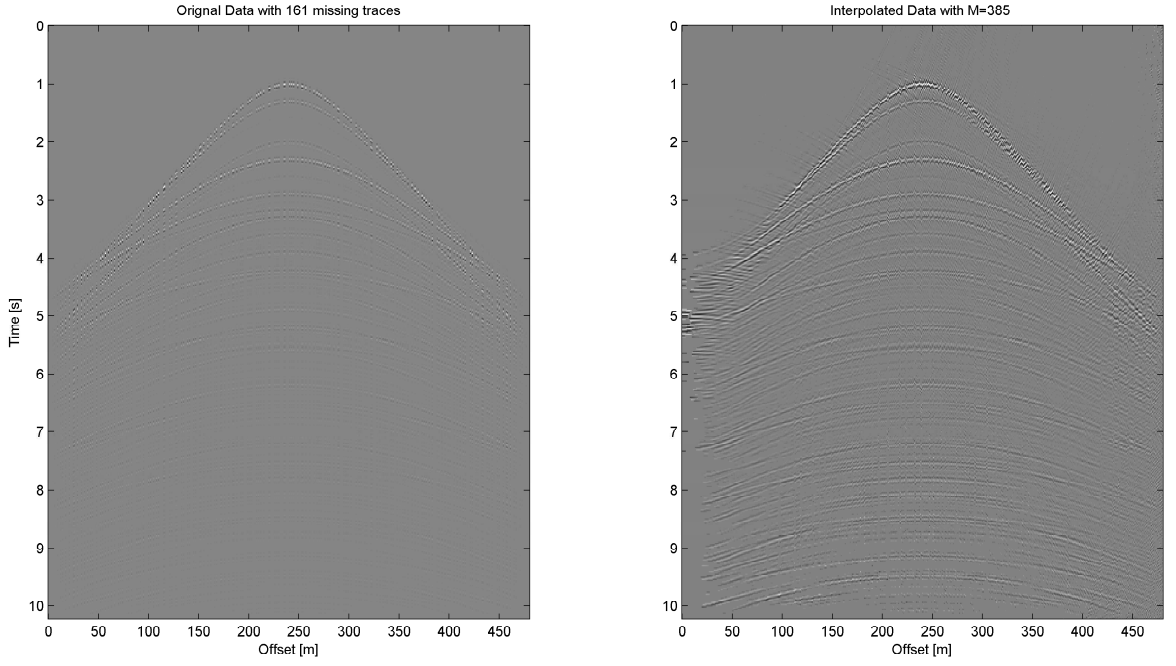

(b)

Figure 4.8: (a)Interpolation of missing seismic traces using Radon transform with total number of traces 481. Total number of missing traces are 161. (N=481, M=481).(b) provides the result with 20% compression respectively(M=381).

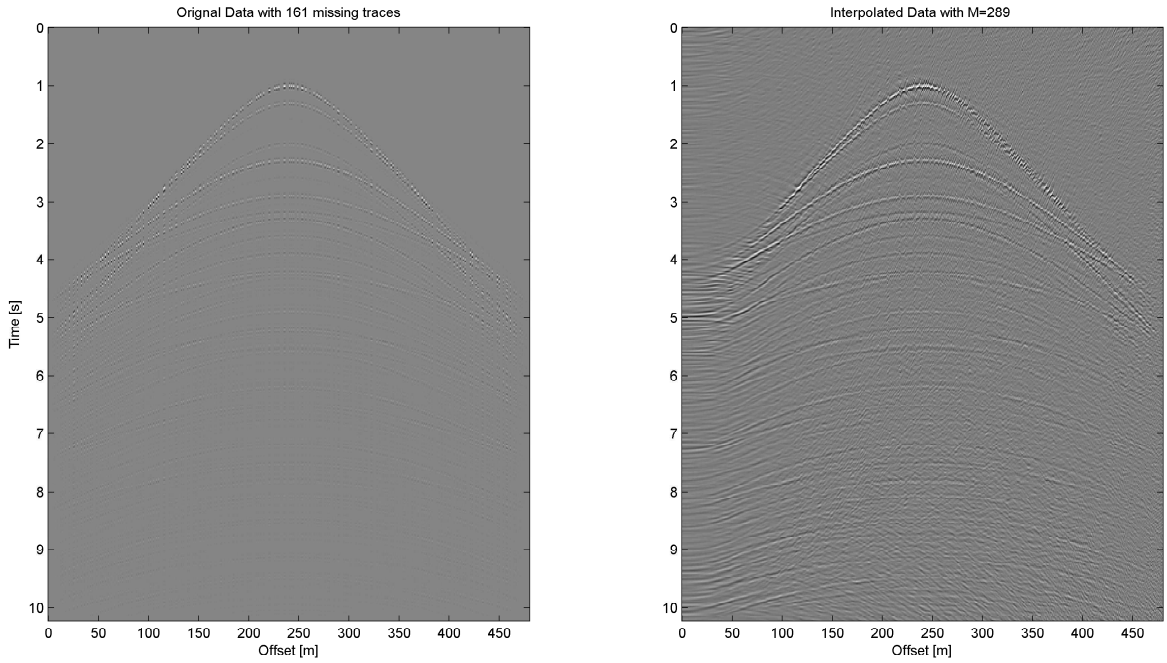

(a)

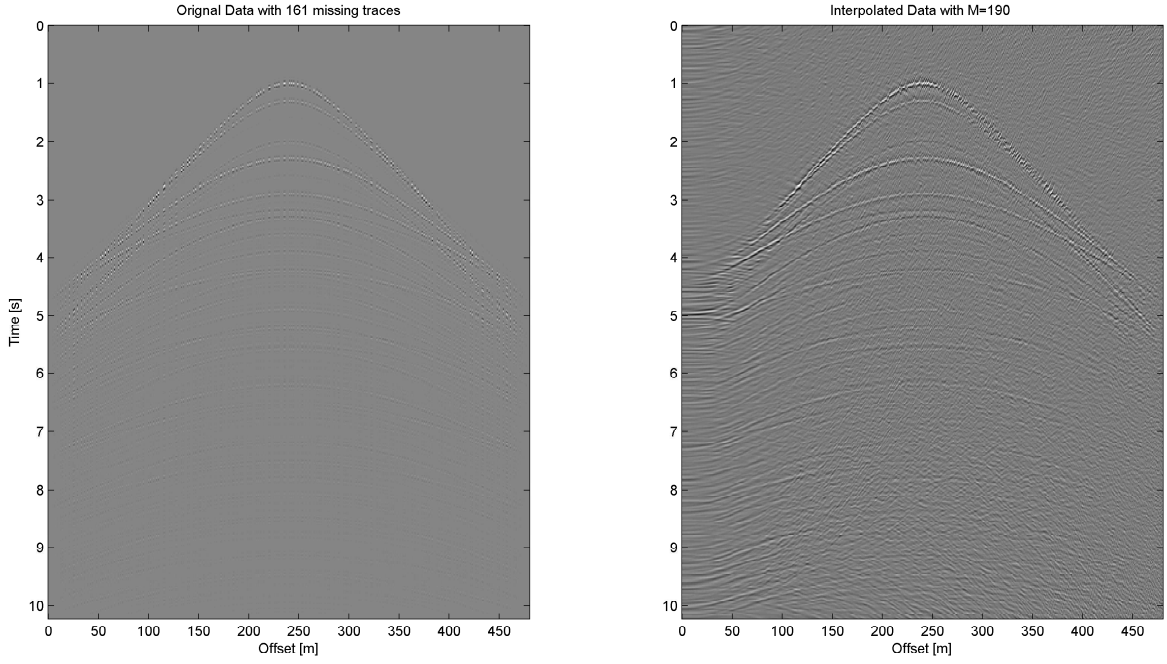

(b)

Figure 4.9: Interpolation of missing seismic traces using Radon transform with total number of traces 481. Total number of missing traces are 161. (a),(b) provides the result with 40 and 60 % compression respectively(M=289,190).

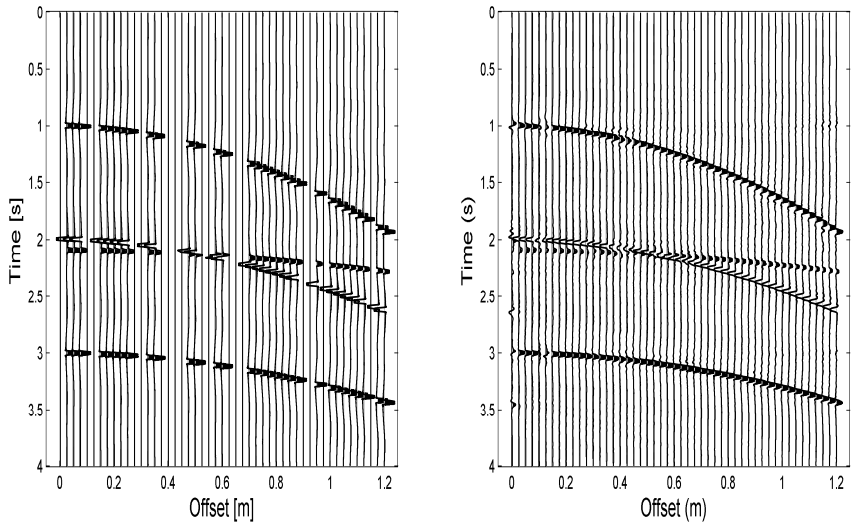

(a) (b)

Figure 4.10: Interpolation of missing seismic traces using compressive sensing with Curvelet transform N=50

Comparison with curvelet transform

Similar to the linear Radon case, comparison with curvelet is presented here. Results for same data with different noise level using curvelet is presented in Figure 4.10, and 4.11.

The result for real data interpolation using curvelet transform is presented in Figure 4.12. The curvelet works well for the high intensity curves. But unlike Radon it does not increase the resolution. Parabolic Radon transform, interpolates the missing traces even for high noise levels and low compression levels. On the other hand, curvelet transform does not perform well when SNR is low. Besides the performance issue a major difference between the Curvelet and the proposed setup is the computation time.

Table 4.1 shows the run time for different level of compression for proposed setup and curvelet transform for 0 % noise. The comparison for different noise level

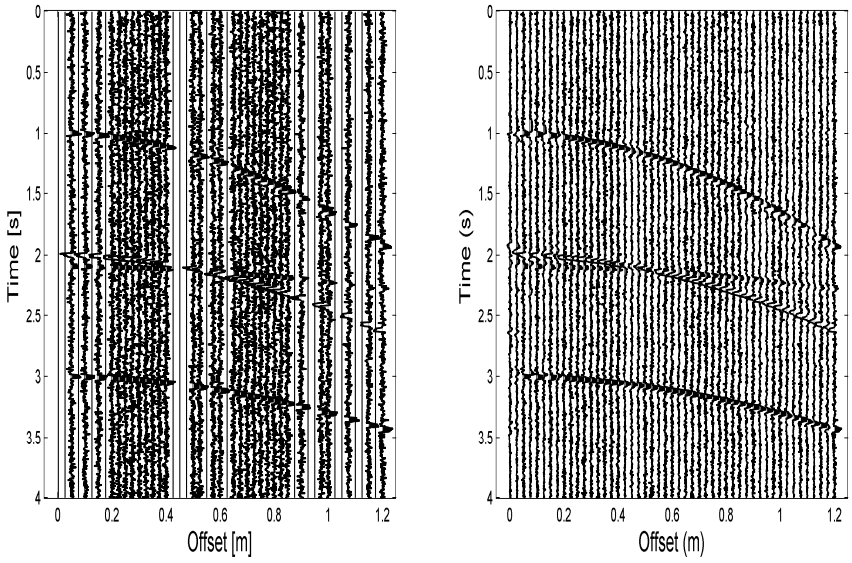

(a) (b)

Figure 4.11: Figure (b) shows the interpolation of the synthetic data using curvelet transform as the sparsifying transform for the compressive sensing with 40% noise.

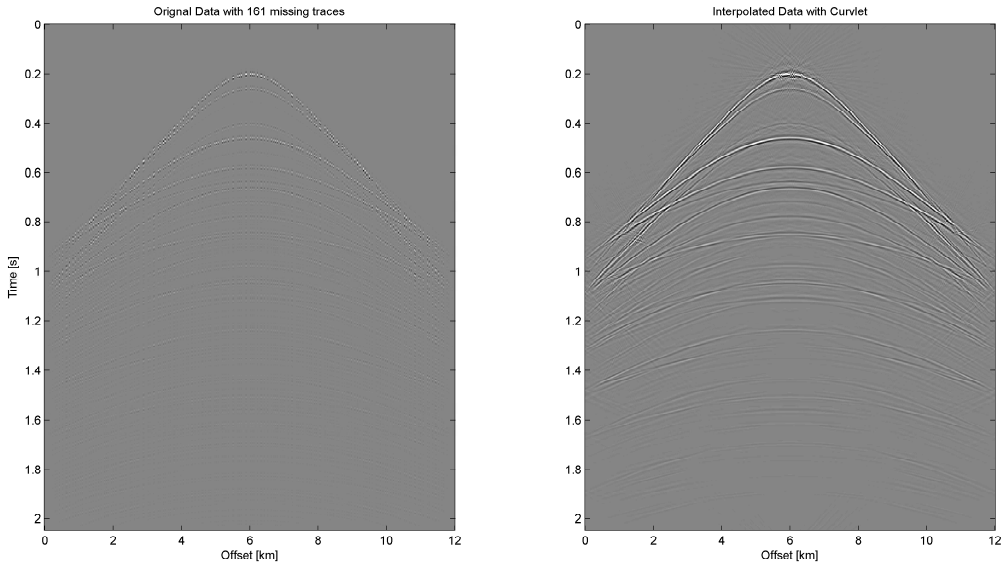

Figure 4.12: Interpolation of missing seismic traces of the data using compressive sensing with Curvelet

is presented in table 4.2. Also the computation time for real data interpolation is tabulated in table 4.3.From the results it is clear that proposed algorithm is about 25 times faster than the curvelet.

Transform Type	Compression	Time
Radon Transform	20%	1.231985 seconds
Radon Transform	40%	1.250185 seconds
Radon Transform	60%	1.303519 seconds
Radon Transform	80%	1.298178 seconds
Curvlet Transform	-	20.584001 seconds

Table 4.1: Time comparison: Parabolic Radon transform vs Curvelet transform, Noise-less case

Noise	Time Radon	Time Curvlet
0 %	1.27 seconds	20.58 seconds
10%	1.28 seconds	20.83 seconds
20%	1.28 seconds	21.01 seconds
30%	1.29 seconds	22.28 seconds
40%	1.30 seconds	25.26 seconds

Table 4.2: Time comparison: Parabolic Radon transform vs Curvelet transform

Transform Type	Compression	Time
Radon Transform	20	3.11 seconds
Radon Transform	40	3.28 seconds
Radon Transform	60	3.48 seconds
Curvelet Transform	-	53.55 seconds

Table 4.3: Time comparison: Parabolic Radon transform vs Curvelet transform (Data II)

Interpolation of Missing Seismic Events by Hybrid Radon transform

Previously, linear and parabolic Radon transform are used for the interpolation of linear and non linear seismic events respectively. Here a new scheme for interpolation, based on hybrid Radon transform, is tested on a real dataset. Hybrid

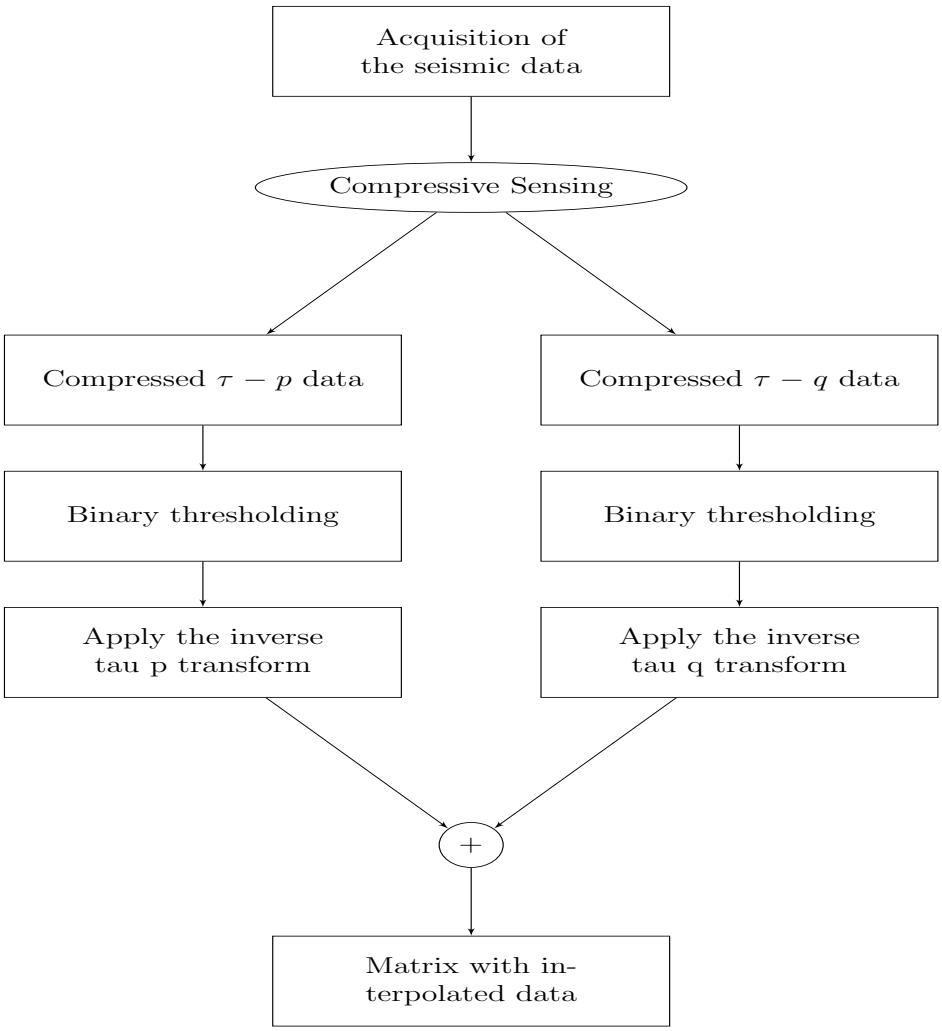

Figure 4.13: Workflow of the proposed technique for interpolation seismic events

Radon transform [130] uses linear and parabolic Radon transform at the same time. Overall work-flow is presented in the 4.13.

The proposed method is applied on the data set from Yilmaz (2001). Shot gather 6 (Figure 4.14a), which consists of 48 traces with sampling time 4 ms and spacing 100m. Out of 48 traces, 20 traces are randomly missing as shown in Figure 4.14b. The result after the interpolation of the missing data shown in 4.14c.

The results for 60% compression are shown in Figure 4.15. The Comparison with curvelet is also presented in Figure 4.16.

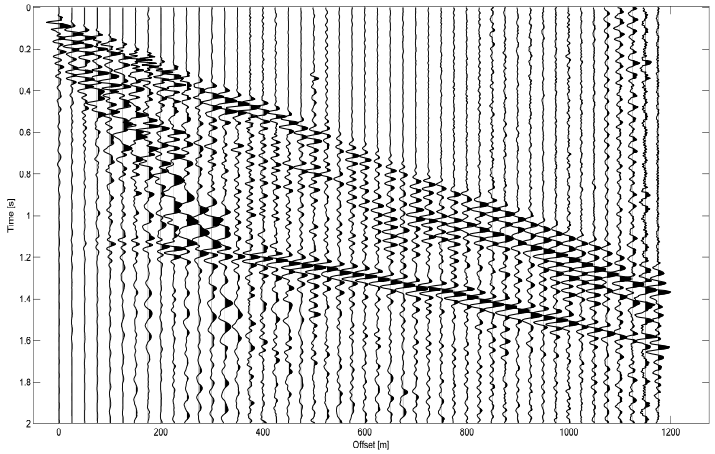

(a)

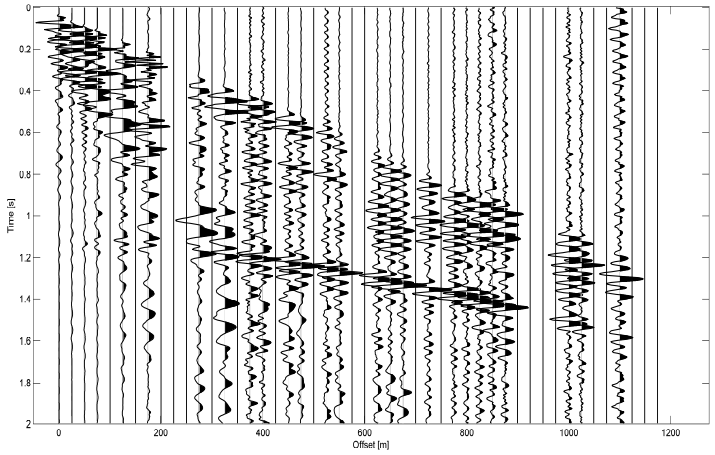

(b)

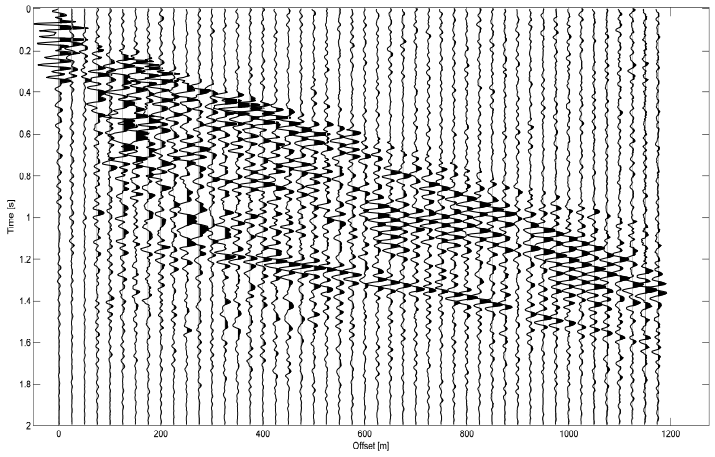

(c)

Figure 4.14: (a) The real data set(shot record 6) from Yilmaz (2001). Same data with randomly missing 20 traces is shown in (b). The interpolated data after applying the proposed hybrid algorithm is presented in (c) with M= 40

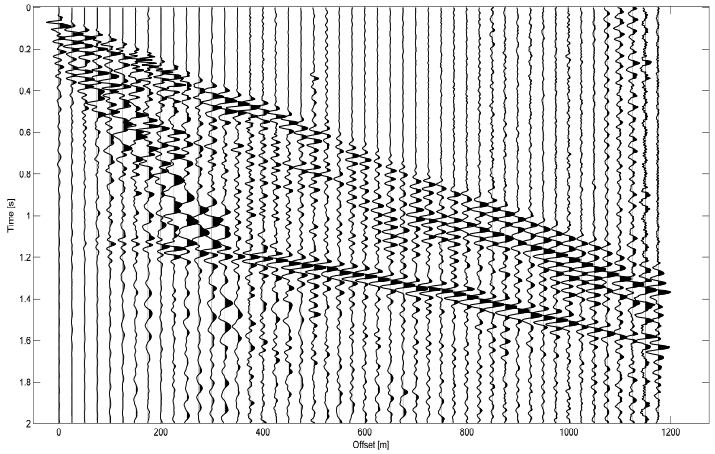

(a)

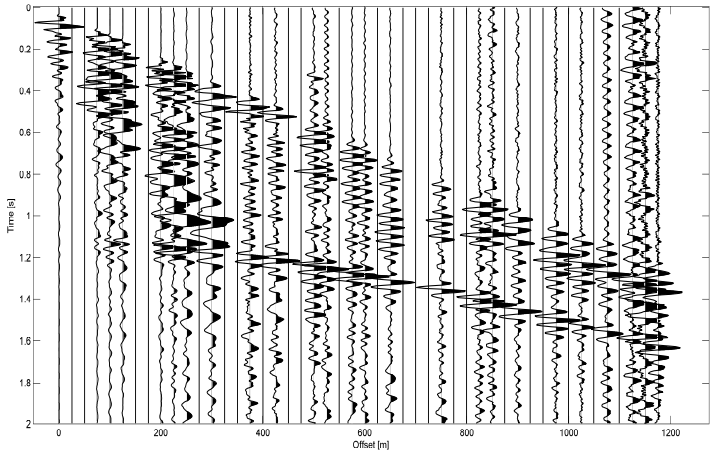

(b)

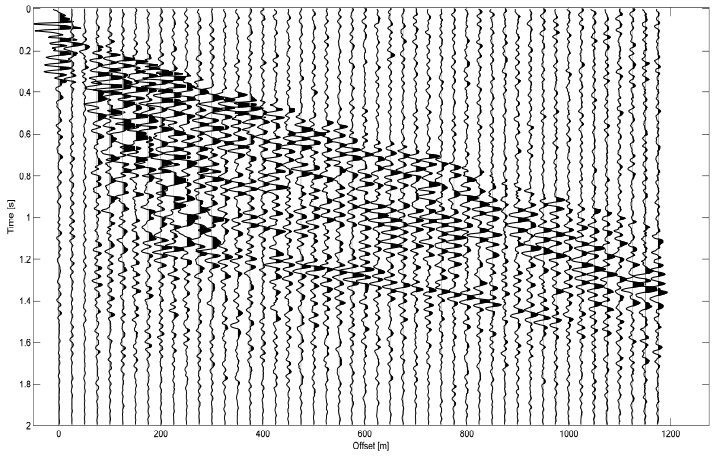

(c)

Figure 4.15: (a) The real data set(shot record 6) from Yilmaz (2001). Same data with randomly missing 20 traces is shown in (b). The interpolated data after applying the proposed hybrid algorithm is presented in (c) with M= 20

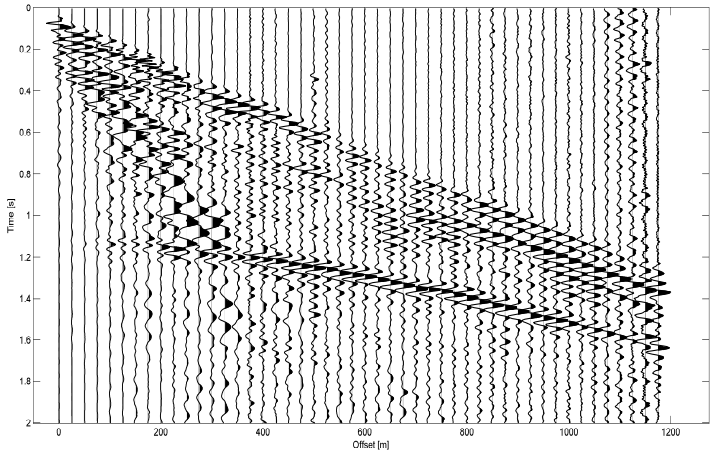

(a)

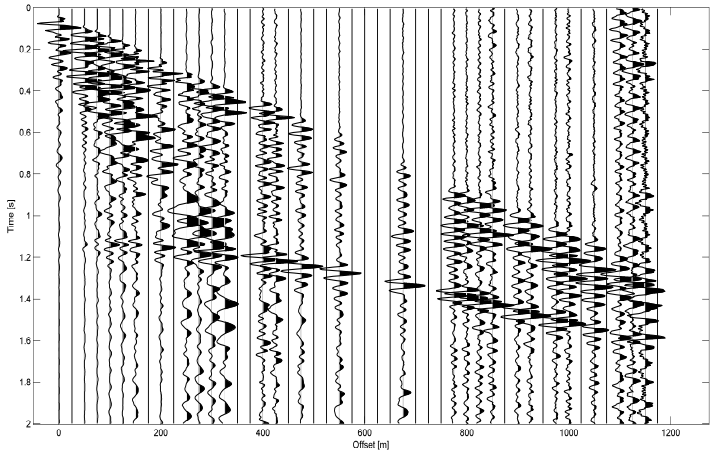

(b)

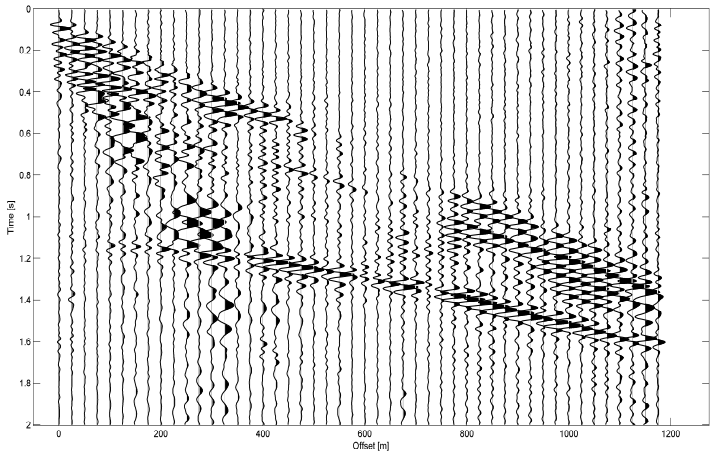

(c)

Figure 4.16: Interpolation : Compressive sensing with Curvelet Transform

4.6 Classification: Separation Of Non-Linear Seismic Events

Parabolic Radon transform as a sparsifying transform for the compressive sensing can also be used for the extraction of non-linear events like primary reflections and multiple reflection. By combining Parabolic Radon transform and compressive sensing, these non-linear events can be separated at the time of acquisition. We can capture only the parabolic events . By using compressive sensing we can separate the non linear events at the time of acquisition. Basic model remains the same as discussed in the case of interpolation. For the separation of non-linear events, the fact that non-linear event mapped to single point in $\tau - q$ domain, is used. On the other hand, the linear events spreads out in $\tau - q$ domain. Spread out events have lower value than the non-linear events, hence these events can be muted by doing some thresholding.

4.6.1 Simulation Results

For the simulation, synthetic data(4.17) is used. The data contain total 7 events, out of these 7 events 4 are linear and 3 are non-linear events. The results after applying the Parabolic Radon transform along with the compressive sensing are presented with different compression level in figure 4.18. To test the robustness of the proposed method result, after the addition of the 10% and 30% random noise, are presented in Figure 4.19 and Figure 4.20.

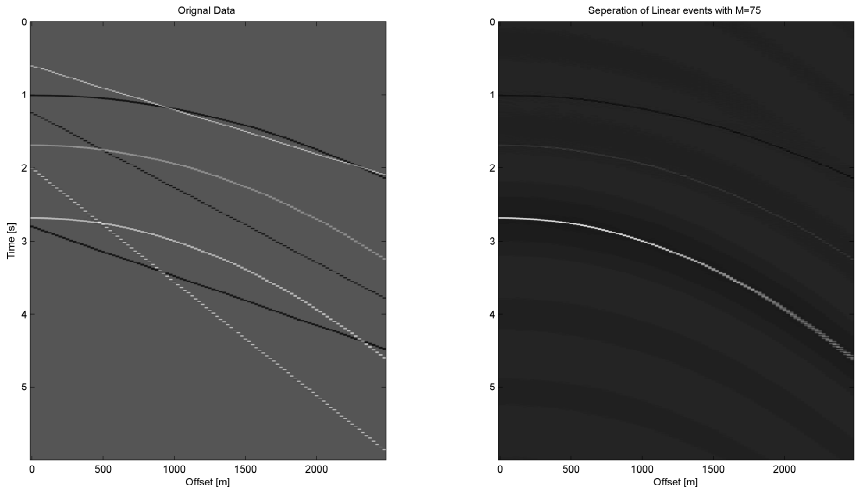

Figure 4.17: Separation Of non-Linear Seismic Events with N=100 and M=75.

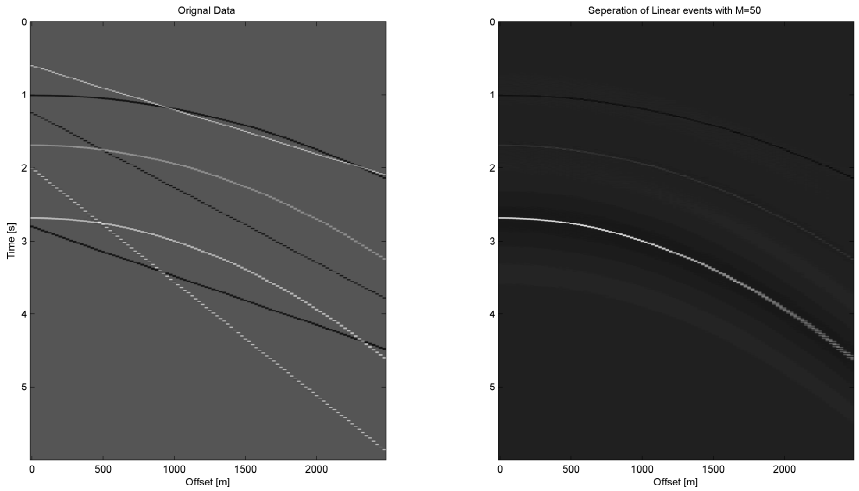

(a)

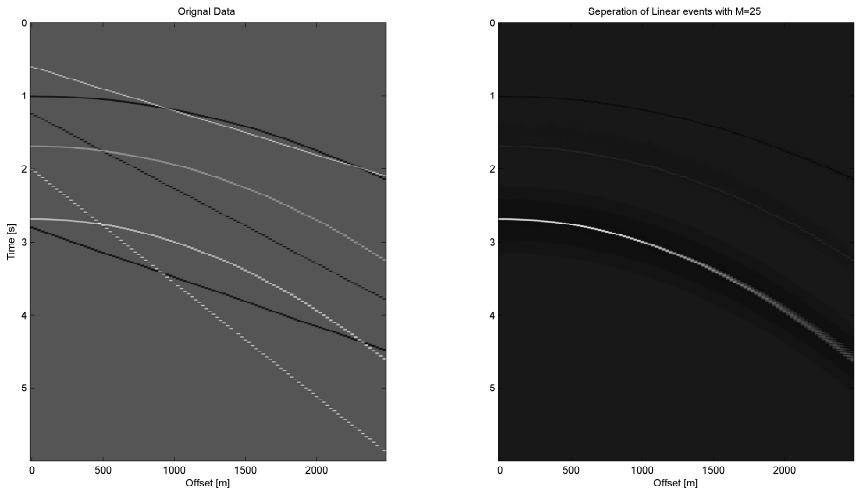

(b)

Figure 4.18: (a)Separation Of Linear Seismic Events with N=100, M=50 (50% compression). (b) Seperation with M=25 (25% compression)

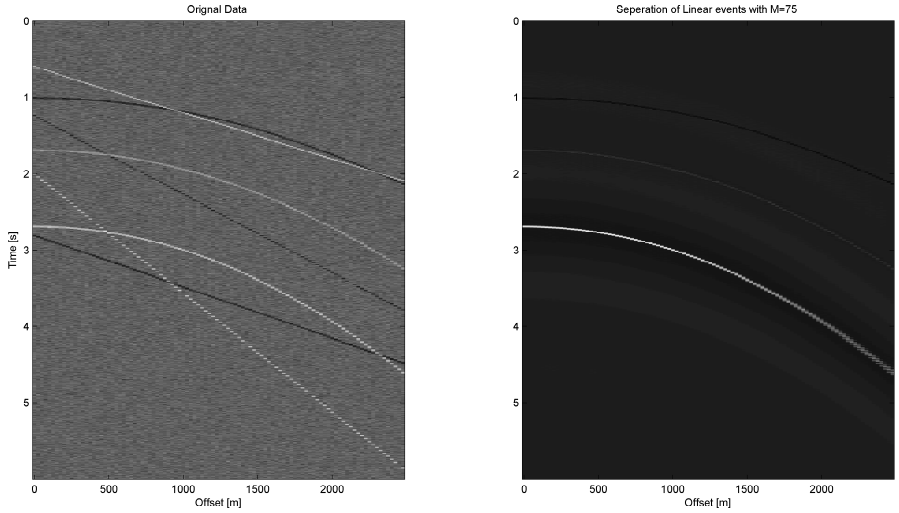

(a)

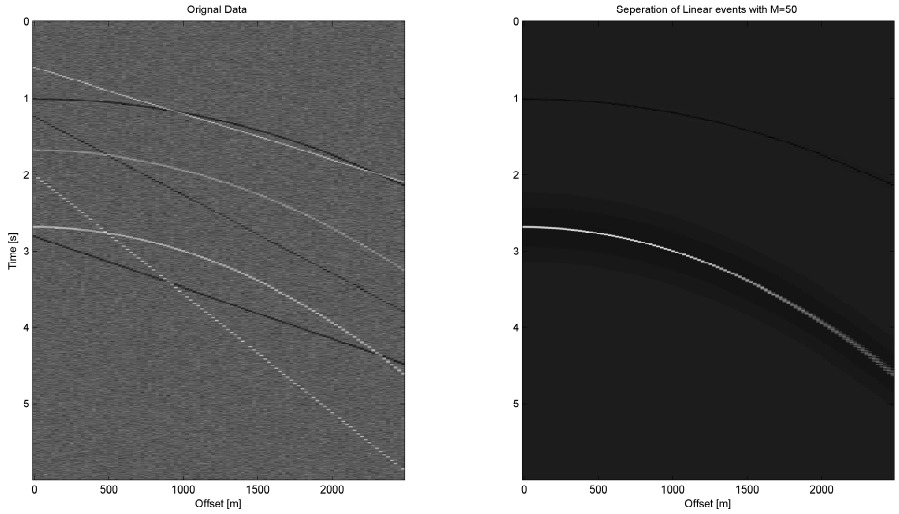

(b)

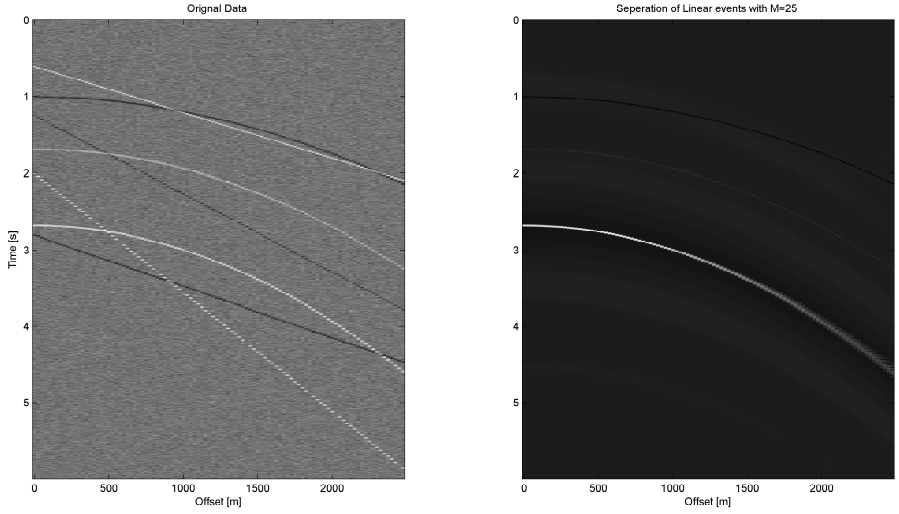

(c)

Figure 4.19: Separation Of Linear Seismic Events with 10% Noise with N=100. (a), (b) and (c) presents the results with M=75,50,25 respectively

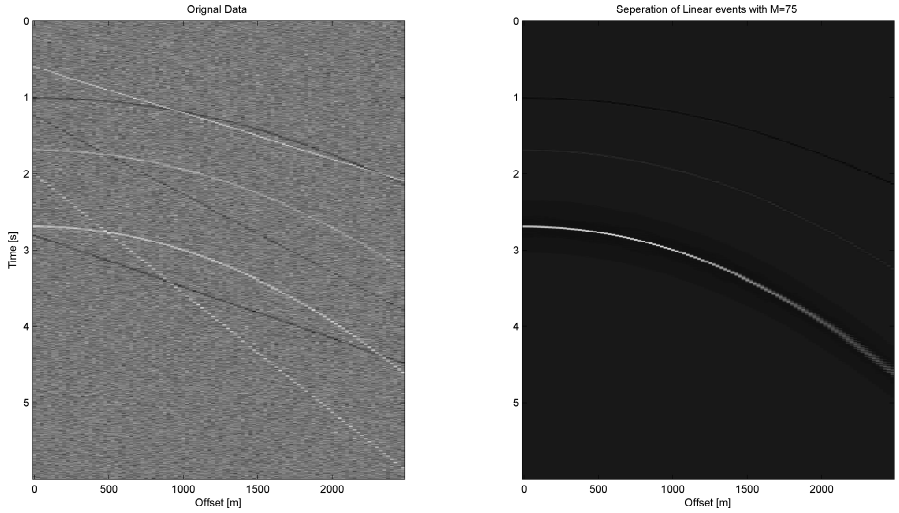

(a)

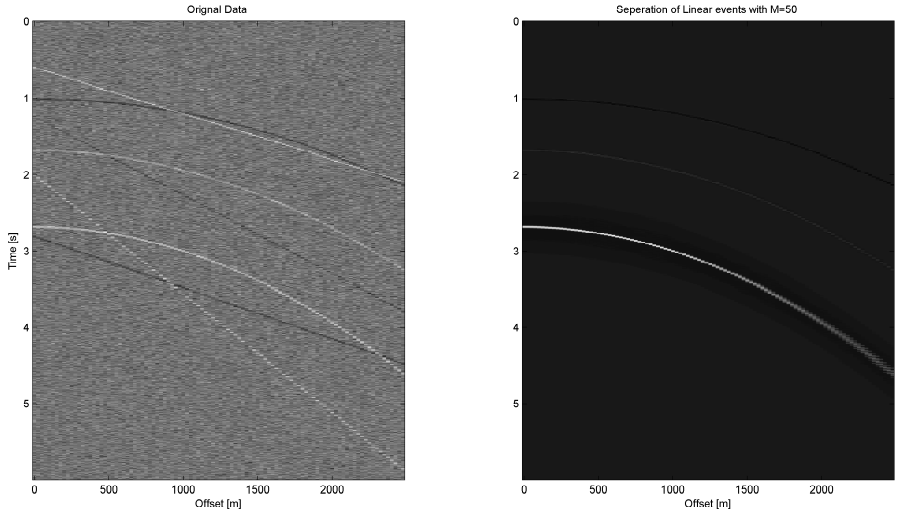

(b)

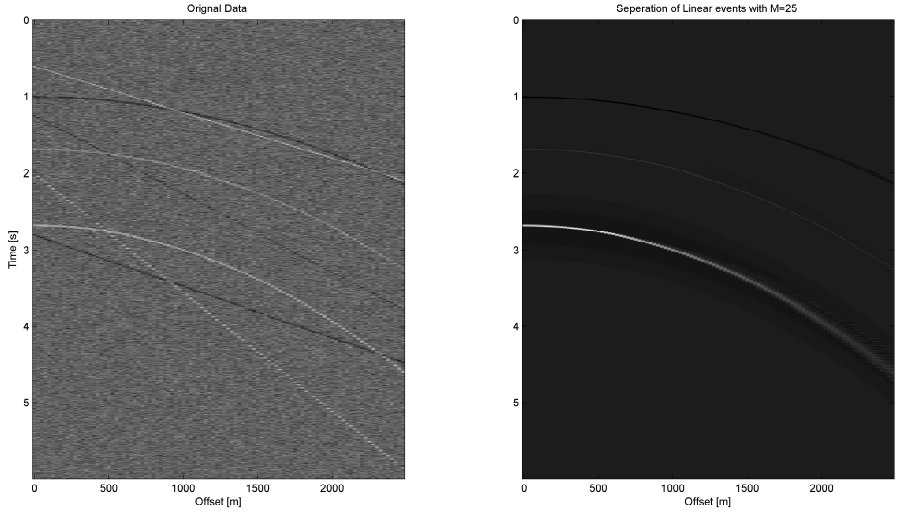

(c)

Figure 4.20: Separation Of Linear Seismic Events with 20% Noise with N=100. (a), (b) and (c) presents the results with M=75,50,25 respectively

4.7 Deconvolution

Deconvolution is used to retrieve the reflectivity from the seismic data. It is a filtering process in which wavelet is removed from the captured seismic data. Most common way of deconvolution is the use of Weiner filter, transferring one wavelet into another in least square sense. There are many deconvolution techniques has been proposed for seismic data such as predictive.

Maximum entropy based entropy was introduced by Burg (1967) [101–103]. This effective technique is known as spiking deconvolution but it is sensitive to noise variance. To minimize the effect of noise a consistent relative entropy method is discussed in [104–106]. Deconvolution based on zero-lag is presented in [107, 108]. The most famous type of deconvolution is predictive deconvolution [109, 110]. Predictive deconvolution is independent of the lag value and uses the relative entropy concept. It removes the multiples and even increase the resolution. Commercially a combination of deterministic and predictive deconvolution is used.

In this paper a new technique for the seismic deconvolution, based on Radon transform and a new sampling scheme, compressive sensing, is presented. The Radon transform as a sparsifying transform for the compressive sensing can be used for seismic deconvolution at the fly. Finally the data is converted back from the Radon domain to t-x domain.

Algorithm

Given a seismic record, the proposed compressive sensing with Radon transform method for seismic deconvolution is stated as follows:

1. Use the compressive sensing to acquire the seismic data in the compressed fashion as described in the previous section.

2. Use the following facts to generate an automatic mask:

   (a) The curves are converted to single points in the Radon domain.

   (b) These points have higher value than the points corresponding to the noise or irrelevant curves.

3. Multiply the mask with the compressed Radon domain. This will leave only the curves in the Radon domain.

4. Apply the inverse linear Radon transform to the previous step result.

4.7.1 Simulation Results

The synthetic data contains four reflections as shown in Figure 4.21a. The total number of traces in the data are 50(N=50) with spatial sampling interval 25m and sampling interval 4m/s. Figure 4.21b shows the compressed $\tau - q$ domain with M=40. Now based on the third step of the proposed algorithm the Radon domain after muting of the non-significant part is presented in the Figure 4.21b. Finally the results after the application of the inverse parabolic Radon transform

Transform Type	Compression	Time
Radon Transform	80%	0.225 seconds
Radon Transform	60%	0.226 seconds
Radon Transform	40%	0.233 seconds
Radon Transform	20%	0.234 seconds
Fx deconvolution	-	0.322 seconds

Table 4.4: Time comparison: Parabolic Radon transform vs FX-deconvolution

are presented in Figure 4.21d, which shows the deconvolution results with 20% compression. The estimated noise is presented in Figure 4.21e.

Seismic deconvolution results for 40% and 60% compression are presented in Figure 4.22 and 4.23.

It is evident from the results, the proposed deconvolution algorithm provides reasonable good results even for high compression level. One of the most common technique of seismic deconvolution is the fx-deconvolution. Figure 4.24 provides the deconvolution results with fx-deconvolution.

Computationally the comparison between the both technique is presented in the table 4.4. Algorithm was tested on Intel Core i7 processor. The proposed algorithm is faster than the fx-deconvolution but the major difference is in the number of samples needed for the both technique.

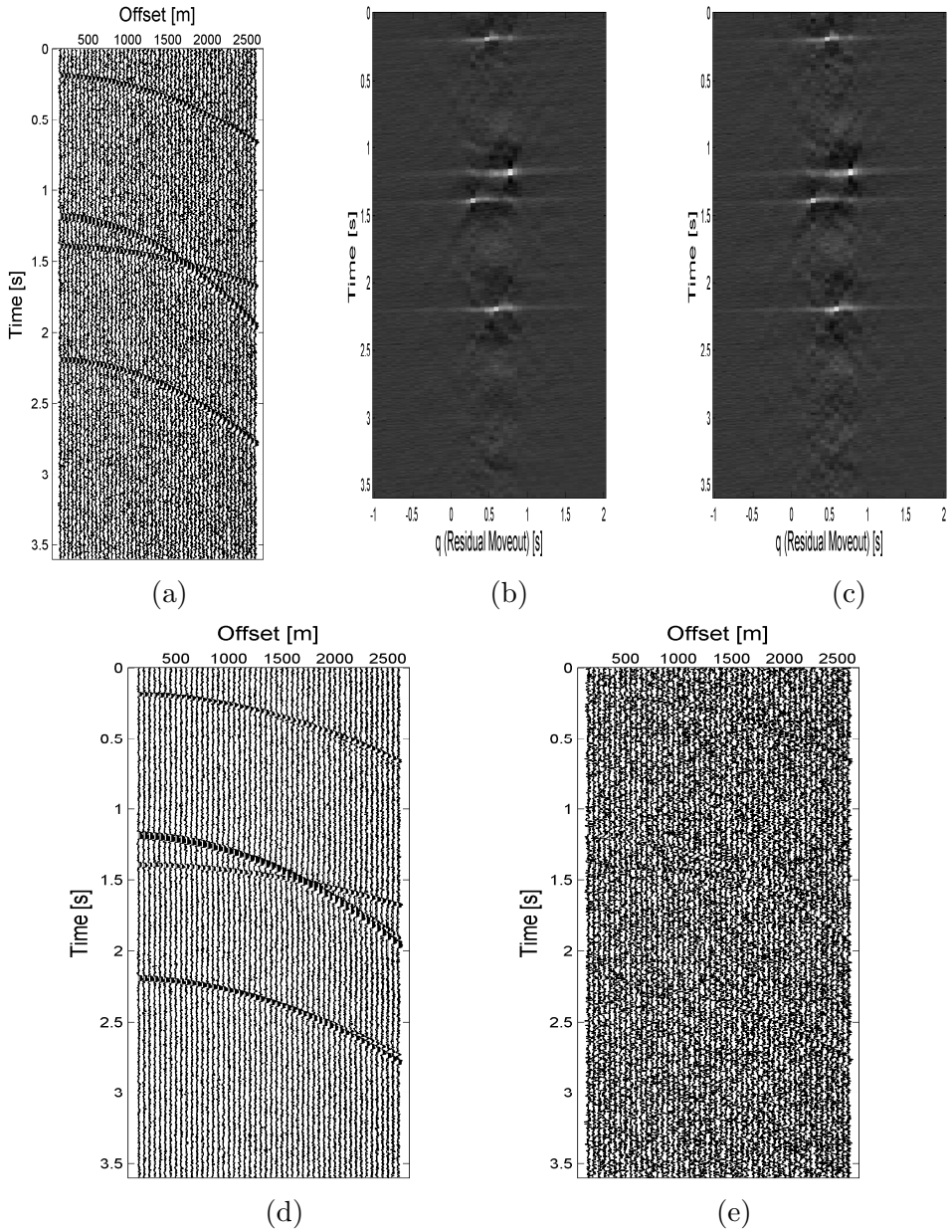

Figure 4.21: Deconvolution of seismic data using Compressive sensing With N=50 (a) The synthetic data used for deconvolution. (b) The compressed $\tau - q$ transform of (a), after the acquisition in compressed fashion with M=40 (20%compression). (c) The $\tau - q$ domain after the muting of the non-significant data. (d) The seismic data after taking the inverse parabolic Radon transform, of the (c). The estimated noise is shown in (e).

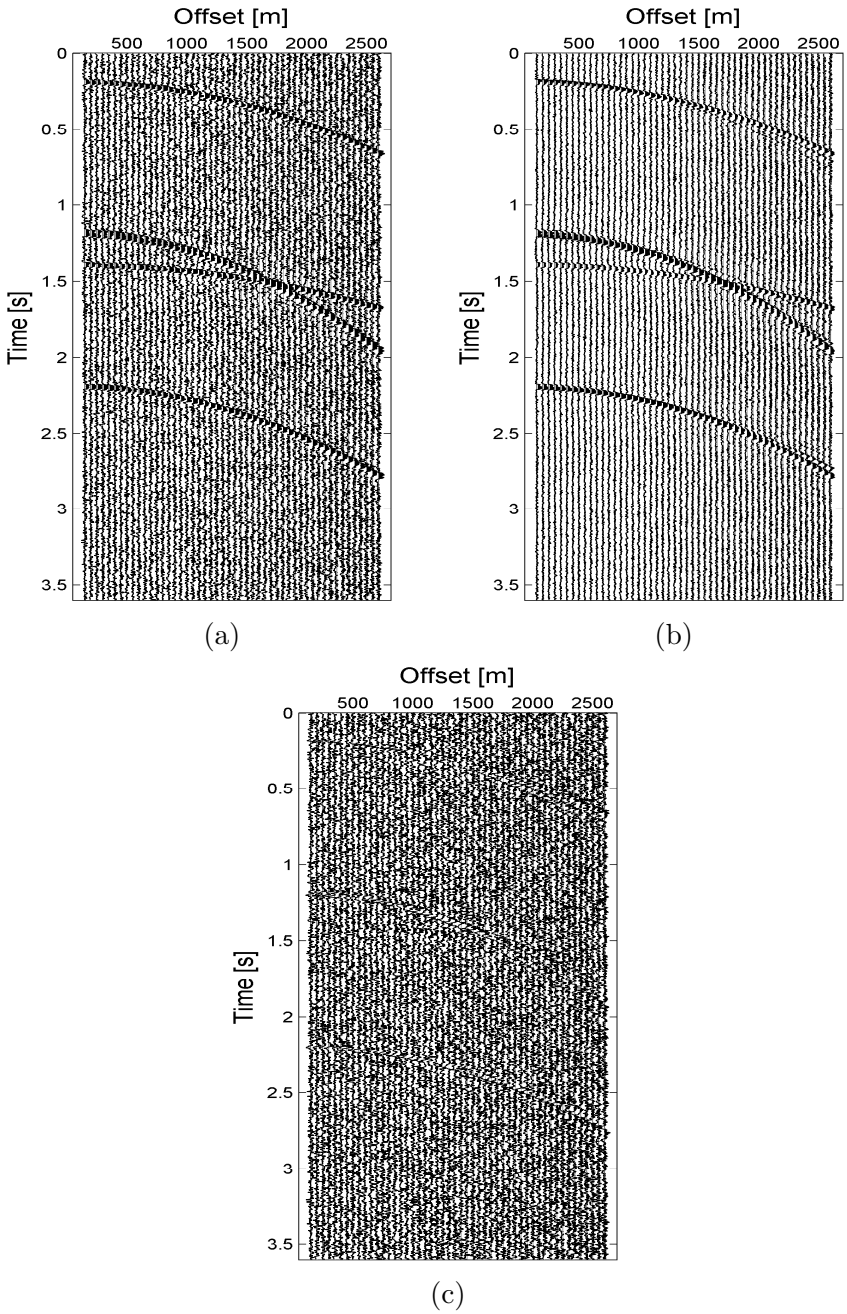

Figure 4.22: Deconvolution removal of seismic data using Compressive sensing With N=50 (a) The synthetic data used for the deconvolution. (b) The seismic data after deconvolution with M=30 (40% compression). The estimated noise is shown in (c).

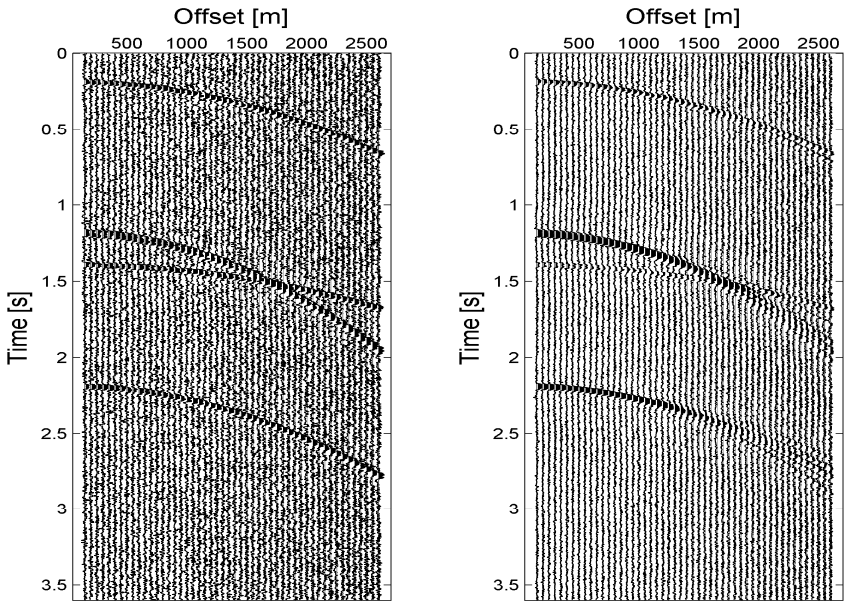

(a)

(b)

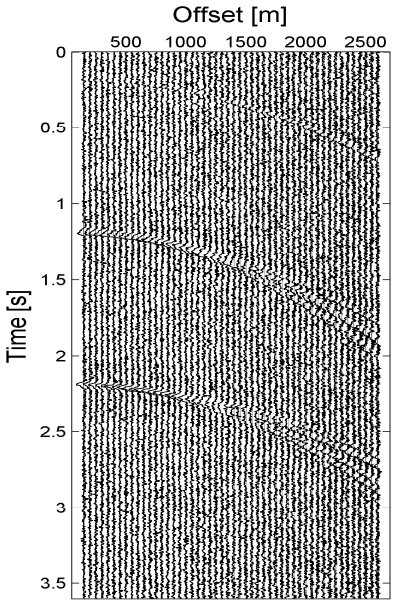

(c)

Figure 4.23: Deconvolution of seismic data using Compressive sensing With N=50 (a) The synthetic data used for the deconvolution. (b) The seismic data after deconvolution with M=20 (60% compression). The estimated noise is shown in (c).

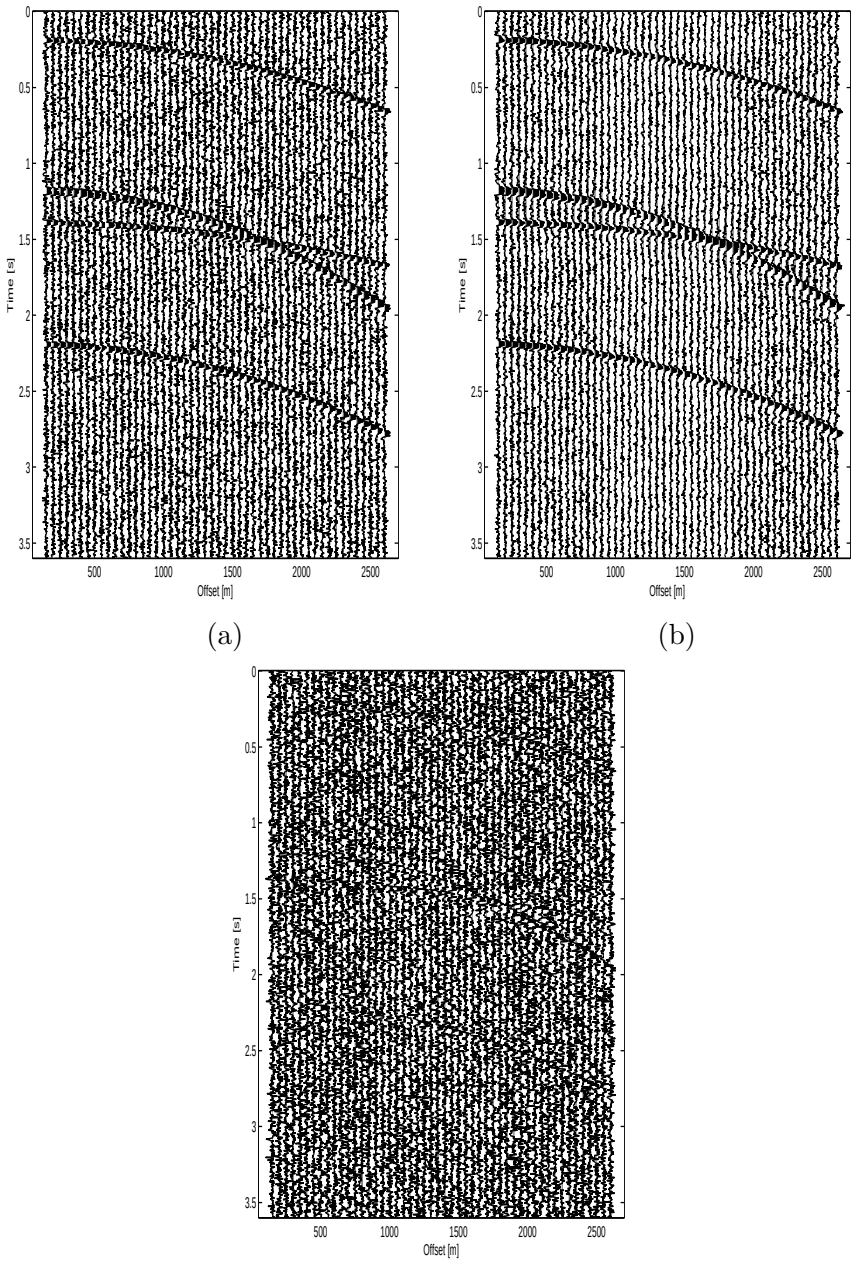

(a) (b)

(c)

Figure 4.24: Deconvolution of seismic data using fx deconvolution (a) The synthetic data used for the deconvolution. (b) The seismic data after deconvolution . The estimated noise is shown in (c).

4.8 Multiple Removal

The captured data contain multiple reflections from the same earth layer. Due to the complex geological conditions, different kinds of multiple reflections are generated; these reflections significantly reduce the resolution of recorded seismic data as they get mixed with primary waves. These reflections interfere with the primary reflections, which in turn make the processing of seismic data more difficult. Besides difficulty in identification of primary reflections we also face difficulties in the data analysis and interpretation. Attenuation of multiple reflections from the recorded seismic data is one of the key issues in the field of seismic data processing, so we can obtain the accurate description of the concerned surface as accurately as possible.

The captured data along with primary reflections contain many undesired components such as multiple reflections, refractions, diffractions etc. Presence of these unwanted components make the processing more difficult. Migrations and inversion schemes also require seismic data without these multiple reflections. So presence of these multiples limit the performance of the algorithm used for seismic signal processing. So attenuation of multiple reflections is very important step in seismic data processing. A lot of algorithm has been presented for the multiple attenuation. Methods depending upon the moveout and different transform has been discussed in [94] . In transformed domain, the unwanted regions are muted and we end up with only the primary reflections. Methods based on prediction and extraction of multiples are also presented. Wave-field extrapolation and predictive

deconvolution are the example of these techniques. These techniques work well with surface-related multiple removal. These techniques are presented in [131] and [132]. These methods are time consuming so adaptive algorithms are presented in [94, 133, 134]. There are some techniques which uses independent component analysis for the multiple removal as discussed in [135–137].

The parabolic Radon transform as a sparsifying transform for the compressive sensing can be used to remove the multiple reflection at the fly. The primary reflection and multiple reflection have same value of q once the data is represented in $\tau - q$ domain. This fact can be used to remove the multiples from the $\tau - q$ domain. Removal is done by muting all the points except one, with same value of q. By taking the inverse Radon transform will produce the image without the multiples.

Algorithm

Given a seismic record, the proposed compressive sensing with $\tau - q$ method for automatic multiple reflections removal is stated as follows:

1. Use the compressive sensing to acquire the seismic data in the compressed fashion as described in the previous section.

2. Use the following facts to generate an automatic mask (one for the primary reflections, zero for multiple reflections):

   (a) In the $\tau - q$ domain, primary reflection and multiple reflections have same value of q.

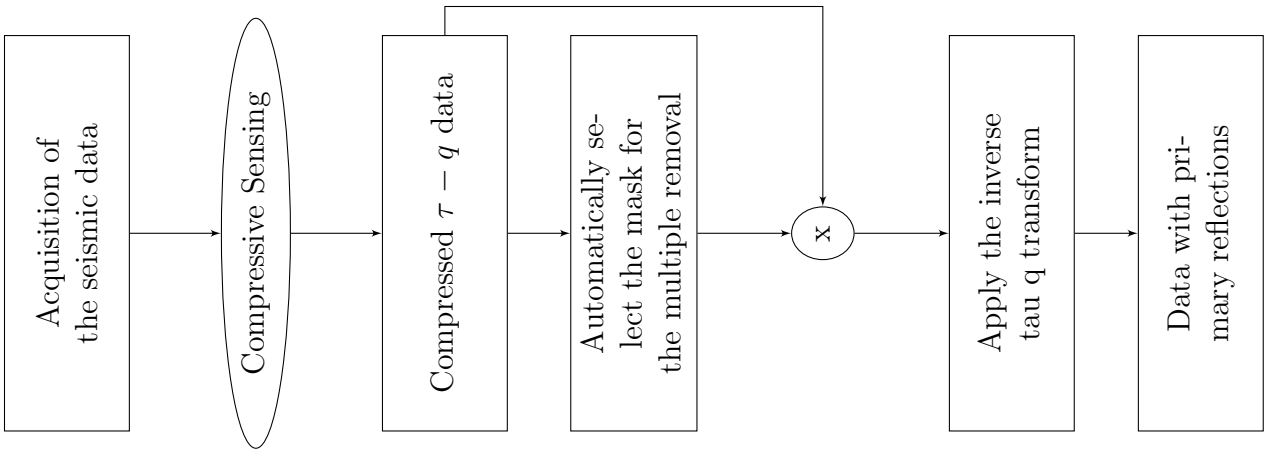

Figure 4.25: Workflow of the proposed technique for Multiple removal

(b) For that particular value of q, the value with the lowest t corresponds to the primary reflection.

3. Multiply the mask with the compressed $\tau - q$ domain. This will leave only the primary reflections in the $\tau - q$ domain.

4. Apply the inverse parabolic Radon transform to the previous step result.

Overall algorithm is presented in the Figure 4.25.

4.8.1 Simulation Results

The synthetic data contains two primary and two multiple reflections as shown in Figure 4.26a. The total number of traces in the data are 100(N=120) with spatial sampling interval 25m and sampling interval 4m/s. Figure 4.26b shows the compressed $\tau - q$ domain with M=80. Now based on the third step of the proposed algorithm the Radon domain after the muting of the multiple is presented in the Figure 4.26c. Finally the results after the application of the inverse parabolic

Radon transform are presented in Figure 4.26d, which shows the data without the multiple reflections with 20% compression.

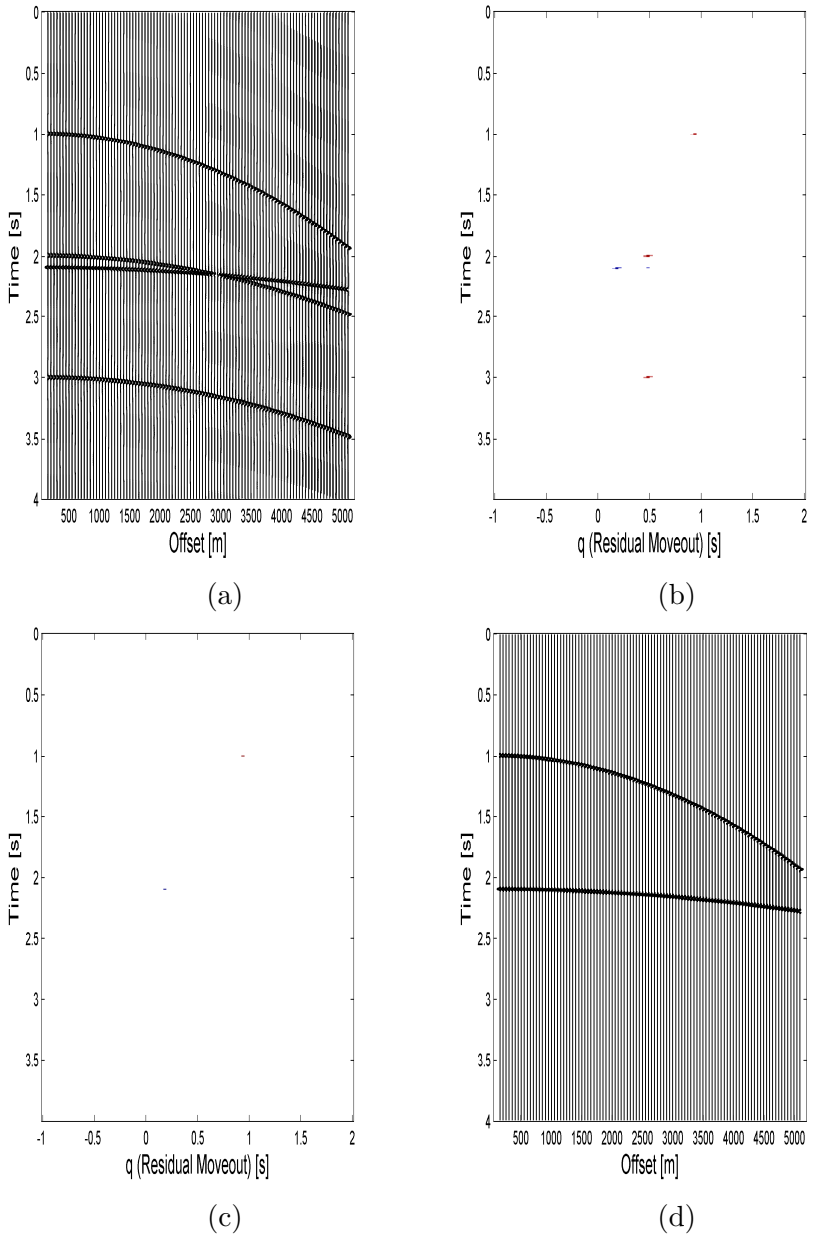

Figure 4.26: Multiple reflection removal of seismic data using Compressive sensing With N=100 (a) The synthetic data used for the multiple removal. (b) The compressed $\tau - q$ transform of (a), after the acquisition in compressed fashion with M=80 (20%compression). (c) The $\tau - q$ domain after the muting of the multiples. (d) The seismic data after taking the inverse parabolic Radon transform, of the (c).

The Figure 4.27 and 4.28 presents the results for the multiple removal with 60% and 80%compression level respectively.

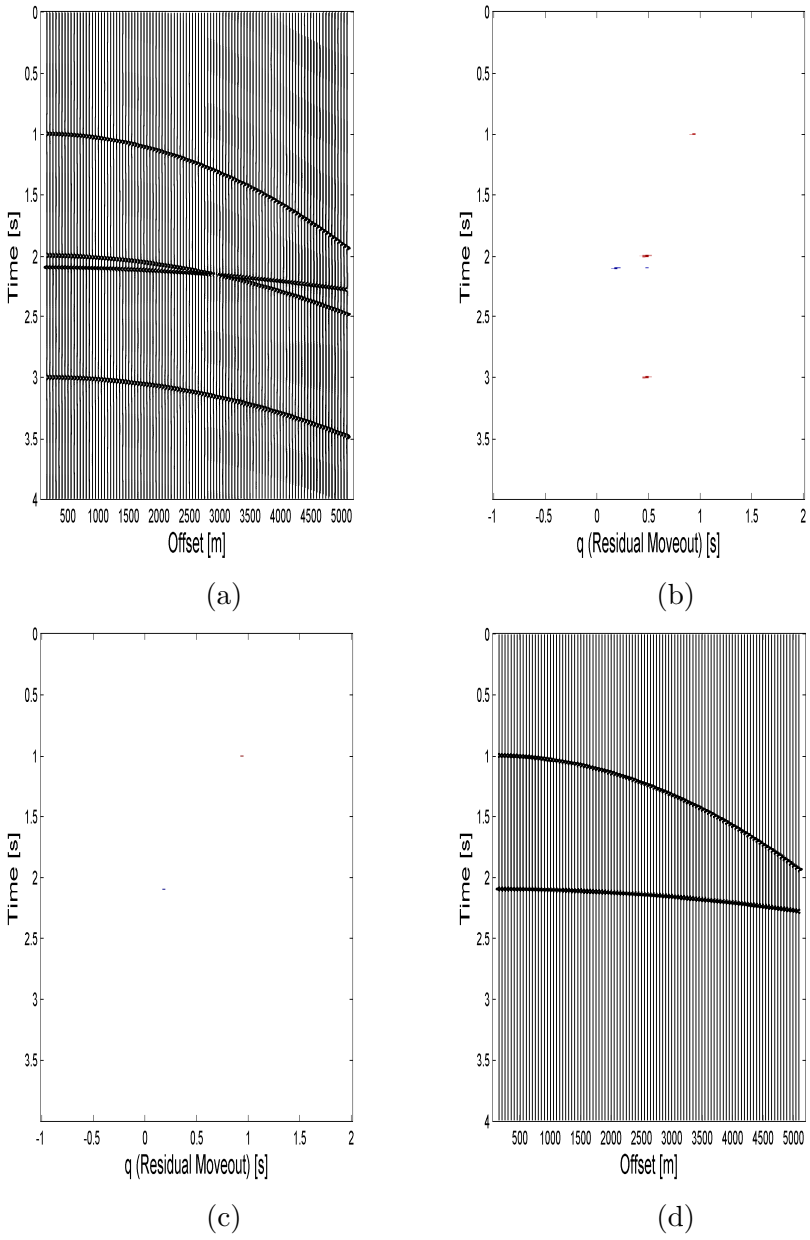

Figure 4.27: Multiple reflection removal of seismic data using Compressive sensing With N=100 (a) The synthetic data used for the multiple removal. (b) The compressed $\tau - q$ transform of (a), after the acquisition in compressed fashion with M=40 (60%compression). (c) The $\tau - q$ domain after the muting of the multiples. (d) The seismic data after taking the inverse parabolic Radon transform, of the (c).

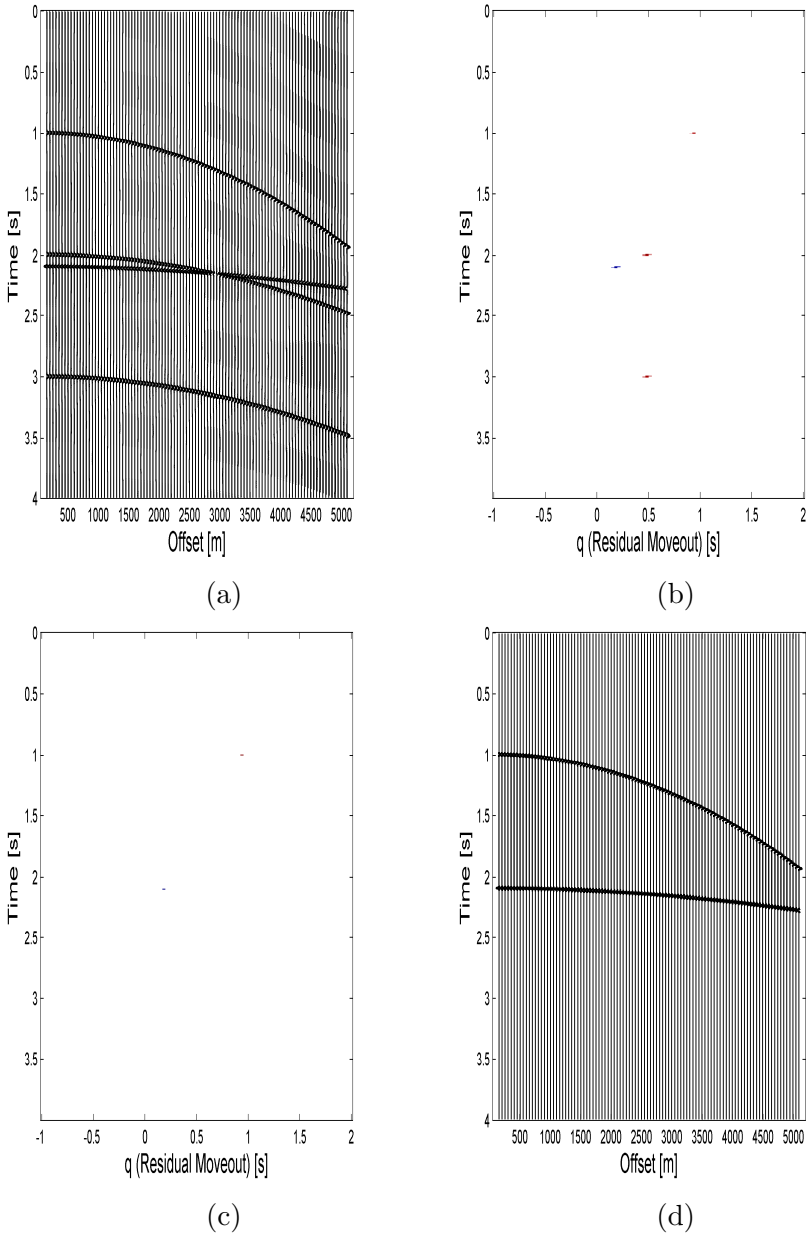

Figure 4.28: Multiple reflection removal of seismic data using Compressive sensing With N=100 (a) The synthetic data used for the multiple removal. (b) The compressed $\tau - q$ transform of (a), after the acquisition in compressed fashion with M=20 (80%compression). (c) The $\tau - q$ domain after the muting of the multiples. (d) The seismic data after taking the inverse parabolic Radon transform, of the (c).

To test the robustness of the proposed setup, the algorithm was applied to the data with different level of white Gaussian noise. The results of multiple removal, using the proposed algorithm, after the addition of 10% white Gaussian noise and 75% compression, are presented in Figure 4.29.

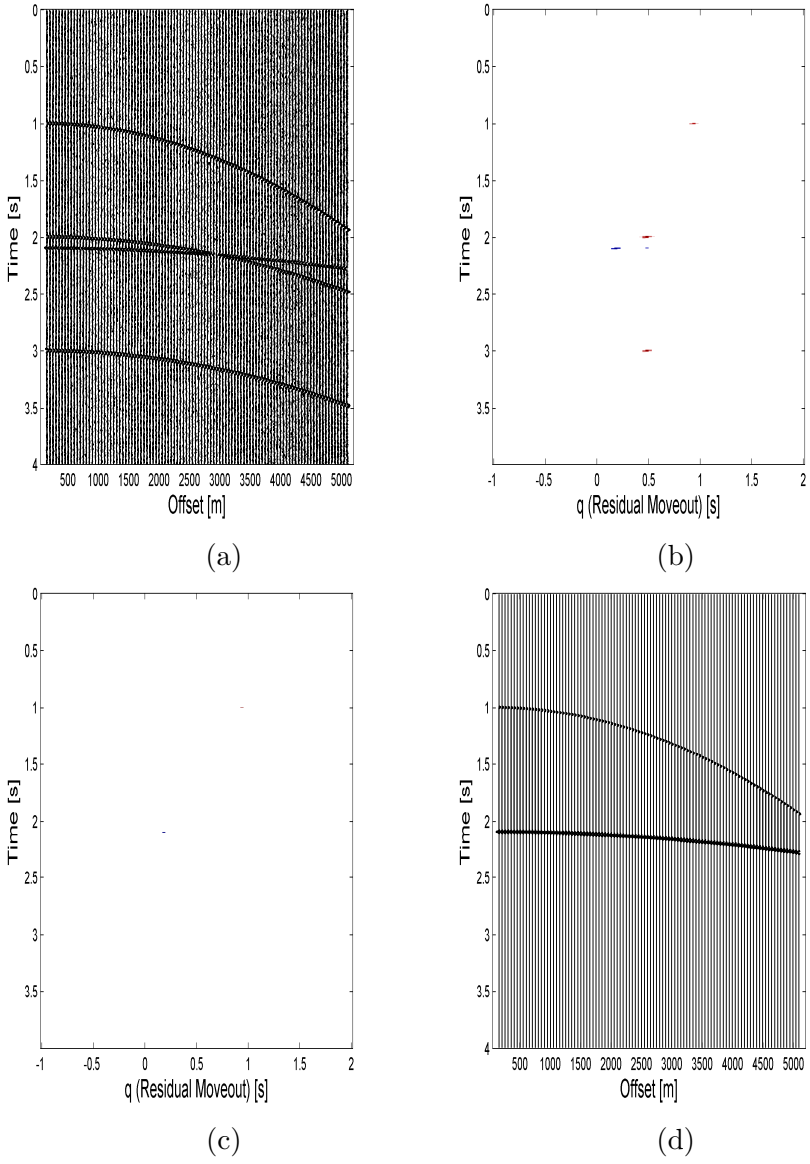

Figure 4.29: Multiple reflection removal of seismic data using Compressive sensing With N=100 with 10% Noise(a) The synthetic data used for the multiple removal. (b) The compressed $\tau - q$ transform of (a), after the acquisition in compressed fashion with M=25 (75%compression). (c) The $\tau - q$ domain after the muting of the multiples. (d) The seismic data after taking the inverse parabolic Radon transform, of the (c).

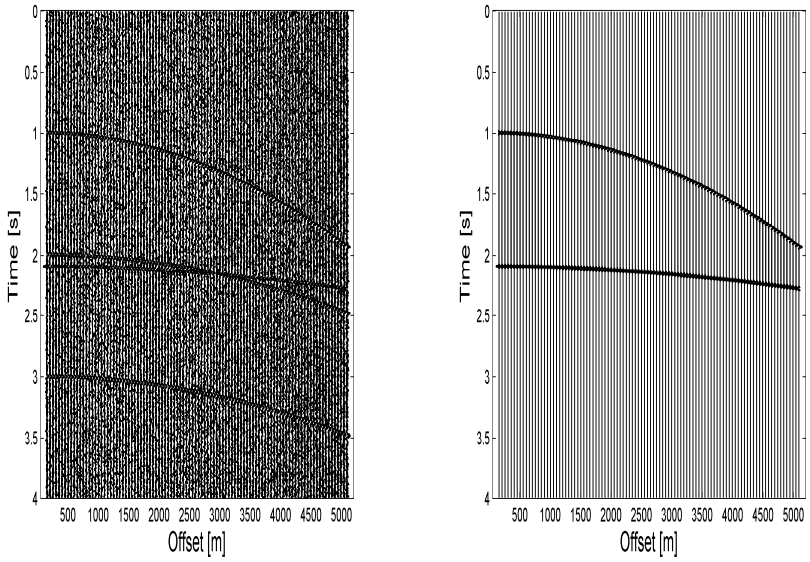

(a) (b)

Figure 4.30: Multiple reflection removal of seismic data using Compressive sensing With N=100 with 20% Noise(a) The synthetic data used for the multiple removal. (b) The seismic data after the multiple removal with M=25 (75%compression).

The proposed algorithm works well for even higher noise level and high compression level. The results of the proposed algorithm with 20% and 40% white noise are presented in figure 4.30 and 4.31.

The same algorithm is tested on a real dataset of the Gulf of Mexico as shown in Figure 4.32a. The total number of traces in the data are 92(N=92) with spatial sampling interval 25m and sampling interval 4m/s. The result after the multiple removal, with 50 % compression, is presented in figure 4.32b. To show the effect of the proposed algorithm, a part of the database along with the final result is shown in Figure 4.33.

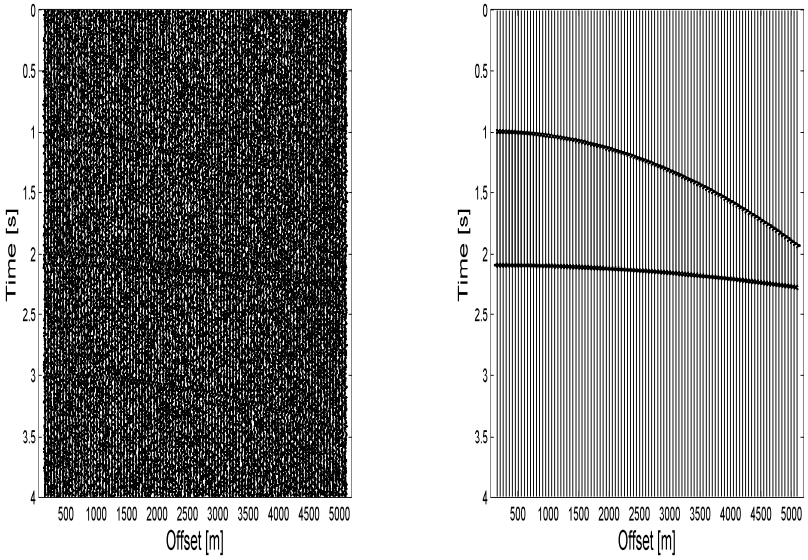

(a) (b)

Figure 4.31: Multiple reflection removal of seismic data using Compressive sensing With N=100 with 40% Noise(a) The synthetic data used for the multiple removal. (b) The seismic data after the multiple removal with M=25 (75%compression

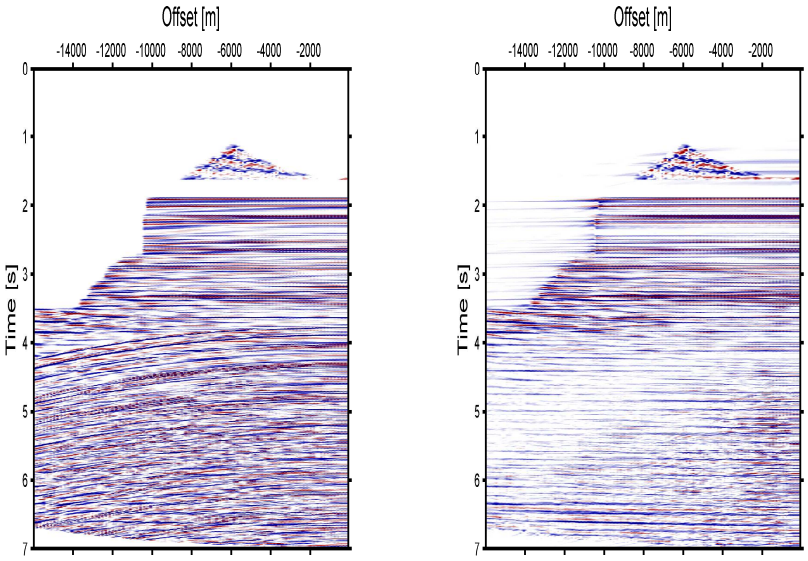

(a) (b)

Figure 4.32: Multiple reflection removal of Gulf of Mexico using Compressive sensing With N=92 (a) The real data used for the multiple removal. (b) The seismic data after the multiple removal with M=46 (50%compression).

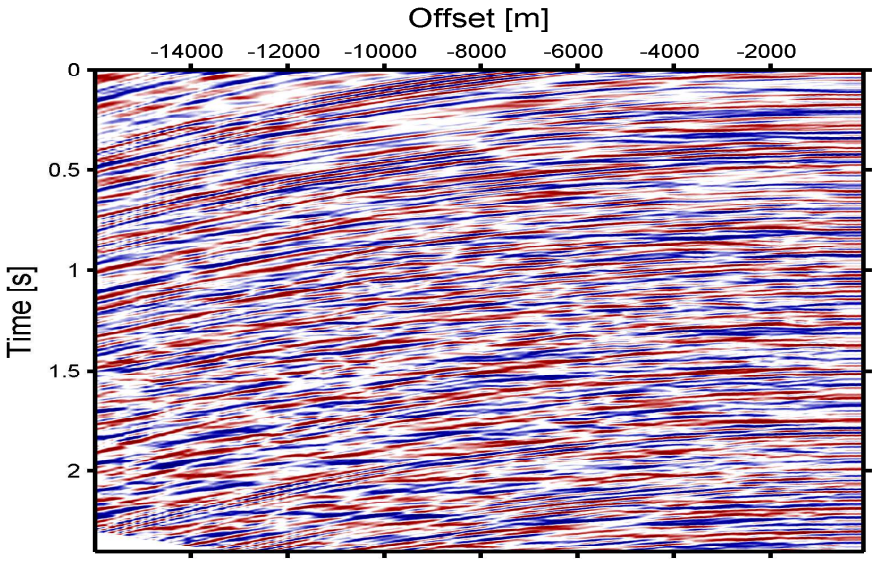

(a)

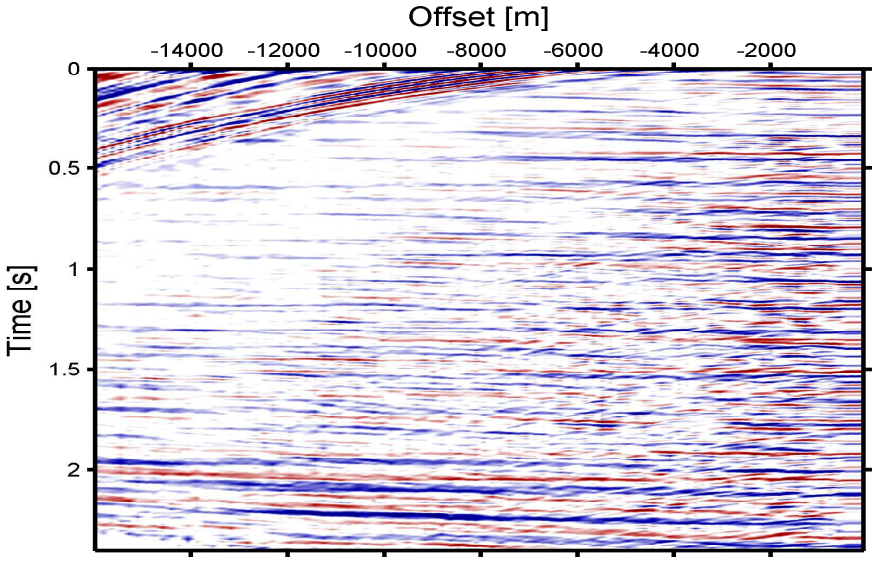

(b)

Figure 4.33: Multiple reflection removal of Gulf of Mexico using Compressive sensing With N=92 (a) The real data used for the multiple removal. (b) The seismic data after the multiple removal with M=46 (50%compression).

4.9 Conclusion

In the first section of this chapter a brief review of parabolic Radon transform is presented. Parabolic Radon transform and its types are discussed. Besides basic theory of parabolic Radon transform, Radon transform of point source, linear and non-linear events is presented.

In the second part of the chapter, compressive sensing using parabolic Radon transform as sparsifying transform is presented. The proposed algorithm is used for the interpolation of missing traces. From the comparison with the curvelet transform, it became evident that Radon is much faster than the curvelet transform. Moreover Radon transform is robust and works for low SNR signals as well.

Compressive sensing with parabolic Radon transform as a sparsifying transform can be used to separate the non-linear events from the non-linear Radon transform at the time of acquisition. Deconvolution using Radon transform is also presented in this chapter. The deconvolution results are compared with the famous fx-deconvolution.

At the end of this chapter, multiple reflection problem is tackled using the proposed algorithm. From the detailed simulation results, it is clear that Radon transform with compressive sensing, not only reduce the number of measurements but it is also quite robust and provides accurate detection of the primary reflection.

CHAPTER 5

CONCLUSION

In this research work, the Radon Transform is used as the sparsifying transform for the Compressive sensing of seismic exploration data. Radon transform is robust in both the linear domain $(\tau - p)$ or parabolic domain $(\tau - q)$. The $\tau - p$ and $\tau - q$ domain provides the sparse representation of the linear and parabolic(or hyperbolic) seismic events, respectively. The concept was proved, as shown via the results, for several important seismic processing steps.

The applications that are discussed in this thesis are

- Interpolation of linear and non-linear missing seismic traces
- First arrival picking of the seismic refraction data
- Classification of different seismic events of the acquired data
- Deconvolution of seismic data
- Multiple reflection removal from seismic data

From the results, it is interesting to see how compressive sensing with Radon transform can be used for various application of seismic signal processing. The

Radon transform does not only work well with compressive sensing but it is significantly more faster than the existing proposed transform for seismic signal processing like curvelet transform. Computationally Radon transform is much less expensive than the curvelet as it is evident from the simulation results. Radon Transform is also quite robust and even works well for quite low SNR. The fact that the linear events and non linear events are sparse in $\tau - p$ and $\tau - q$ domain respectively, can be used to only record linear/non-linear seismic events. Linear Radon transform can be used to detect the first break of the refraction data. Similarly parabolic Radon transform can be used to remove the multiple reflections from the seismic reflection data.

5.1 Future Suggestions

In this research, Radon transform is used with frequency domain representation. Instead of using frequency domain Radon transform representation, time-domain high resolution Radon transform can be used. Time-domain Radon transform will map the seismic events into the single points, more accurately at the cost of computational time.

Other variants of Radon can be tested like instead of parabolic, hyperbolic Radon transform/Hybrid Radon transform can be used. Resolution can be increased by local Radon transform.

Instead of l_1 norm minimization, other recovery algorithm can be utilized for the compressive sensing.

To further prove or negate the concept that Radon transform can be used as sparsifying transform for compressive sensing of the seismic data processing, the technique can be tested experimentally.

REFERENCES

[1] O. Yilmaz and S. M. Doherty, *Seismic data processing*. Society of Exploration Geophysicists Tulsa, 1987, vol. 2.

[2] J. L. Ahern, "Seismic Reflection Method," p. http://principles.ou.edu/, 2007.

[3] B. P. Inc, "Seismic Exploration Overview."

[4] U. NERL, "Marine Seismic Methods, Environmental Geophysics ,US EPA."

[5] O. Yilmaz, *Seismic Data Analysis: Processing, Inversion, and Interpretation of Seismic Data, Volume 1*. SEG Books, 2001.

[6] P. Pecholcs, R. Al-Saad, M. Al-Sannaa, J. Quigley, C. Bagaini, A. Zarkhidze, R. May, M. Guellili, S. Sinanaj, and M. Membrouk, *A broadband full azimuth land seismic case study from Saudi Arabia using a 100,000 channel recording system at 6 terabytes per day: acquisition and processing lessons learned*, 2012, ch. 772, pp. 1–5.

[7] F. Herrmann, M. Friedlander, and O. Yilmaz, "Fighting the Curse of Dimensionality: Compressive Sensing in Exploration Seismology," *IEEE Signal Processing Magazine*, vol. 29, no. 3, pp. 88–100, May 2012.

[8] D. L. D. L. Donoho, "Compressed sensing," *IEEE Transactions on Information Theory*, vol. 52, no. 4, pp. 1289–1306, 2006.

[9] R. Baraniuk, "Compressive sensing," *Signal Processing Magazine, IEEE*, no. July, pp. 118–121, 2007.

[10] T. Blumensath, "Compressed sensing with nonlinear observations," *preprint*, pp. 1–9, 2010.

[11] E. J. Candes and M. B. Wakin, "An Introduction To Compressive Sampling," *IEEE Signal Processing Magazine*, vol. 25, no. 2, pp. 21–30, Mar. 2008.

[12] E. Candès, L. Demanet, D. Donoho, and L. Ying, "Fast Discrete Curvelet Transforms," *Multiscale Modeling & Simulation*, vol. 5, no. 3, pp. 861–899, Jan. 2006.

[13] L. Demanet and L. Ying, "Wave atoms and sparsity of oscillatory patterns," *Applied and Computational Harmonic Analysis*, vol. 23, no. 3, pp. 368–387, 2007.

[14] E. Candès and L. Demanet, "Curvelets and Fourier Integral Operators," *Comptes Rendus Mathematique*, vol. 336, no. 5, pp. 395–398, 2003.

[15] F. Matus and J. Flusser, "Image representation via a finite Radon transform," *Pattern Analysis and Machine Intelligence, IEEE Transactions on*, vol. 15, no. 10, pp. 996–1006, 1993.

[16] T. M. Lehmann, C. Gonner, and K. Spitzer, "Survey: Interpolation methods in medical image processing," *Medical Imaging, IEEE Transactions on*, vol. 18, no. 11, pp. 1049–1075, 1999.

[17] Z. Cao, "Analysis and application of the Radon transform," *Masters Abstracts International*, 2007.

[18] P. Kuchment, "Generalized transforms of Radon type and their applications," *Proceedings of Symposia in Applied Mathematics*, pp. 1–32, 2006.

[19] F. Natterer, "Inversion of the attenuated Radon transform," *Inverse problems*, vol. 17, no. 1, p. 113, 2001.

[20] M. Sacchi, D. Verschuur, and P. Zwartjes, "Data reconstruction by generalized deconvolution," *74th Annual International Meeting, Expanded Abstracts*, no. October, 2004.

[21] W. Mousa and A. Al-Shuhail, "Enhancement of first arrivals using the τ-p transform on energy-ratio seismic shot records," *Geophysics*, 2012.

[22] D. Trad, T. Ulrych, and M. Sacchi, "Latest views of the sparse Radon transform," *Geophysics*, vol. 68, no. 1, pp. 386–399, Jan. 2003.

[23] S. Tong, R. Wang, H. Liu, J. Zhang, and C. Bu, "High Resolution Radon Transform and its Applications in Multiple Suppression of Seismic Data in Deep-Sea," *2009 2nd International Congress on Image and Signal Processing*, vol. 2, no. 1, pp. 1–4, Oct. 2009.

[24] Z. Cao and J. Bancroft, "A Semblance Weighted Radon Transform on Multiple Attenuation," *CSEG National Convention*, vol. 2, no. 1917, pp. 298–301, 2005.

[25] V. Minaeian, A. Javaherian, and A. Moslemi, "Multiple Attenuation by FX Parabolic Radon Transform," *1st International Petroleum Conference & Exhibition*, no. May 2009, pp. 4–6, 2009.

[26] J. R. Thorson and J. F. Claerbout, "Velocity stack and slant stack stochastic inversion," *Geophysics*, vol. 50, no. 12, pp. 2727–2741, Dec. 1985.

[27] P. Toft, "The Radon Transform theory and Application," Ph.D. dissertation, Technical University of Denmark, 2003.

[28] G. Beylkin, "Discrete radon transform," *IEEE Transactions on Acoustics, Speech, and Signal Processing*, vol. 35, no. 2, pp. 162–172, Feb. 1987.

[29] M. Ng and M. Perz, "High resolution Radon transform in the tx domain using" intelligent" prioritization of the Gauss-Seidel estimation sequence," in *2004 SEG Annual Meeting*, 2004.

[30] J. Romberg, "Compressive sensing by random convolution," *SIAM Journal on Imaging Sciences*, vol. 2, no. 4, pp. 1098–1128, 2009.

[31] F. Herrmann, Y. Erlangga, and T. Lin, "Compressive simultaneous full-waveform simulation," *Geophysics*, vol. 2, no. August, pp. 1–20, 2009.

[32] G. Hennenfent and F. Herrmann, *Sparseness constrained data continuation with frames: applications to missing traces and aliased signals in 2/3D*, 2005, ch. 551, pp. 2162–2165.

[33] F. Herrmann, "Sub-Nyquist sampling and sparsity: How to get more information from fewer samples," *2009 SEG Annual Meeting*, 2009.

[34] J. Cao, Y. Wang, J. Zhao, and C. Yang, "A review on restoration of seismic wavefields based on regularization and compressive sensing," *nverse Problems in Science and Engineering*, pp. 679–704, 2011.

[35] F. J. Herrmann and X. Li, "Efficient least-squares imaging with sparsity promotion and compressive sensing," *Geophysical prospecting*, vol. 60, no. 4, pp. 696–712, 2012.

[36] Y. Wang, J. Cao, and C. Yang, "Recovery of seismic wavefields based on compressive sensing by an l1-norm constrained trust region method and the piecewise random subsampling," *Geophysical Journal International*, vol. 187, no. 1, pp. 199–213, 2011.

[37] H. J. Landau, "Sampling, data transmission, and the Nyquist rate," *Proceedings of the IEEE*, vol. 55, no. 10, pp. 1701–1706, 1967.

[38] A. Jerri, "The Shannon sampling theorem ;Its various extensions and applications: A tutorial review," *Proceedings of the IEEE*, vol. 65, no. 11, pp. 1565–1596, 1977.

[39] H. Xue, "Compressed Sensing," pp. 1–41, 2011.

[40] E. Candes, J. Romberg, and T. Tao, "Robust uncertainty principles: exact signal reconstruction from highly incomplete frequency information," *IEEE Transactions on Information Theory*, vol. 52, no. 2, pp. 489–509, Feb. 2006.

[41] R. Baraniuk and M. Davenport, "A simple proof of the restricted isometry property for random matrices," *Constructive Approximation*, pp. 253–263, 2008.

[42] E. J. Candes and T. Tao, "Near-optimal signal recovery from random projections: Universal encoding strategies?" *Information Theory, IEEE Transactions on*, vol. 52, no. 12, pp. 5406–5425, 2006.

[43] M. Zibulevsky and B. A. Pearlmutter, "Blind source separation by sparse decomposition in a signal dictionary," *Neural computation*, vol. 13, no. 4, pp. 863–882, 2001.

[44] D. MacKenzie, "Compressed sensing makes every pixel count," *What's Happening in the Mathematical Sciences*, no. July, pp. 114–127, 2009.

[45] M. Duarte and M. Davenport, "Single-pixel imaging via compressive sampling," *IEEE Signal Processing Magazine*, 2008.

[46] J. Haupt and R. Nowak, "Compressive sampling vs. conventional imaging," *Image Processing, 2006 IEEE International*, 2006.

[47] A. Sankaranarayanan, "Compressive acquisition of dynamic scenes," *Computer VisionECCV*, 2010.

[48] J. Ma, G. Plonka, and M. Hussaini, "Compressive video sampling with approximate message passing decoding," *Circuits and Systems for Video Technology, IEEE Transactions on , vol.22, no.9*, 2012.

[49] S. Pudlewski, "Compressed-sensing-enabled video streaming for wireless multimedia sensor networks," *Mobile Computing, IEEE Transactions on*, 2012.

[50] H. Chen, N. Xi, B. Song, L. Chen, and J. Zhao, "Infrared Camera Using a Single Nano-photodetector," *Sensors Journal, IEEE*, 2013.

[51] M. Duarte and S. Sarvotham, "Distributed compressed sensing of jointly sparse signals," *Asilomar Conf. Signals, Sys.*, 2005.

[52] E. Candes and T. Tao, "Decoding by linear programming," *Information Theory, IEEE Transactions on*, vol. 40698, no. December, pp. 1–22, 2005.

[53] S. Cotter and B. Rao, "Sparse channel estimation via matching pursuit with application to equalization," *Communications, IEEE Transactions on*, 2002.

[54] A. Gomaa and N. Al-Dhahir, "A new design framework for sparse FIR MIMO equalizers," *Communications, IEEE Transactions on*, 2011.

[55] C. Berger and S. Zhou, "Sparse channel estimation for multicarrier underwater acoustic communication: From subspace methods to compressed sensing," *IEEE Transactions on Signal Processing*, 2010.

[56] J. Meng, W. Yin, and Y. Li, "Compressive sensing based high-resolution channel estimation for OFDM system," *Selected Topics in Signal Processing*, 2012.

[57] G. Gui, W. Peng, and F. Adachi, "High resolution compressive channel estimation for broadband wireless communication systems," *Journal of Communication Systems*, 2012.

[58] M. Lustig, D. Donoho, and J. Pauly, "Rapid MR imaging with compressed sensing and randomly under-sampled 3DFT trajectories," *Proc. 14th Ann. Meeting ISMRM*, 2006.

[59] ——, "Sparse MRI: The application of compressed sensing for rapid MR imaging," *Magnetic Resonance in Medicine*, 2007.

[60] M. Lustig and D. Donoho, "Compressed sensing MRI," *Signal Processing Magazine, IEEE 25.2*, 2008.

[61] H. Yu and G. Wang, "Compressed sensing based interior tomography," *Physics in medicine and biology*, 2009.

[62] J. Provost and F. Lesage, "The application of compressed sensing for photo-acoustic tomography," *Medical Imaging, IEEE Transactions on*, 2009.

[63] E. Candès, "The restricted isometry property and its implications for compressed sensing," *Comptes Rendus Mathematique*, vol. 346, pp. 589–592, 2008.

[64] D. Needell and R. Vershynin, "Uniform uncertainty principle and signal recovery via regularized orthogonal matching pursuit," *Foundations of computational mathematics*, pp. 1–18, 2009.

[65] F. J. Herrmann, "Compressed sensing and sparse recovery in exploration seismology," Tech. Rep., 2009.

[66] F. Herrmann, D. Wang, G. Hennenfent, and P. Moghaddam, "Curvelet-based seismic data processing: A multiscale and nonlinear approach," *Geophysics*, pp. 1–18, 2007.

[67] F. Herrmann and G. Hennenfent, "Nonparametric seismic data recovery with curvelet frames," *Geophysical Journal . . .*, 2008.

[68] T. Lin and F. Herrmann, "Compressed wavefield extrapolation with curvelets," *SEG International Exposition and 77th Annual Meeting*, no. 3, pp. 1997–2001, Jan. 2007.

[69] C. Sastry, G. Hennenfent, and F. Herrmann, "Signal reconstruction from incomplete and misplaced measurements," *European Association of Geoscientists & Engineers*, no. June 2007, pp. 11–14, 2007.

[70] G. Hennenfent and F. J. Herrmann, "Simply denoise: Wavefield reconstruction via jittered undersampling," *Geophysics*, vol. 73, no. 3, pp. V19–V28, May 2008.

[71] W. Tang, J. Ma, and F. Herrmann, "Optimized compressed sensing for curvelet-based seismic data reconstruction," *preprint*, pp. 1–28, 2009.

[72] Y. Yang, J. Ma, and S. Osher, "Seismic data reconstruction via matrix completion," *UCLA CAM Report*, pp. 1–16, 2012.

[73] T. Lin and F. Herrmann, "Unified compressive sensing framework for simultaneous acquisition with primary estimation," *2009 SEG Annual Meeting*, no. 1, 2009.

[74] F. J. Herrmann, U. Böniger, and D. J. E. Verschuur, "Non-linear primary-multiple separation with directional curvelet frames," *Geophysical Journal International*, vol. 170, no. 2, pp. 781–799, Aug. 2007.

[75] H. Mansour, H. Wason, T. T. Lin, and F. J. Herrmann, "Randomized marine acquisition with compressive sampling matrices," *Geophysical Prospecting*, vol. 60, no. 4, pp. 648–662, Jul. 2012.

[76] F. J. Herrmann and H. Wason, "Compressive Sensing in Marine Acquisition and Beyond," in *74th EAGE Conference & Exhibition - Workshops*, Jul. 2012.

[77] A. Gholami and M. Sacchi, "A Fast and Automatic Sparse Deconvolution in the Presence of Outliers," *Geoscience and Remote Sensing, IEEE Transactions on*, 2012.

[78] F. Herrmann, "Compressive-wavefield simulations," *SAMPTA'09, International Conference on Sampling Theory and Applications*, pp. 2–5, 2009.

[79] S. Helgason, *The Radon Transform(Google eBook)*. Springer, 1999.

[80] T. G. Feeman, *The Mathematics of Medical Imaging*, ser. Springer Undergraduate Texts in Mathematics and Technology. New York, NY: Springer New York, 2010.

[81] S. Helgason, *The radon transform*, 1999.

[82] P. Algorithm, *Image Reconstruction from Projections : Radon Transform : Example 2 Sinogram*, 2004.

[83] C. H. Chapman, "Generalized Radon transforms and slant stacks," *Geophysical Journal of the Royal Astronomical Society*, vol. 66, no. 2, pp. 445–453, 1981.

[84] M. Sarajæ rvi, "Inversion of the Linear and Parabolic Radon Transform," Ph.D. dissertation, University of Bergen, 2010.

[85] N. Temme, "The Radon transform; first steps," *CWI Newsletter*, 1987.

[86] P. W. Cary, "The simplest discrete Radon transform," *SEG Technical Program Expanded Abstracts 1998*, pp. 1999–2002, Jan. 1998.

[87] B. Zhou and S. Greenhalgh, "Linear and parabolic τ-p transforms revisited," *Geophysics*, vol. 59, no. 7, pp. 1133–1149, 1994.

[88] S. Mendelson, "Uniform uncertainty principle for Bernoulli and subgaussian ensembles," *Constructive Approximation*, 2008.

[89] D. Trad, "Interpolation and multiple attenuation with migration operators," *Geophysics*, 2003.

[90] B. Liu and M. Sacchi, "Minimum weighted norm interpolation of seismic records," *Geophysics*, 2004.

[91] G. Hennenfent and F. J. Herrmann, "Application of stable signal recovery to seismic data interpolation," *SEG Technical Program Expanded Abstracts 2006*, vol. 1, no. 4, pp. 2797–2801, Jan. 2006.

[92] S. Spitz, "Seismic trace interpolation in the FX domain," *Geophysics*, 1991.

[93] R. Kumar, a. Y. Aravkin, H. Mansour, B. Recht, and F. J. Herrmann, "Seismic Data Interpolation and Denoising Using SVD-free

Low-rank Matrix Factorization," in *75th EAGE Conference & Exhibition incorporating SPE EUROPEC 2013*, 2013.

[94] A. Berkhout and D. Verschuur, "Imaging of multiple reflections," *Geophysics*, 2006.

[95] W. Curry and G. Shan, "Interpolation of Near Offsets with Multiples and Prediction-Error Filters," in *68th EAGE Conference & Exhibition*, Jun. 2006.

[96] Y. Wang, Y. Luo, and G. Schuster, "Interferometric interpolation of missing seismic data," *Geophysics*, 2009.

[97] J. Cao, Y. Wang, and C. Yang, "Seismic Data Restoration Based on Compressive Sensing Using Regularization and ZeroNorm Sparse Optimization," *Chinese Journal of Geophysics*, vol. 55, no. 2, pp. 239–251, 2012.

[98] F. Herrmann, D. Wang, and G. Hennenfent, "Multiple prediction from incomplete data with the focused curvelet transform," *Geophysics*, 2007.

[99] H. Mansour, F. J. Herrmann, and O. Ylmaz, "Improved wavefield reconstruction from randomized sampling via weighted one-norm minimization," *Geophysics*, vol. 78, no. 5, pp. V193–V206, Sep. 2013.

[100] E. Candes, L. Demanet, and L. Ying, "CurveLab Toolbox, Version 2.0. 3," 2005.

[101] W. Hongyu, "Maximum Entropy Spectral Analysis," *Journal of China Institute of*, 1982.

[102] C. Vanbatenburg, "Maximum entropy spectral analysis," *NASA STI/Recon Technical Report N*, 1984.

[103] T. Ulrych and T. Bishop, "Maximum entropy spectral analysis and autoregressive decomposition," *Reviews of Geophysics*, 1975.

[104] J. Shore and R. Johnson, "Axiomatic derivation of the principle of maximum entropy and the principle of minimum cross-entropy," *Information Theory, IEEE Transactions ...*, 1980.

[105] J. Shore, "Minimum cross-entropy spectral analysis," *Acoustics, Speech and Signal Processing, IEEE ...*, 1981.

[106] J. Shore and R. Johnson, "Properties of cross-entropy minimization," *Information Theory, IEEE Transactions on*, 1981.

[107] J. Parrish, "Relative entropy spectrum deconvolution," *... Geophysicists International Exposition and 67th Annual ...*, 1997.

[108] ——, "Applying minimum relative entropy spectrum deconvolution," *1999 SEG Annual Meeting*, 1999.

[109] ——, "Signature after predictive deconvolution," *ASEG Extended Abstracts*, 2002.

[110] K. Peacock and S. Treitel, "Predictive deconvolution: Theory and practice," *Geophysics*, 1969.

[111] O. Yilmaz, *Seismic data analysis: processing, inversion, and interpretation of seismic data*, 2001.

[112] M. Cox, E. Scherrer, and R. Chen, "Static corrections for seismic reflection surveys," *Society of Exploration Geophysicists Tulsa*, 1999.

[113] R. Peraldi and A. Clement, "Digital processing of refraction data study of first arrivals," *Geophysical Prospecting*, 1972.

[114] P. Hatherly, "A computer method for determining seismic first arrival times," *Geophysics*, 1982.

[115] B. Gelchinsky and V. Shtivelman, "Automatic Picking of First Arrivals and Parameterization of Traveltime Curves," *Geophysical Prospecting*, 1983.

[116] F. Coppens, "First arrival picking on common offset trace collections for automatic estimation of static corrections," *Geophysical Prospecting*, 1985.

[117] U. Spagnolini, "Adaptive Picking of Refracted First arrivals," *Geophysical prospecting*, 1991.

[118] M. Murat and A. Rudman, "Automated First Arrival Picking: a Neural Network APPROACH1," *Geophysical Prospecting*, 1992.

[119] S. Yung and L. Ikelle, "An example of seismic time picking by third-order bicoherence," *Geophysics*, 1997.

[120] F. Boschetti, M. Dentith, and R. List, "A fractal-based algorithm for detecting first arrivals on seismic traces," *Geophysics*, 1996.

[121] L. Jiao and W. Moon, "Detection of seismic refraction signals using a variance fractal dimension technique," *Geophysics*, 2000.

[122] I. M. I. Tibuleac, E. T. Herrin, J. M. Britton, R. Shumway, and A. C. Rosca, "Automatic Determination of Secondary Seismic Phase Arrival Times Using Wavelet Transforms," *Seismological Research Letters*, vol. 74, no. 6, pp. 884–892, Nov. 2003.

[123] D. Trad, T. Ulrych, and M. Sacchi, "Accurate interpolation with high resolution time variant Radon transforms," *Geophysics*, vol. 67, no. 2, pp. 644–656, 2002.

[124] M. Sacchi and M. Porsani, "Fast high resolution parabolic Radon transform," *Society of Exploration Geophysicists 69th Annual International Meeting, SPRO P. Vol. 1. No. 1*, 1999.

[125] M. Sacchi, "A Tour of High Resolution Transforms," *cseg.ca*, no. 2, pp. 665–668, 1999.

[126] A. Gholami and H. R. Siahkoohi, "Simultaneous constraining of model and data smoothness for regularization of geophysical inverse problems," *Geophysical Journal International*, vol. 176, no. 1, pp. 151–163, Jan. 2009.

[127] Y. Luo, J. Xia, R. D. Miller, Y. Xu, J. Liu, and Q. Liu, "Rayleigh-wave mode separation by high-resolution linear Radon transform," *Geophysical Journal International*, vol. 179, no. 1, pp. 254–264, Oct. 2009.

[128] S. T. Kaplan, M. Naghizadeh, and M. D. Sacchi, "Data reconstruction with shot-profile least-squares migration," *Geophysics*, vol. 75, no. 6, pp. WB121–WB136, Nov. 2010.

[129] E. van den Berg, "Sparco: A testing framework for sparse reconstruction," *.... ca/labs/scl/sparco*, 2007.

[130] T. J. Trad, D. ; Sacchi, M. D. ; Ulrych, "A hybrid linear-hyperbolic Radon transform," *Journal of Seismic Exploration*, 2001.

[131] A. Berkhout, *Seismic Migration: Imaging of Acoustic Energy by Wave Field Extrapolation: Imaging of Acoustic Energy by Wave Field Extrapolation*, 1984.

[132] D. Verschuur, "Surface-related multiple elimination, an inversion approach," Ph.D. dissertation, 1991.

[133] D. Verschuur and A. Berkhout, "Estimation of multiple scattering by iterative inversion, Part II: Practical aspects and examples," *Geophysics*, 1997.

[134] D. J. Verschuur, "Seismic Multiple Removal Techniques: Past, Present and Future," *EAGE publications*, 2006.

[135] D. Donno, "Improving multiple removal using least-squares dip filters and independent component analysis," *Geophysics*, 2011.

[136] S. Kaplan and K. Innanen, "Adaptive separation of free-surface multiples through independent component analysis," *Geophysics*, 2008.

[137] W. Lu, "Adaptive multiple subtraction using independent component analysis," *Geophysics*, 2006.

Vitae

- Name: Arbab Latif
- Nationality: Pakistan
- Date of Birth: Feb 15,1987.
- Email: *arbablatif@gmail.com*
- Permanent Address: Gujranwala Cantt, Punjab, Pakistan
- BE Electrical Engineering: National University of Sciences and Technology, Pakistan
- Submitted Technical Papers:

  "Reconstruction of missing seismic traces using Compressive sensing and Radon Transform", IEEE Transactions on Geoscience and Remote Sensing

  "Automatic picking of the first arrival event using Compressive Sensing and $\tau - p$ Transform", Geophysics

  "Multiple reflection removal using Compressive Sensing with Radon Transform", Geophysics

  "Seismic Deconvolution using Compressive Sensing with Radon Transform", Geophysics